NTNU
Norwegian University of
Science and Technology

The Effect of Alginate G-block Treatment on the Extracellular Matrix

Trine Tønnesson

Biotechnology (5 year)
Submission date: February 2018
Supervisor: Kurt Ingar Draget, IBT
Co-supervisor: Cathrine Taylor Nordgård, IBT

Norwegian University of Science and Technology
Department of Biotechnology and Food Science

Preface

This master thesis was conducted at the Institute for Biotechnology and Food Science and the Institute for Molecular Genetics and Cancer Research at the Norwegian University of Science and Technology (NTNU). It is a part of the five year integrated master program in biotechnology-MBIOT5. The project was carried out from January 2017 til February 2018. This thesis was written with professor Kurt Ingar Draget as the main supervisor and Dr. Catherine Taylor Nordgård as co-supervisor.

Trondheim, February 16th, 2018

Trine Tønnesson

Acknowledgment

I would like to sincerely thank my supervisors professor Kurt Ingar Draget and dr. Catherine Taylor Nordgård for giving me the opportunity to work on this project. You have given me such great guidance and knowledge within laboratory work and scientific writing. In addition, a big thank you goes to Ann Sissel T. Ulset for helping me during the process of fault-tracking.

I would like to express my sincere gratitude to dr. Shalini Rao for giving me the opportunity to work on my thesis at St. Olavs Hospital. In addtion, for giving me such good help and feedback as well as for helping me to learn to evaluate immunohistochemical staining. I would also like to thank Bjørn Munkvoll for showing me and training me within the field of immunohistochemistry. In addition I would like to extend a great thank you to pathologist dr. Patricia Mjønes for evaluation the final staining for my three proteins, providing an expert opinion on the results obtained and also for great tips and advises in general. Furthermore, a general thank you to all the people I met at the 3^{rd} floor north at Gastrosenter for welcoming me there and for all the helpful conversations, hints and tips in the lab.

I would like to say a huge 'Thank you!' to my parents, you are great! Thank you for letting me vent out my frustration and for always being here for me. Lastly, a big thank you goes out to my friends and boyfriend for moral support through this process.

T. T

Abstract

Dense extracellular matrix and alterations of extracellular matrix are two of the hallmarks of solid tumors. The resulting highly fibrotic extracellular matrix is associated with several types of cancer. These solid tumors can pose a physiological resistance to cancer treatment, in part by preventing delivery of blood-borne drugs to cancer cells. This in turn causes a high mortality rate for solid tumors. RiXOVA is an anti-cancer drug candidate based on G-block technology that is hypothesized to target the extracellular matrix. Experimental *in vivo* studies on pancreatic cancer xenografted in a mouse model treated with G-block has shown a reduction in tumor growth both with G-block a single vehicle and in combination with the chemotherapy Gemcitabine. A hypothesized mode of action concerning G-block is that G-blocks are able to reduce the barrier created by the extracellular matrix in certain cancer types (e.g breast and pancreatic cancer) easing the delivery of drugs into the tumor microenvironment and increasing the drug bioavailability.

The aim of this thesis is to investigate the effect of G-block on collagen IV, fibronectin and α-smooth muscle actin in a xenografted pancreatic tumor model by using immunohistochemistry and attempting to quantify the results obtained with ImmunoRatio. In addition to that rheological properties (e.g gelling kinetic, setting time and deformation response) of collagen gel with and without added G-block were investigated to elucidate possible effects of G-block on collagen.

Within immunohistochemistry the addition of G-block demonstrated a significant difference in amount of fibronectin, quantified as a DAB+/nuclear staining, for mice that received 10 doses of G-block. There were no significant differences for collagen IV or α-smooth muscle actin in G-block treated tumor versus control tumor. Regarding rheology, addition of G-block in the collagen gel caused a shift in the gelling kinetics. There was a significant difference in the temperature in which the elastic modulus was at 20% of its maximum value for collagen gel with G-block added relative to collagen gel without G-block added. G-block did not influence the setting of collagen as both collagen with and without G-block appeared to not reach apparent equilibrium during the isothermal hold time. Collagen gels both with and without G-block appeared to exhibit a frequency dependence at 1-10 Hz in the frequency sweep suggesting that the collagen gel could be a physical gel. G-block at a 5.00 mg/ml concentration appeared to affect the strength of the gel causing a potential shift from a weak gel to a strong gel.

Sammendrag

Endring i extracellulær matrise og oppregulering av extracellulær matrise komponenter er to av karakteristikkene assosiert med solide tumorer. Dette fører til en høy-fibriotisk extracellulær matrise som er assosiert med flere forskjellige kreft typer. Disse solide tumorene skaper en barriere som fører til problemer relatert til levering av medisin i kreftvev. Dette fører igjen til at solide tumorer har en høy mortalitets-rate. RiXOVA er en kreftmedisin-kandidat og er basert på G-blokk teknologi som antas å potensielt påvirke extracellulær matrise. Eksperimentelle *in vivo* studier på bukspyttkjertel-kreft implantert i mus som har blitt behandlet med G-blokk har demonstrert en reduksjon i vekst av tumor med G-blokk alene samt også ved kombinasjon med kjemoterapien Gemcitabine. En hypotetisert effekt av G-blokk relatert til kreftvev er at G-blokk kan redusere barrieren skapt av extracellulær matrise gjennom signaler fra tumor i enkelte krefttyper (f.eks bryst- og bukspyttkjertel-kreft), dette kan lette transport og levering av medisin inn til tumor og øke den behandlende medisinens biotilgjengelighet.

Målet med denne oppgaven er å undersøke effekten G-block kan ha på kollagen IV, fibronektin og α-glatt muskel aktin i en bukspyttkjertel-kreft modell xenografert i mus. Dette ble gjort ved å bruke immunohistokjemi, et forsøk på å kvantifisere fargningen oppnådd i immunohistokjemi ble gjort med ImmunoRatio. I tillegg til dette ble rheologiske egenskaper (f.eks. gellings kinetikk og deformasjons respons) til kollagen geler med og uten tilsats av G-blokk undersøkt for å avdekke mulige effekter G-blokk kan ha på kollagen.

Innenfor immunohistokjemi vev behandlet med G-blokk viste en signifikant forskjell i mengde fibronektin, kvantifisert som en DAB+/celle-kjerne farging, for mus som fikk 10 doser med G-blokk over tid. Det var ingen signifikante forskjeller for kollagen IV eller α-glatt muskel aktin i G-blokk behandlede tumorer vs kontroll tumorer. For rheologi førte tilsats av G-blokk til et skift i gellings kinetikk for kollagen gel ved å øke temperaturen hvor den elastiske modulus var på 20% av sin maksimums verdi. G-blokk påvirket ikke settingen av kollagen gel da hverken kollagen gel alene eller kollagen gel med G-blokk oppnådde ekvilibrium i den isotermiske hold tiden. Kollagen gel med og uten G-blokk hadde begge en frekvens avhengig respons i 1-10 Hz vinduet i frekvens sveip, dette kan indikere at kollagen gelen var en fysisk gel. Kollagen gel med G-blokk konsentrasjon 5.00 mg/ml kan synes å påvirke styken på kollagen gelen og føre til et potensielt skift fra svak gel til sterk gel.

Acronyms

α-SMA α-Smooth muscle actin

δ Phase angle

η Viscosity

γ Shear strain

$\dot{\gamma}$ Shear strain rate

τ Stress

1h RT One hour incubation in room temperature

DAB+ 3,3'-Diaminobenzidine

DPBS Dulbecco's phosphate-buffered saline without calcium and magnesium

ECM Extracellular matrix

G α-L-Guluronic acid

G' Elastic, in-phase, storage modulus

G" Viscous, out-of-phase, loss modulus

G* Complex modulus

H&E Hematoxylin and eosin

Ig Immunoglobulin

IHC Immunohistochemistry

kDa Kilo Dalton- molecular weight unit

LVR Linear viscoelastic region/regimen

M β-D-Mannuronic acid

MMP Matrix metalloprotease

M_w Molecular weight

O.N Over night incubation at 4°C

Pa Pascal- unit of stress and/or pressure

PDAC Pancreatic ductal adenocarcinoma

PanIN Pancreatic intraepithelial neoplasia

RGD-motif An amino acid sequence of Arg-Gly-Asp

Contents

List of Figures

List of Tables

Chapter 1

Introduction

1.1 Cancer

Due to the decline in infections diseases in the western world cancer has now become the second leading cause of death only surpassed by heart disease (Owen et al. (2013)). In addition, it is estimated that approximately one of five deaths will be as a result of cancer (Alberts et al. (2008a)). Cancer is defined by the loss of tissue organization as well as the aberrant behavior exhibited by cancerous cells. The transformations cells undergo when they become cancerous are a result of genetic mutations and epigenetic alterations (Frantz et al. (2010)). Cancer cells are defined by the following two hereditary properties: (a) they defy normal rules of reproduction and (b) the cells invade and colonize in areas belonging to other cells. A tumor or neoplasm is the result of such an abnormal cell that grows and divides out of control, however, as long as the neoplastic cells do not become invasive it is said to be a benign tumor. By destroying the mass of a benign tumor the patient will usually be completely cured. On the other hand, a tumor is defined as malignant if the neoplastic cells have acquired the ability to invade surrounding tissue (Figure 1.1). Once a malignant tumor has had a chance to invade surrounding tissue and these cells have ended up in the blood or lymphatic stream these cells can be transported to other sites in the body and give rise to secondary tumors. This process is called metastasis (Alberts et al. (2008a)). The metastatic ability of cancers is one of the major causes of cancer related mortality (Decock et al. (2011)).

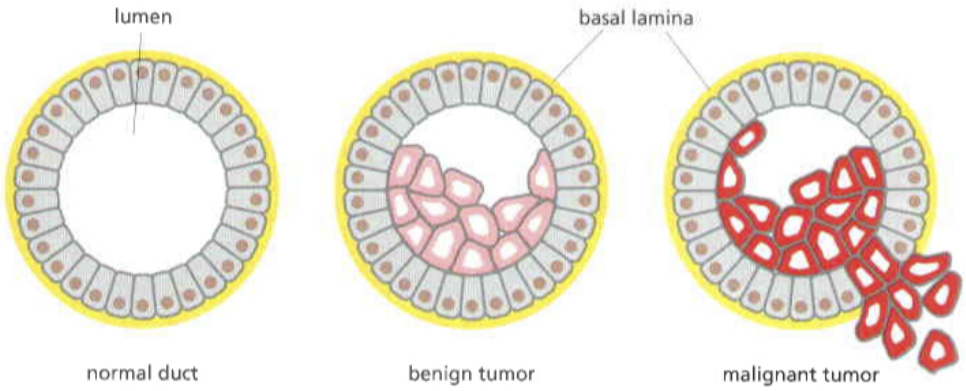

Figure 1.1: Normal ductal tissue versus benign and malignant tumor ductal tissue. The malignant tumor cells shown are in the process of destroying the integrity of the duct and attempting metastasis. Obtained from (Alberts et al. (2008a)).

Names of cancer are given based on what type of cells and tissue they originate from. For instance, cancers arising from epithelial cells are named carcinomas, cancers arising from connective tissue or muscle cells are named sarcomas (Owen et al. (2013)). Cancer is, as mentioned above, caused a single abnormal cell. This single cell experienced some sort of heritable change or mutation, which it passed on to its daughter cells via cell division. These daughter cells then experience additional changes which allow them to outgrow, out-divide and outlive healthy normal cells. It is however not enough for a single mutation to occur in a cell to cause cancer, malignant cells harbor many mutations. Tumors can develop for years before they are discovered and by the time of discovery they will already contain about a billion neoplastic cells (Alberts et al. (2008a)).

1.1.1 Pancreatic ductal adenocarcinoma

In the United States it was estimated that over 40 000 new cases and 39 000 deaths were attributed to pancreatic cancer in 2014, and pancreatic ductal adenocarcinoma (PDAC) represents the vast majority of these deaths. Pancreatic cancer itself was in 2014 the 12th most common type of cancer in the US but it is ranked as the 4th most common cause of cancer related deaths (Stark and Eibl (2015)). By 2030 pancreatic cancer is projected to become the second leading cause of cancer-related deaths in USA, with the leading cause of cancer-related deaths is projected to be lung cancer (Hessmann et al. (2017)).

The high lethality of pancreatic cancer is attributed to both the lateness of discovery and diag-

nosis, as well as the resistance to current treatments posed by the cancer (e.g chemotherapy). In addition, PDAC has a high instance of early metastasis and more than 80 % afflicted by PDAC have unresectable tumors. The majority of these cases of pancreatic cancers also present with a metastatic disease due to the aggressiveness of the cancer type (Bailey et al. (2008)).

The pancreas, where the primary tumor of pancreatic cancer occurs, can be divided into four anatomic regions: the uncinate process (Figure 1.2 bottom right part of head region), the head, the body and the tail (Figure 1.2). With regards to PDAC the four regions are reduced to two, the head (with the uncinate process) and the body/tail. 60-70% of PDAC arise from the head of the pancreas whilst 20-25% arise from the body/tail. Tumors arising from the head of the pancreas will cause a phenomenon called ”painless jaundice” (yellowing of skin and the whites of the eyes) as the head of the pancreas is located in close proximity of the common bile duct (Figure 1.2) and a tumor growth there will compress the bile duct. This leads to an accumulation of bile in the blood and this can in turn prompt an imaging study that can reveal an underlying tumor. Tumors of the body/tail will in contrast not produce jaundice and will come to clinical attention later when other symptoms like weight loss and pain appear (Stark and Eibl (2015)).

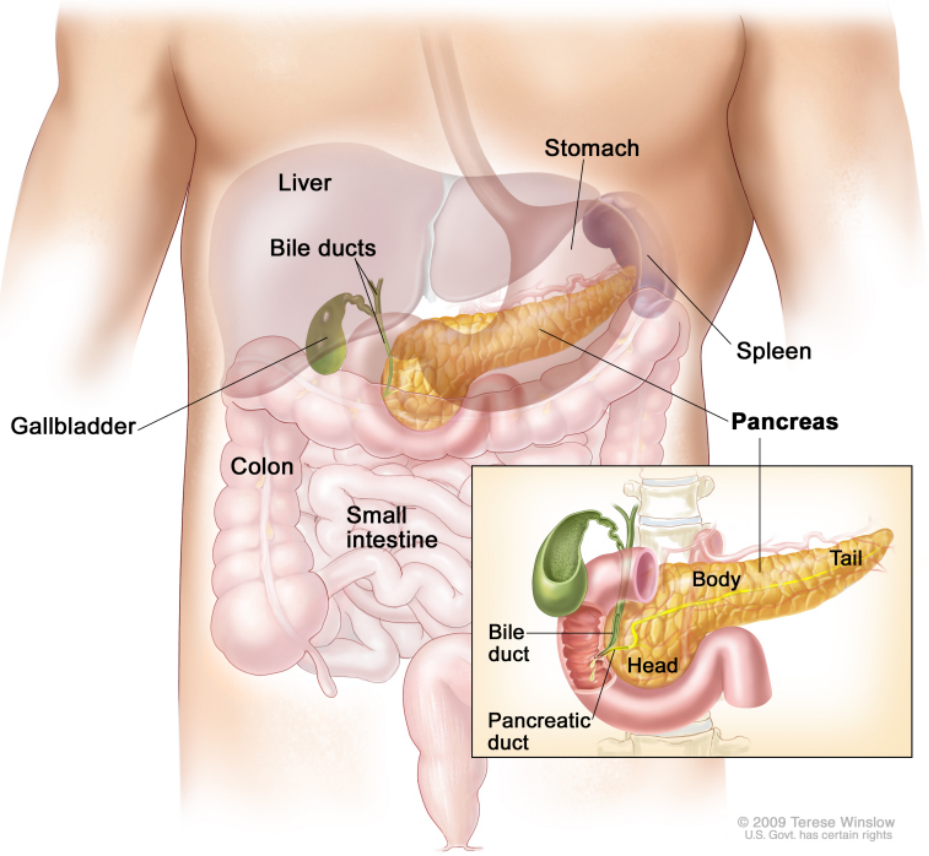

Figure 1.2: Overview of the location of the pancreas in the body relative to other organs and its gross anatomy in the smaller image on the lower right. Note that the pancreatic duct stretches all through the entirety of the pancreas. The pinkish tube that wraps around the head of the pancreas is the duodenum. Obtained from Winslow (2009).

PDAC is an epithelial tumor type that arises from cells of the pancreatic duct (Figure 1.2, pancreatic duct in inserted image) (Stark and Eibl (2015)). This type of tumor is defined as a solid tumor and the neoplastic cells form glands and infiltrate into surrounding tissues (Wolfgang et al. (2013)). Further, this formation of a solid tumor is thought to be caused by the presence of a dense stroma comprised of, among others, fibroblasts and inflammatory cells. Histopathologic analyses of PDAC tissue compared with normal pancreatic tissue shows dense collagen (type I and III) bundles associated with fibroblasts. This dense expression of collagen is in turn assco-ciated with a loss of basement membrane integrity which promotes invasion and metastasis of malignant cells into the interstitial matrix within other tissues and organs (Mahadevan and Von Hoff (2007)). The tissues invaded by the PDAC include lymphatic tissue, spleen and peritoneal cavity, with metastasis to the liver and lungs (Hezel et al. (2006)).

It is believed that the development of PDAC occurs over an extended period of time and it is thought that PDAC follows a stepwise progression like other carcinomas. It starts with a transition from a normal pancreatic duct to a pre-invasive precursor lesion. This is known as pancreatic intraepithelial neoplasia (PanIN) and PanIn can ultimately develop into PDAC (Stark and Eibl (2015)). The mutation of the oncogene K-ras, found on chromosome 12 (Wolfgang et al. (2013)) is thought to be a common genetic marker for this type of cancer (Bailey et al. (2008)), (Deer et al. (2010)). Mutation in the K-ras gene occurs in almost all primary tumors of PDAC (95%) (Wolfgang et al. (2013)) and are present at early stages of the disease (Deer et al. (2010)). The protein product of K-ras is a member of the RAS family of GTP-binding proteins that mediate a wide variety of cellular functions including proliferation, differentiation, and survival (Hezel et al. (2006)). Another potentially important mutation occurs in the SMAD4 gene. This is a tumor suppressor gene located on chromosome 18 and the protein product of this gene- Smad4 is involved in the transforming growth beta (TFG β) cell signaling pathway (Wolfgang et al. (2013)). A deletion of this transcription factor can cause cells to proliferate in an uncontrolled manner (Gopinathan et al. (2015)). This mutation is associated with poor patient prognosis, wide metastasis and seems to occur at later stages of the disease. As such SMAD4 could serve as a marker for tumor progression (Wolfgang et al. (2013)).

The chemotherapy gemcitabine has through the past several decades remained the standard of care when dealing with PDAC, in addition to surgery, despite it only having a marginal proven effect on patient survival (Hessmann et al. (2017)). Surgery is currently the only option that offers a definitive chance for a cure, however- only 10-20% of patients with PDAC have tumors that can be surgically resected (Stark and Eibl (2015)). An other problem with PDAC is the formation of abundant tumor stroma (Wolfgang et al. (2013)) by up-regulating production and secretion of fibronectin, collagen and hyaluronan among others. This is thought to be one of the problem areas of the treatment of PDAC. By forming a dense stroma around the afflicted areas a type of barrier is formed and this is thought to impede drug delivery into the tumor, causing its resistance to conventional drug therapy (Hessmann et al. (2017)).

Despite the bleak fate for patients diagnosed with PDAC currently there have been advances in understanding the genetic behind this disease, surgical techniques have improved, radiation therapy has had a lowering in toxicity and novel drug combinations have shown to improve chances of survival according to a review published by Wolfgang et al. (2013).

1.2 Extracellular matrix and tumor microenvironment

The extracellular matrix (ECM) fills the area surrounding the cells within all tissues and organs (Frantz et al. (2010)). The ECM is comprised of a variety of proteins and polysaccharides secreted from cells in close proximity and it is organized in a meshwork close to the surface of the secreting cells (Figure 1.3, left image) (Alberts et al. (2008b)). In addition, each type of tissue has an ECM with a unique composition and topology, generated during tissue development (Frantz et al. (2010)). The ECM plays an active role in regulation of adjacent cells with regards to their development, survival, shape and function- among others (Alberts et al. (2008b)). Furthermore, ECM play an important role in both tissue and organ development, function and in repairing injuries. Diseases such as cancer can either be caused by or cause of changes in the organization or integrity of the extracellular matrix (Miner (2010)). Remodeling of the ECM can occur when cells express or activate enzymes like metalloproteinases (MMPs) that degrade components of the ECM (like collagen and fibronectin) and synthesize new matrix proteins (Avraamides and Varner (2010)).

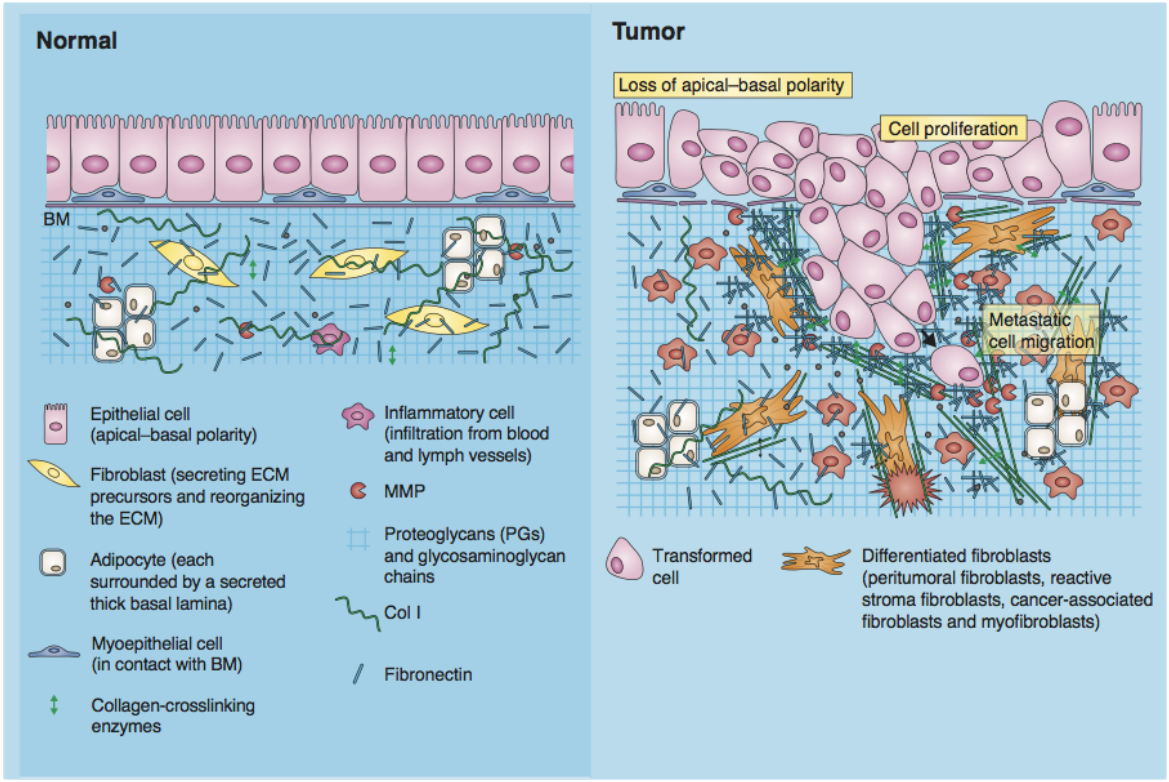

Figure 1.3: The components and the composition of the extracellular matrix in normal healthy tissue (left) and in tumor afflicted tissue (right). The basement membrane (BM) can be seen as a thin sheet that separates the ECM from the epithelial cells. Adapted from Frantz et al. (2010).

Important parts of the ECM are the basement membrane and interstitial matrix. The basement membrane is produced by epithelial, endothelial and stroma cells (e.g. fibroblasts) to separate epitelium from endothelium. The interstitial matrix however is primarily produced by stroma cells. The basement membrane (Figure 1.3, BM) is a specialized ECM and it is more compact and less porous than the interstitial matrix. It contains type IV collagen, laminins, fibronectin and linker protein like nidogen and entaction. These linker proteins connect collagen with other protein components. The interstitial matrix is on the other hand rich in fibrillar collagens (e.g. type I, II, II), proteoglycans, and various glycoproteins and is thus highly charged, hydrated, and contributes greatly to the tensile strength of tissue (Lu et al. (2012)). The interstitial matrix/ stroma encompasses the tissue compartments that lie between functional compartments and serve as a sort of glue that binds the tissue together. Many of the proteins found here are produced by interstitial fibroblasts in mature organs or by migrating mesenchymal cells during organogenesis (Miner (2010)). The interstitial matrices forms the majority of the connective tissue found in the body and it is as mentioned above rich in fibrillar collagen I. This collagen type is cross-linked into a stable mesh work that provides 3D structural support to the interstitial matrix (Sodek et al. (2008)).

The ECM can influence a myriad of processes within tumor stricken tissue, like tumor growth and tumor metastasis- by promoting the growth of neoplastic cells, development of new blood vessels (angiogenesis) and new lymphatic vessels (lymphangiogenesis) from pre-existing vessels, invasion of stromal cells and introduction of tumor cells into the blood circulation. All of this leads to tumor cell proliferation at distant sites where the cycle repeats it self and this in turn produces additional metastases in other locations of the body (Avraamides and Varner (2010)).

1.2.1 Matrix metalloproteinases

A total of 23 proteases make up the family of matrix metalloproteinases (MMPs). These MMPs can be divided into five categories, depending on their domain structure and substrate specificity: collagenases, gelatinases, stromelysins, matrilysins and membrane-type MMPs (Decock et al. (2011)). Collectively MMPs are able to digest all of the components that make up the ECM. The tumor cells use MMPs to their advantage when invading and metastasizing to secondary sites in the body by having parts of the ECM degraded (Fingleton and Lynch (2010)). Basement memebrane remodelling is primarily done by the gelatinases MMP-2 and MMP-9 as well as

transmembrane MMPs (Sodek et al. (2008)). In order to maintain stability and expression of enzymatic activity MMPs require both zinc ions and calcium ions (Nagase and Woessner (1999), Visse and Nagase (2003)). The ability to degrade both stroma and basement membranes makes MMPs necessary in the tumor microenvironment. Certain MMPs also have the ability to act as growth factors and cytokines (Fingleton and Lynch (2010)).

1.2.2 Interstitial matrix/ Stroma

The interstitial matrix/stroma is comprised of connective tissue that contains fibroblasts, myofibroblasts, inflammatory white blood cells, endothelial cells of blood and lymphatic vessels and smooth muscle cells. In addition, these cells secrete a variety of proteins and polysaccharides (Alberts et al. (2008b)). These structures within the stroma provides the framework for tumors and are essential for facilitating cross-talk between tumors and between stroma cells and tumor cells (Feitelson et al. (2015)). The cancer cells of a carcinoma can induce changes in the stroma by secreting signal proteins which alter stroma cell behavior and cause the secretion of proteolytic enzymes. These proteolytic enzymes (e.g. MMPs) have the power to modify the ECM. The stroma in turn can influence the cancer cells by secreting signal proteins to stimulate cancer cell growth and division (Alberts et al. (2008b)).

1.3 Proteins

1.3.1 Collagen

Collagen I (molecular weight (M_w) of 290 kDa) (Alberts et al. (2008b)) along with among collagen II and III (Kalluri (2003)) belongs to a family of fibrous proteins and are secreted in large quantities by connective tissue (Alberts et al. (2008b)). Currently, there are 28 types of collagen discovered, however, not all of them are components of the ECM (Muiznieks and Keeley (2013)). They differ in terms of amino acid composition, structure, length, biological role and abundance. Collagen is also a major component in skin and bone and can undergo a variety of transformations; fibril formation, gelation, denaturation and hydrolysis. The most typical characteristic for this protein group is its abilitiy to undergo aggregation into a filamentous form referred to as collagen fibrils. Collagen fibrils can further aggregate to form collagen fibers (Figure 1.4) (Kezwon and Wojciechowski (2014)).

The structure of collagen consists of a rigid triple stranded helix where three left-handed collagen polypeptide chains (α-chains) are woven around each other- resembling a ropelike structure (Alberts et al. (2008b)). Its triple helix is then right-handed and has three residues per turn and there are cross-linkages between the α-chains made up of intermolecular bonds and intramolecular bridges (Kezwon and Wojciechowski (2014)).

There are many types of vertebrate collagen but they generally have the following distribution of amino acids: 35% glycine (Gly), 11% Alanine (Ala), and a total of 21% for Proline (Pro) and 4-Hydroxyproline (4-Hyp) (Nelson and Cox (2013)). Hydroxyproline is a imino acid that is associated uniquely with collagen and its triple helical structure serves to stabilize the structure (Djabourov et al. (2013b). Collagen is very rich in both proline and glycine and these two amino acids are important in the triple helix formation. Proline contains a ring structure that also contributes to stabilize the helix conformation for each α-chain and glycine is regularly spaced at every third residue in the central region of the α-chain (Alberts et al. (2008b)). Thus, glycine causes a repeating tripeptide consisting of a Gly-X-Y motif where X is often Pro and Y is 4-Hyp, however- Lysine (Lys) and Histidine (His) can also be found in the X and Y positions and form covalent bonds (Nelson and Cox (2013)). Further, glycine is a small amino acid and because of this it allows the three α-chains to pack tightly to form the triple helix. These properties enable

collagen fibrils to be good at withstanding stretching forces (Alberts et al. (2008b)).

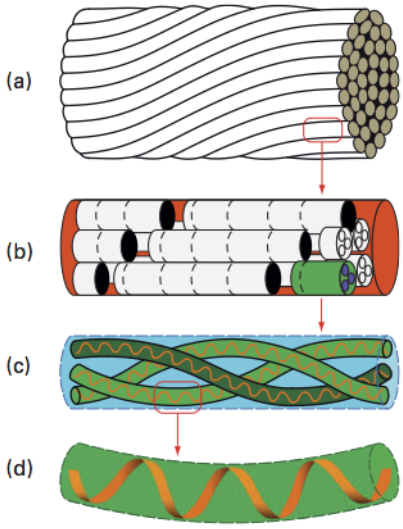

Figure 1.4: Structure of collagen fibers. (a) collagen fibers are formed from bundles of twisted fibrils, (b) fibrils are made from rods that are arranged in parallel and staggered arrays, (c) each rod consists of a right-handed triple helix, (d) a single collagen strand with a left-handed helix. Obtained from Djabourov et al. (2013b)

In addition to the fibrilar forming types of collagen there are also network-forming collagen (Muiznieks and Keeley (2013), Kalluri (2003)). Collagen type IV is one of these and it is an important component of the basement membrane/basal lamina. It differs from for instance collagen I in its shape. Where collagen I forms a straight rope-like structure, is fibrillar and is found in the interstitial matrix, type IV collagen consists of three long protein chains and is mainly associated with the basement membrane (Figure 1.3). These chains have been separately synthesized, but they also twist together to form a superhelix like type I collagen, but differ as the type IV collagen has interruptions in more than 20 domains. These interrupted domains in turn allow the formation of kinks and bends in the superhelix. These kinks and bends causes the formation of a felt-like network which in turn provides the basement membrane with a certain amount of tensile strength (Alberts et al. (2008b)).

1.3.1.1 Gelatin

Gelatin is extracted from collagen and this extraction is achieved by hydrolytic degradation of collagen (Ross-Murphy (1992)). The main molecular unit of collagen is a superhelix, also referred to as tropocollagen rod, that contains three polypetide chains with a sequence of Gly-Pro-X

where X often is hydroxyproline (Djabourov et al. (2013b)). The amount of proline and hydroxyproline within a collagen helix affects the gelation and denaturation temperature of collagen and subsequently gelatin (te Nijenhuis (2007)).

For extraction of gelatin from collagen the collagen fibers need to be disrupted by both chemical and thermal treatments. There are two ways of chemical disruption that leads to gelatin extraction: alkali and acidic. By extracting with alkali the isoelectric point is changed to a pH = 5, when applying an acidic extraction the isolectric point is at pH = 8-9 which is the same as for native collagen (Djabourov et al. (2013b)). Gelatin solutions can be prepared at variable pHs and ionic strengths. The most important requirement for a gelatin solution to be prepared is the temperature, it needs to be above 30°C and the pH needs to be different than the isoelectric point. This can be achieved by adjusting the pH or by adding salts to the solution (Djabourov et al. (1993)). If gelatin is in an aqueous solution above the denaturation temperature the gelatin molecules are in a random coil state, when the gelatin solution is cooled down well below the denaturation temperature parts of the random coils are involved in a reverible coil-helix transition (te Nijenhuis (2007)). When the gelatin solution is cooled down it forms a transparent gel (Ross-Murphy (1992)). Only small parts of the gelatin molecule are able to undertake this coil-helix transition. Because of this only a small number of triple helices are formed, and this can only happen if the concentration of gelatin in a aqueous solution is high enough ($>$2% gelatin) (te Nijenhuis (2007)).

1.3.2 Fibronectin

Fibronectin is a large molecular weight extracellular glycoprotein. It is present at low concentration in basement membranes but at high concentrations in remodeling extracellular matrices, more precisely in the interstitial matrix (Avraamides and Varner (2010)). Fibronectin is expressed by endothelial cells during both embryonic and tumor development but it is poorly expressed in normal healthy tissue (Alberts et al. (2008b)). Fibronectin is important with regards to cell adhesion, growth, migration and differentiation. Further, it has been found to be overexpressed in several types of cancer and its also thought that fibronectin might limit tumor cell responsiveness to therapy (Wang and Hielscher (2017)).

Fibronecitn is encoded by a single gene on the human chromosome 2, however, with alternative

splicing fibronectin can present in multiple isoforms (Avraamides and Varner (2010)). The alternative splicing of a single pre-mRNA can generate as many as 20 variants of fibronectin in humans. Because of alternative splicing of pre-mRNA from the single fibronectin gene, fibronectin has the capacity to produce a large number of variants. This in turn generates fibronectin with different properties related to cell-adhesion, ligand-binding, and solubility that provide a mechanism for cells to alter the composition of the ECM (Pankov and Yamada (2002)).

Fibronectin presents like a dimer (M_w of 220–250 kDa) composed of two large sub-units. The sub-units are held together by disulfide bonds at the carboxy-terminal (Avraamides and Varner (2010)). The sub-units themselves are folded into a series of functionally distinct domains and the domains are separated by regions of flexible polypeptide chains (Alberts et al. (2008b)). Both of the monomers that make up the dimers contain 12 type I, 2 type II and 15-17 type III protein domains (Figure 1.5) (Avraamides and Varner (2010), Pankov and Yamada (2002)). The type I is found at both the amino- and carboxy terminals and form antiparallel β-pleated sheets. The type II domains also form β-pleated sheets but these comprise collagen binding domains. The type III forms β-barrels with extended protein interaction loops (Avraamides and Varner (2010)).

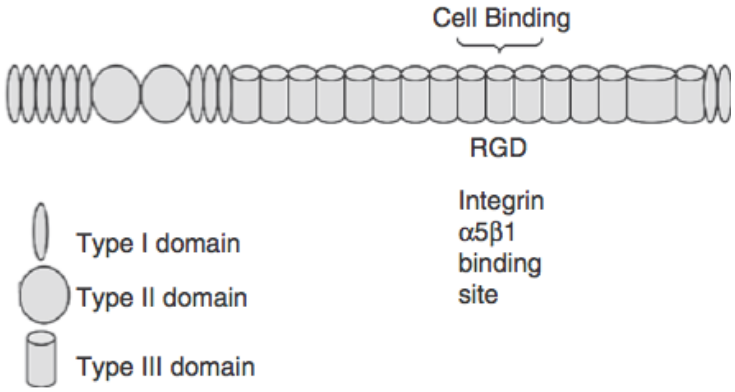

Figure 1.5: The basic structure of a fibronectin monomer. The monomer contains 12 type I domains, 12 type II domains and 15-17 type III domains. Interprotein intercations often take place in type III domains. The RGD (Arg-Gly-Asp) motif is found on the 10th type III domain. Adapted from Avraamides and Varner (2010)

Fibronectin exists mainly in two forms, the soluble and insoluble form. In the insoluble form the dimer assembles into disulfide bonded oligomers and fibrils, while the soluble form remains in the dimeric form (Avraamides and Varner (2010)). The soluble from of fibronectin is found in circulating blood and other body fluids while the insoluble form is found in the ECM of tissue

and organs (Pankov and Yamada (2002)).

The receptors associated with fibronectins are integrins, they are a large family of heterodimeric membrane protein receptors. Integrins anchors the ECM to the intracellular cytoskeleton. The RGD-motif (amino acid sequence Arg-Gly-Asp (Miner (2010)) is a type of integrin binding site that is located on the 10th type III domain repeat of fibronectin (Figure 1.5) (Pankov and Yamada (2002)). This motif is a binding site for several integrin receptors (Miner (2010)). Integrins are dependent upon divalent cations (Ca^{2+} and Mg^{2+}) as these cations form salt bridges with ligands (Avraamides and Varner (2010)).

Increased fibronectin levels lead to an increase in tissue stiffness, loss of epithelial cell polarity as well as enhanced proliferation. In normal tissue, as mentioned previously, the ECM does not contain fibronectin and because of this the tissue is quite soft. However, during oncogenesis the basement membrane changes and collagens and fibronectin are deposited within tumor areas and this is one of several mechanisms which enhance tumor cell proliferation. Increased levels of fibronecitn also plays a role in metastasis by sending out signals that promote cell migration (Avraamides and Varner (2010)).

1.3.3 α-Smooth muscle actin

Actin is one of the best conserved eukaryotic proteins. It has six isoforms where four of them represent differentiation markers of muscle tissue and the remanding two can be found in both muscle cells and non-muscle cells (Skalli et al. (1986)). The α-smooth muscle actin (α-SMA) is encoded by the ACTA2 gene (Yuan (2015)) and the expression of the various types of isoactin is dependent upon cell and tissue type (Herman (1993)). The overall sequence homology exhibited by the actin isoforms are $>$90% (Skalli et al. (1986)). The amino terminal end of the protein is thought to be the modulator of certain specific isoform fuctions like actin-actin, actin-myosin and actin-actin-binding protein interactions (Herman (1993)) and it is also thought to be the molecules main antigenic region (Skalli et al. (1986)). α-SMA contributes to cell-generated mechanical tension and to the maintenance of cell shape and movement. The motility of cells are very much dependent on the actin cytoskeleton (Lee et al. (2013)).

After a tissue injury fibroblasts differentiate into contractile and secretory myofibroblasts, these

cells express α-SMA (Hinz et al. (2007), Desmoulière et al. (1993)). Furthermore, these cells contribute to tissue repair during wound healing but this can severely impair organ function when ECM protein secretion become excessive as this causes fibrosis (Hinz et al. (2007)). However, these myofibroblast cells also present in stroma-reactions of epithelial tumors and may help promote the progression of cancer invasion since tumor cells also use actin bundles to help break away from the primary tumor site and subsequently invade into surrounding tissue (Hinz et al. (2007), Lee et al. (2013)).

1.4 Alginate

Alginate is a polysaccaride derived from brown algae (e.g *Laminaria hyperborea*) (Christensen (2016)) in addition to some types of bacteria (e.g. *Azotobacter Vindelandii* and some *Pseudomonas*-species) (Smidsrød and Moe (2008)). It is a linear binary copolymer composed of β-D-mannuronic acid (M) and α-L-guluronic acid (G). These are bound together in a 1$\rightarrow$4 linkage (Draget and Taylor (2011)). The molecular weight of commercial available alginate can be obtained in the range of 32000 to 400000 g/mol with a wide variety of compositions of M and G (Lee and Mooney (2012)).

The G-monomer is modified from the M-monomer and this modification can be done by C-5 epimerase which causes the carboxyl group on C-5 to flip (Figure 1.6 a). When M is converted to G the conformation of the molecules shifts from a $^1C_4$ conformation to a $^4C_1$ conformation (Figure 1.6 b). The change in conformation causes the glycosidic linkages in the polymer to shift which can influence various properties of the alginate. The link between M-M remains diequatorial while the linkage between M-G becomes equatorial-axial and linkage between G-G becomes diaxial (Figure 1.6 b) (Smidsrød and Moe (2008)).

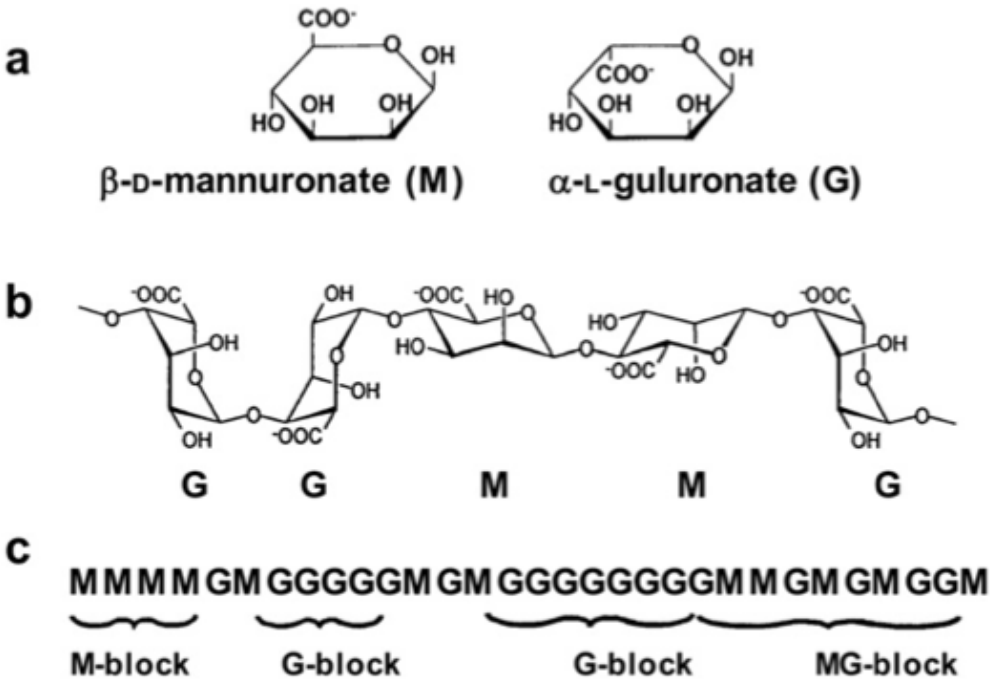

Figure 1.6: a) The structures for both α-L-guluronic acid and β-D-mannuronic acid, b) chain conformation of M and G, G is in a $^4C_1$ conformation and M is in a $^1C_4$ conformation, c) examples of block distribution. Obtained from Draget and Taylor (2011)

The epimerisation of M to G influences, as mentioned, certain properties of alginate. Examples of the change in properties and function can be the ability to form gels with divalent cations (e.g Ca^{2+}), immunogenic responses (Lee and Mooney (2012)) and also how well alginate is dissolved by acid hydrolysis (Haug et al. (1967)). Alginate with a high content of M was reported to be immunogenic and 10 times more potent in stimulating cytokine production as opposed to high G content alginate (Lee and Mooney (2012)). Further, alginate rich in M-blocks cannot form ionic gels, but they can form acidic gels (Draget et al. (1994)).

The diaxial linkage seen in G-blocks gives an ”egg-box” model (Figure 1.7 A) where the glycosidic bond between two adjacent guluronic acids causes a cavity in the polymer chain (Grant et al. (1973)). Within this cavity the Ca^{2+} can bind to several -OH and $-COO^{-}$ and this leads to gelation when there are enough cross-links formed between Ca^{2+} and guluronic acid residues on two alginate strands (Figure 1.7 A, B) (Lee and Mooney (2012), Tønnesen and Karlsen (2002)).

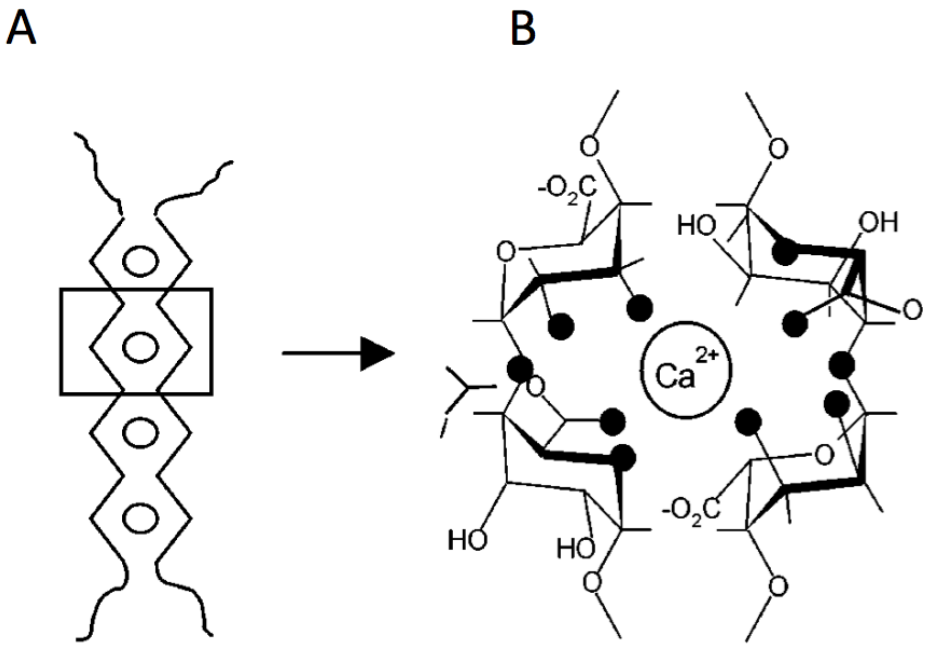

Figure 1.7: Binding mode between G-blocks in alginate and calcium that causes the egg-box structure. (A) shows the egg-box structure created when two strands rich in G-blocks bind to the same Ca^{2+} atoms and (B) shows the oxygen (black dots) in the hydroxy and carboxy groups thought to be involved in the binding of Ca^{2+}. Adapted from Braccini and Pérez (2001).

There are three major compositions of monosaccarides in alginate: M-blocks, G-blocks and MG-blocks (Figure1.6c). The length of the blocks as well as the composition of the three variants can be determined by what type of organism it originates from (Christensen (2016)). The non-random block structure is attributed to a biosynthetic pathway where guluronic acid residues

are introduced into a preformed mannuronan polymer. This change is achieved by a family of isoenzymes with C-5 epimerase activity. The bacterium *A. vindelandii* encodes for seven of these epimerases (AlgE1-AlgE7) and these epimerases introduce either GMG or GG blocks of various lengths, ranging from very long G-blocks to short G-blocks, into the mannuronan polymer chain (Aarstad et al. (2012), Draget and Taylor (2011)).

In order to extract alginate from seaweed the seaweed is treated with a dilute alkaline solution (often NaOH) (Lee and Mooney (2012)). The extract, alginic acid, is filtered and either sodium chloride or calcium chloride is added to the filtrate in order to convert it to either sodium alginate or calcium alginate (Lee and Mooney (2012), Tønnesen and Karlsen (2002)). The alginate salt can be transformed into alginic acid again by treating it with dilute HCl to allow for further purification (Lee and Mooney (2012)). By using ^{1}H NMR spectroscopy it is possible to determine the composition and sequence of G and M in alginate, as demonstrated by Grasdalen (1983) .

Acid based hydrolysis is a much used way to selectively degrade alginate. As previously mentioned, the composition of M- and G-monomers in alginate influences how well alginate is dissolved in acid hydrolysis. Acid hydrolysis of glycosides was first suggest by Edward (1955) as mentioned in Timell (1964) and consists of (I) rapid protonation of the glycosidic oxygen that join together two alginate monomers, (II) this protonation gives a corresponding conjugate acid, then (III, IV) the slow rate-determining step where the acid decomposes and forms an alcohol and a carbonium-oxide ion causing a half-chair formation of the carbonium-oxide ion, (V) then water is rapidly added and the result is the transformation of the carbonium-oxide ion into a reducing end (Timell (1964)). The differences in the chemical composition of alginate (amount of guluronic acid and mannuronic acid) affects the solubility of alginate in relation to acid based hydrolysis (Haug et al. (1974)). Alginate from *L. hyperborea* has a high prevalence of G-blocks while *Ascophyllum nodosum* has a high prevalence of M-blocks (Haug et al. (1967)). Haug et al. (1967) demonstrated that the amount of material dissolved by acid hydrolysis for *L. hyperborea* was at 23% while *Ascophyllum nodosum* had a larger portion (55 %) of its material dissolved. It is also reported that time, pH and temperature influences the results of acid based hydrolysis (Tønnesen and Karlsen (2002))

Alginate is obtained and extracted from a natural source and it is possible that a variety of impurities are present in the raw product. These impurities could be heavy metals, proteins and endotoxins. To reduce the chances of e.g. unwanted immune-responses when using alginate as a

part of a pharmacological product it is important to ensure that the alginate is properly purified (Tønnesen and Karlsen (2002)) as ultra-pure alginate has proven to not produce any significant foreign body reaction when implanted into animals (Lee and Mooney (2012)).

1.5 RiXOVA

RiXOVA is an anti-cancer drug candidate that is currently in the pre-clinical stage of testing. It is intended as a drug candidate for any type of cancer where ECM acts as a treatment barrier. Cancers such as pancreatic, ovarian and breast cancers develop highly fibriotic ECM and RiXOVA is thought to be of relevance especially to these cancer types. The avaliability of drug candidates that target the ECM is largely lacking within of drug discovery projects. RiXOVA is developed by Professor Kurt I. Draget and Dr. Catherine T. Nordgård at the Norwegian Univeristy of Science and Technology in Trondheim. RiXOVA in mice has undergone an extensive toxicological study following systemic injection. The results from Statens Serum Institute in Copenhagen showed no toxicity, even at high doses. Further, the drug also shows no immunogenic reactions (Draget and Nordgård (2015)).

The drug is based on G-blocks as discussed in section 1.4. The versatility of G-block as a drug is reflected in its other application that is intended for the treatment of respiratory diseases such as cycstic fibrosis (CF) and chronic obstructive pulmonary disease. The formulation of G-blocks pertaining to CF has successfully passed phase I of clinical trials. This indicates that the safety of the drug as a human drug is high and a phase IIb trail in CF patients is well on its way to completion(Draget and Nordgård (2015)).

RiXOVA has proven capable of enhancing the effect of chemotherapies like Gemcitabine by reducing the tumor size further than with Gemcitabine alone in a Capan-2 human pancreatic tumor xenograft model (Figure 1.8). It has also proven capable of reducing the tumor size alone in the same type of model, as mentioned previously, indicating that it can possibly work as a single agent as well (Figure 1.9) (Draget and Nordgård (2015)).

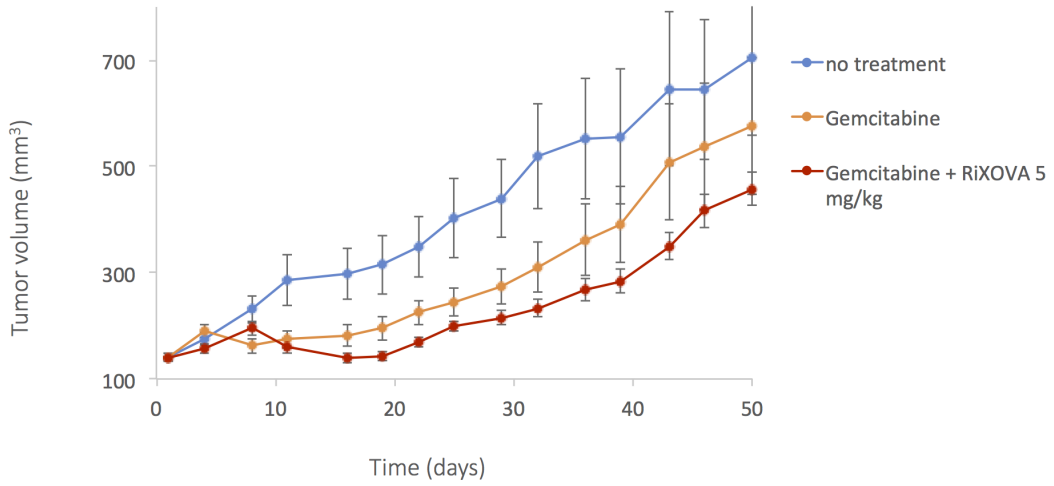

Figure 1.8: The effect of RiXOVA when combined with Gemcitabine, the effect of Gemcitabine alone and the effect of no treatment in an in vivo study of a Capan-2 human pancreatic tumor xenograf model. The different drug combinations were administered intravenously (unpublished data obtained by personal correspondence with Kurt I. Draget).

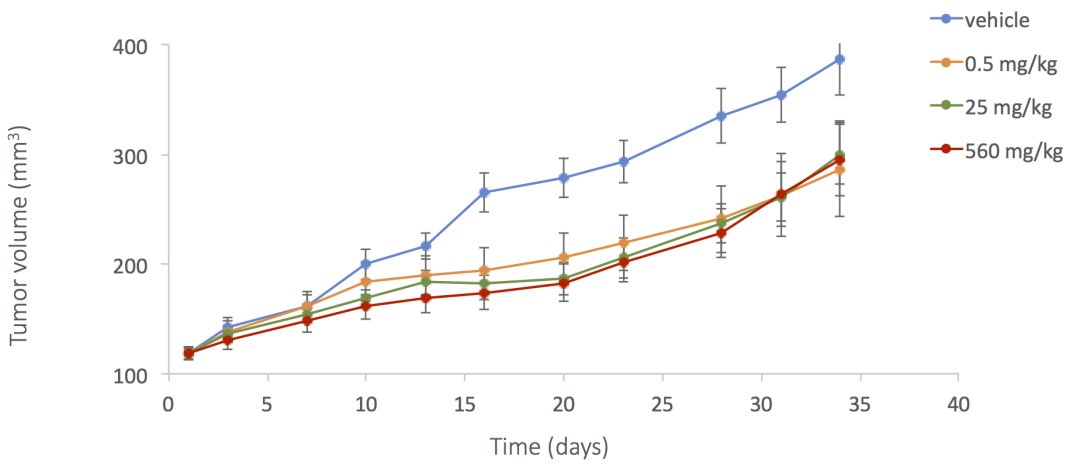

Figure 1.9: Effect of RiXOVA as a single agent in an in vivo study of a Capan-2 human pancreatic tumor xenograf model (unpublished data obtained by personal correspondence with Kurt I. Draget).

1.6 Immunohistochemistry

Immunohistochemistry (IHC) is a widely used diagnostic tool for the determination of the presence of cancer (Duraiyan et al. (2012)). The method was first described in 1958 by Coons (Coons (1958)). In some types of cancer specific antigens are up-regulated or down-regulated. Based on this, specific antibodies can be used to detect and later quantify the presence of specific antigens within a biopsy or tissue section. The principle governing IHC has been in existence since the 1930s but it was not until 1941 the first IHC study was reported. IHC involves specific antigen-antibody binding which can be said to be more precise than more traditional enzyme staining techniques. These can only identify a limited number of proteins, enzymes and tissue structures (Duraiyan et al. (2012)).

In order to perform IHC the tissue or biopsy must either be fixated and embedded in paraffin or fozen. The most common of the two is the paraffin embedded blocks (Renshaw (2007)). The tissue blocks have to be processed into thin slices (between 3-7 μm and then transferred onto glass slidese. Slices thinner than 3 μm would result in very weak immunostaining while slices thicker than 7 μm may lead to loss of tissue on the glass slide or hamper the analysis of the IHC staining result (de Matos et al. (2010)). The prepared slide then has to be dried at around 60 °C in order to increase adherence to the glass and remove any creases caused by the slicing of the sections of tissue (Renshaw (2007)).

1.6.1 Monoclonal- and polyclonal antibodies

Antibodies, or immunoglobulins (Ig) are glycoproteins secreted by specialized B lymphocytes known as plasma cells (Saper (2009)). The structure of the antibody resembles that of the alphabet letter Y. Within the Y shape there are two heavy chains and two light chains. These chains are held together by disulfide and non-covalent bonds. In mammals there are five types of Ig: IgA,IgD, IgE, IgM, IgG (Lipman et al. (2005), Onley (2007)). The majority of antibodies used in research are IgG and IgM (Onley (2007)). The ability of an antibody to bind to an antigen is determined by how well the epitope of an antigen and a paratope on an antibody match. Further, an antibody can also serve as an antigen causing it to attach to a secondary antibody, this is often utilized in IHC to for instance amplify the staining results (Taylor et al. (2006)).

Monoclonal antibodies are produced from a single B lymphocyte clone and because of this the monoclonal antibodies represent a homologous group of antibodies that can bind with high affinity and specificity to one single epitope (Saper (2009)). The specificity of an antibody means its ability to recognize a specific epitope among many epitopes. An antibody which has a high specificity will then have a lower chance of cross-reactivity with other epitopes. The affinity of an antibody for its intended epitope is a measure of binding strength given by the affinity constant K_A. The affinity constant describes the amount of antigen-antibody complex forming at equilibrium (Lipman et al. (2005)).

Polyclonal antibodies are produced from a large number of B lymphocyte clones and this mixture is referred to as polyclonal serum. Polyclonal antibodies are a heterogeneous group and the mixture thus have the ability to bind to several different epitopes, this means that they are less likely to be affected by conformational changes on the targeted molecule. These changes can be caused by pH, temperature and fixation (R&D Systems (2014)). As the polyclonal serum contains a mix of antibodies it is not feasable to determine the affinity constant because the different antibodes within the serum have different affinities. This mix of antibodies can cause the polyclonal serum to give undesired background noise or display cross-reactivity with epitopes/binding sites on other types of proteins (Onley (2007)).

1.6.2 Use of controls

In order to ensure that the final staining achieved is true, it is normal and highly recommended to include certain controls in an IHC experiment. Below is a short overview of the three most important ones.

1.6.2.1 Isotype control

Using an isotype control is most common when working with monoclonal antibodies (R&D Systems (2014)). This type of staining is done to ensure that the specific staining was not caused by non-specific interactions between the antibody and cells/ cellular components(R&D Systems (2014), Taylor et al. (2006)). By using a nonimmune immunoglobulin derived from the same species and at the same dilution as the intended antibody a weak non-specific staining can be

expected (Taylor et al. (2006)). This background staining pattern should therefor be negligible and not resemble the staining pattern produced by the primary antibody when coupled with the secondary antibody (R&D Systems (2014)).

1.6.2.2 Positive control

Tissue samples that are known to express the epitope of interest is important to include in the experiment as these can serve as a guide for the optimization part of an experiment. They also confirm that the primary antibody does in fact bind to what it is expected to bind to (R&D Systems (2014)). It is also important to note that the staining should not appear uniform in the tissue used as a positive control. This is because normal functional tissue express antigens in different proportions based on what part of the tissue is used when performing IHC (Taylor et al. (2006)).

1.6.2.3 Negative control

A negative control is when the tissue slide is incubated without the primary antibody, only the antibody diluent. This is a control that is always necessary in order to prove that the staining with the detection reagent is negligible or that the detection reagent pattern does not resemble the specific staining pattern produced by the antibody (R&D Systems (2014)).

1.6.3 Diaminobenzidine (DAB+) and counterstaining

By using a reporter label the visualization of an antibody bound to an area of interest can be achieved. The label is usually either an enzymatic or fluorescent label and it can be bound directly to the primary antibody (the antibody of interest) or to a secondary antibody, a tertiary antibody or so on in a suitable amplification system Mardle (2007)).

In order to do this visualization tissue sections are incubated with secondary antibodies following the incubation of the tissue with the primary antibody. The secondary antibody, now bound to the primary antibody, was initially conjugated with an enzyme. A popular enzyme-conjugate is horseradish peroxidase (HRP) and this enzyme, still attached to secondary antibody, is exposed

in excess to a chromogen to which it binds to and this causes the bound chromogen to convert into a stable precipitate of a specific color (Figure 1.10). If 3,3'-diaminobenzidine tetrahydrochloride (DAB+) is used the resulting color of the precipitate will be in brown hues. The amount of time it takes for the color signal to appear is dependent upon the amount of target protein or whether or not an amplification system has been used (Mardle (2007)).

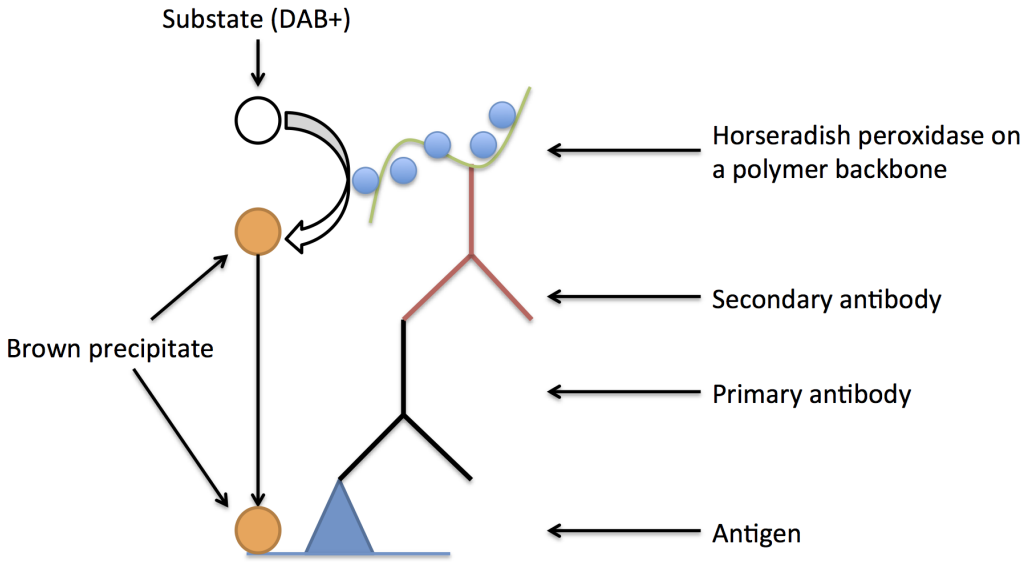

Figure 1.10: Linking of a primary antibody to a secondary antibody causes the formation of a brown percipitate when the conjugated enzyme (horseradish peroxidase) on the secondary antibody is exposed to a chromogen (substrate).

To get an optimal contrast between the stained developed by DAB+ and surrounding tissue, counterstaining is employed. The counter stain hematoxylin will tint a variety of structures in the tissue but most importantly it will stain the nuclei of cells blue (Renshaw (2007)).

1.7 Rheology

Rheology aims to understand and quantify the flow and deformation of materials. Depending on the time scale of observation all real materials will behave as solids at short enough time scales or as liquids at a long enough time scales. A true solid material will deform elastically and return to its original state regardsless of time scale (a Hookean response). A true liquid will flow no matter what time scale it is subjected to (a Newtonian response) (Picout and Ross-Murphy (2003), Zhong and Daubert (2013)). A rubber ball will deform as a response to applied force but upon removal of force the ball will return to its original state. The energy of the deformation was stored in the ball and used to reform it into a spherical shape again (Smidsrød and Moe (2008)).

This in turn leads to the term of viscoelastic materials. Most materials exhibit viscoelastic behaviours when observed at specific time scales. The material will exhibit both the capacity to store and recover as well as loose energy as a response to applied energy (Zhong and Daubert (2013)). The elastic properties of the material characterizes the ability of the material to store the applied energy (e.g force) whilst the viscous properties are related to the loss of applied energy in the form of heat. Silly putty (Figure 1.11) is a material that will flow to fill a container (viscous behavior). If the silly putty is thrown it will ideally bounce back like the abovementioned rubber ball (elastic response) (Smidsrød and Moe (2008)). As such silly putty has viscous properties at long enough time scales and elastic properties at short enough time scales.

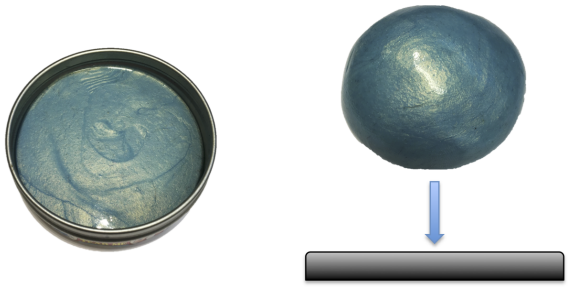

Figure 1.11: Viscous and elastic behavior of silly putty. It will flow to fill a container and when shaped to a sphere and thrown it will bounce back.

To illustrate the importance of time scale in relation to rheology consider a passage in the Bible, ”The Song of Deborah and Barak”. In the 5th verse the following is written:

The mountains melted before the LORD,

even that Sinai from before the LORD God of Israel

(Book of Judges 5.5, King James Bible).

This means that when viewing mountains in the time scale of God (which can be said to be infinite) even the mountains will flow. It is also worth noting that the woman named Deborah in this song gave rise to the dimentionless number dubbed Deborah number used in rheology (Reiner (1964)).

$$D = \frac{time\ of\ relaxation}{time\ of\ observation} \tag{1.1}$$

The Deborah number shows the importance of time scale with regards to deformation. A high Deborah number (D>>1) indicates that the material behaves as a solid-like material. A low Deborah number (D<<1) indicates that the material displays fluid like behavior (Reiner (1964)). Materials with values that fall around 1 will displays viscoelastic behavior. By using silly putty as an example again it will have a high Deborah number at high frequencies or short time scales (elastic response) and a low Deborah number at low frequencies or long time scales (viscous response) (Smidsrød and Moe (2008)). The importance of keeping in mind that the quantitative characterization given to a material, whether it be a solid, viscoelastic or viscous material, is only valid within the time scale given by the time scale of the measurement can not be stressed enough (Smidsrød and Moe (2008), Picout and Ross-Murphy (2003)).

1.7.1 Rheometer

A rheometer (Figure 1.12) is used to characterize the rheology of materials by determining their response to applied deformation or force. Usually such a rheometer can provide data measured by rotation in one direction or by oscillation (Kavanagh and Ross-Murphy (1998)). The majority of modern rheometers are of the stress controlled type but there also exists strain controlled rheometers. A stress controlled rheometer applies a force where as strain controlled applies deformation. If stress is applied by the rheometer a resulting strain response will be measured and if a strain is applied the resulting stress will be measured (Djabourov et al. (2013c)).

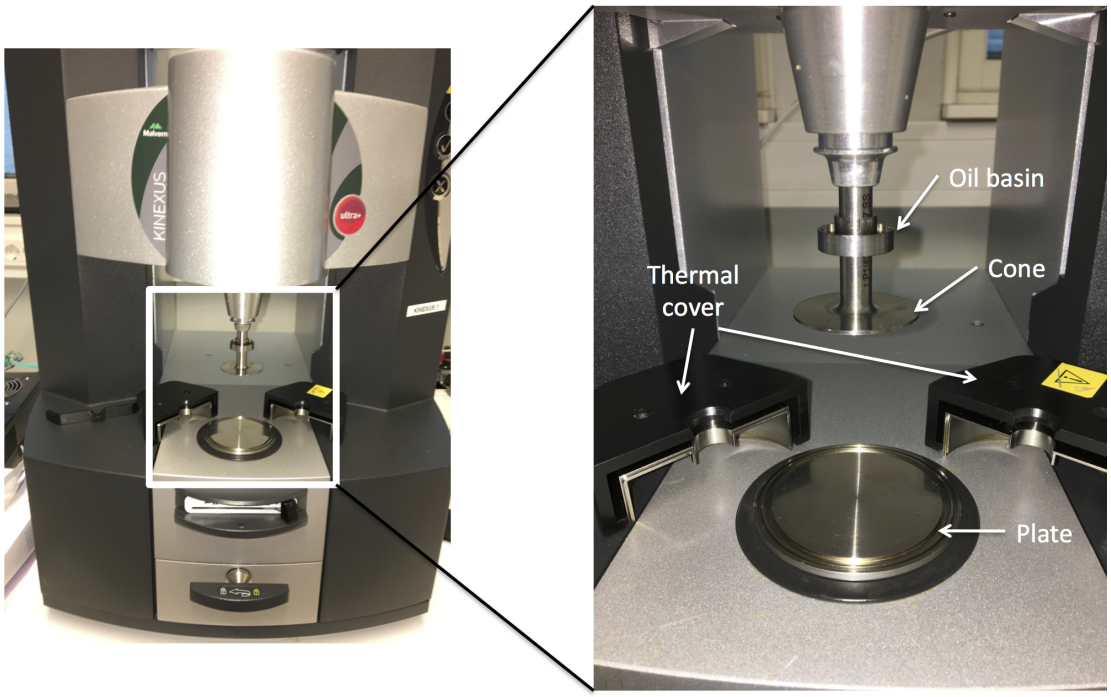

Figure 1.12: The rheometer and components related to the instrument. The cone and the plate together forms the geometry and the oil basin and the thermal covers together form the solvent trap. The sample is placed on the plate and the lowering of the cone onto the sample on the plate is controlled by a computer.

The geometry where the oscillation or rotation takes place consists of two parts. The plate forms the lower element and the cone forms the upper element of the functional unit of the rheometer. The point of the cone is truncated and the gap between the cone and plate is fixed at a specific height so that the two elements do not have contact (Figure 1.13). The cone in the cone and plate geometry uses a numbering system that gives information about the cone angle and the diameter of the cone. For example- a cone labeled 1/25 has a cone angle of 1° and a diameter of 25 mm (Figure 1.13) (Mezger (2014)).

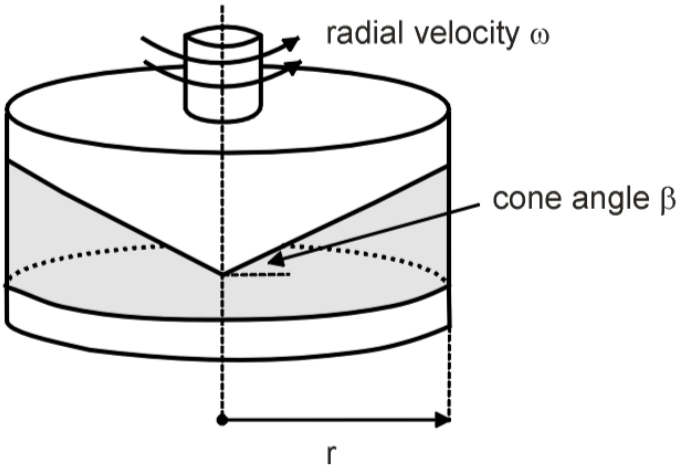

Figure 1.13: Schematic overview of a cone and plate geometry. Obtained from Picout and Ross-Murphy (2003)

The deformation rate (shear stress and shear rate) for a cone and plate geometry is constant within the gap leading to uniform and constant conditions regardless of distance r to the middle of the plate (Figure 1.13) (Zhong and Daubert (2013), Mezger (2014)). With a concentric cylinder geometry or plate-plate geometry the shear rate will vary across the gap, the highest shear rate will occur at the walls for a concentric cylinder or at the edges for a plate-plate geometry (Ross-Murphy (1984), Kavanagh and Ross-Murphy (1998)). The cone and plate geometry is therefor a preferred configuration due to the constant deformation rate achieved. However, if the sample is a very low viscosity fluid or is volatile a concentric cylinder might be a better option as the sample cannot flow out of the chamber surrounding the cylinder (Ross-Murphy (1984)).

1.7.2 Rheological concepts

1.7.2.1 Stress and strain

To measure rheological properties of a material the material is subjected to a rotational force (torque) over an area, this is referred to as stress (τ), and it is here defined as force (F) per unit area (A). By subjecting a material to stress the amount of deformation or induced strain can be measured and this is referred to as shear strain (Figure 1.14). The unit of stress is Pascal (Pa) (Picout and Ross-Murphy (2003), Mezger (2014)).

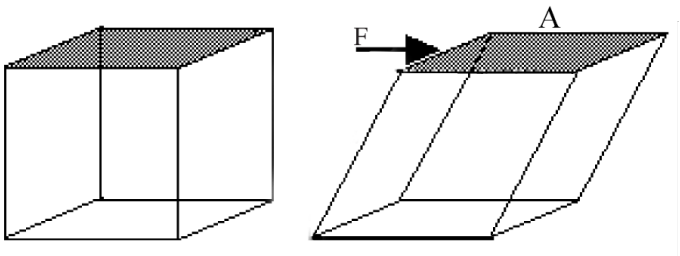

Figure 1.14: Shear deformation of a material by applying force (F) over an area (grey color). Adapted from Goodwin and Hughes (2008)

Stress for an elastic solid is $\tau = \gamma$G and for a viscous fluid it is $\tau = \dot{\gamma}\ \eta$. For a viscoelastic material τ depends upon both the shear strain (γ), the shear strain rate ($\dot{\gamma}$) and also time, as will be explained below. G is the elastic modulus and η is viscosity (Picout and Ross-Murphy (2003), Zhong and Daubert (2013)).

Shear strain (γ) is the resulting change in deformation in a solid sample from an applied stress and is a dimentionless unit (Ross-Murphy (1984)).

Shear strain rate ($\dot{\gamma}$) is the rate of change of deformation of a liquid sample with respect to time (Ross-Murphy (1984)).

In terms of liquid behavior the sample is dependent upon the rate of change of deformation and elastic beehavior is dependent upon the amount of deformation. Because of this, as a viscoelastic material has both elastic and viscous propoerties, the shear stress is a function of both strain, rate of strain and time (Ross-Murphy (1984)).

1.7.2.2 Viscous, elastic and viscoelastic behavior

To describe viscoelastic materials elastic modulus (G') and viscous modulus (G") are important terms (Weitz et al. (2007)) where the unit of G' and G" is given in pascal (Pa) (Smidsrød and Moe (2008)). The elastic modulus (G') is a measure of the elastic properties of a material, high values of G' indicates a more solid-like behavior of the material. The viscous modulus (G") is a measure of the viscous properties of a material, high values of G" indicates more a liquid like response of the material. Complex modulus (G*) is the ratio of stress to strain or strain to stress under oscillatory conditions and it also defines G' and G" (Picout and Ross-Murphy (2003))

(Figure 1.15). By knowing two of the three G values the third can be calculated (Equation 1.2).

$$G^* = (G'^2 + G''^2)^{1/2} \tag{1.2}$$

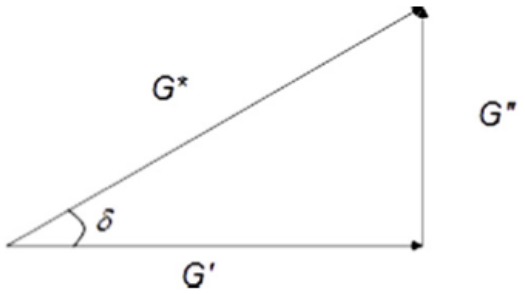

Figure 1.15: The relationship between the elastic modulus (G'), the viscous modulus (G"), the complex modulus (G*) and the phase angle (δ). Obtained from Zhong and Daubert (2013)

If a sinusoidal strain or stress is applied to a material the resulting stress or strain response can be measured (Yan and Pochan (2010), Weitz et al. (2007)). Materials will respond differently to this sinusoidal strain or stress. Ideal elastics respond instantly- meaning there is no lag between input and response resulting in a phase angle (δ) = 0 ° (Figure 1.16, elstic solid). Ideal fluids will be 90 ° out of phase from the input giving ideal fluids a δ= 90 ° (Figure 1.16, viscous fluid) (Kavanagh and Ross-Murphy (1998)). This can in turn be linked to the G' and G" moduli where an alternate name for elastic modulus (G') is in-phase modulus and viscous modulus (G") is called the out of phase modulus.

When viewing sinosodial curves for elastic solids there will be no lag between applied strain or stress and resulting stress or strain, and when viewing the cuve for viscous fluids the response will be 90° out of phase relative to the applied deformation (Figure 1.16). The phase angle (δ) gives a relation between the elastic and viscious responses within the material, or to put it differently: it is the energy lost per cycle (G") divided by the energy stored per cycle (G'). The δ should always be a value between 0° and 90° (Zhong and Daubert (2013)). All real materials (viscoelastic materials included) will give a response that lies between the elastic and viscous response as it will contain a combination of both elastic and viscous properties (Figure 1.16, viscoleastic material) (Weitz et al. (2007)), as such the response will be somewhere between 0 and 90°.

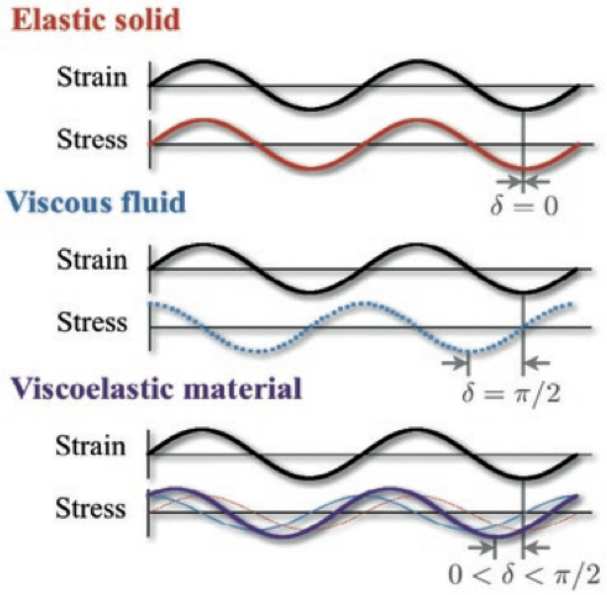

Figure 1.16: The relationship between an applied oscillatory strain and the resultant stress for an elastic solid, a viscous fluid and a viscoelastic material. Obtained from Weitz et al. (2007)

As a more general rule of thumb: if δ>45° (G" >G') the response is generally viscous. If δ<45° (G' >G") the response is generally elastic. When $\delta = 45°$ this indicates transition between the two states. The δ value indicates the properties of the material in the time scale of observation (Smidsrød and Moe (2008)).

1.7.3 Biopolymers as gels

Biopolymers (e.g proteins, nucleic acids and polysaccharides) are often found as liquids in solutions or as soft solids in the shape of gels (Picout and Ross-Murphy (2003)). Smidsrød and Moe (2008) defines a gel as *"a continuous network of molecules with a large amount of solvent molecules (e.g water) trapped inside the network. The network is held together by linkages, with a lifetime exceeding the time of observation. The macroscopic gel behaves as one single substance or phase, consisting of two or more components, polymer and solvent."* To put it differently: the polymeric components of a material like a gel interact to form a network and within the material there is a large amount of solvent.

In order for a gel to form the concentration of the polymer must be above a critical concentration. If the concentration is not high enough there will not be enough polymers to form cross-links within the solvent and the the system will be a dilute solution (Ross-Murphy (1984)).

Polymer networks can be divided into three categories: chemically cross-linked materials, entanglement networks (concentrated solutions) and physical networks (Djabourov et al. (2013a)). Concentrated solutions form entanglement points where the polymer strands cross and loop around each other (MacKintosh et al. (1995)). Covalently cross-linked networks are formed by chemical bonds. Physical gels can be formed from both biological and synthetic polymers (Ross-Murphy (1995)). For biopolymer gels non-covalent cross-links (physical) are formed by e.g hydrogen bonding, hydrophobic interactions or ioninc complexes (Djabourov et al. (2013a)). The biopolymer alginate forms a gel when the G-block content is high enough and the polymer is exposed to divalent cations (ionic complexes) in an aqueous solution (see Chapter 1.4).

Within the category of physical gels there is also a distinction between what is referred to as strong and week gels. Strong gels appear as solids even at large deformations where as weak gels flow like liquids at large deformations (Kavanagh and Ross-Murphy (1998), Ross-Murphy (1995)). Further, if the deformation is large enough a strong gel will rupture, break or fail and they will not heal unless they can be melted and reset, a weak gel will in constrast flow and if the weak gel is given enough time it will recover (Ross-Murphy (1995), Ross-Murphy (1984)).

Kavanagh and Ross-Murphy (1998) defines gelation as: *"that process (or series of processes) which leads to the formation of a gel"*. Polymers must interact with either other parts of the polymer chain or other polymers for this to occur. By interacting with other parts of the same polymer molecule intramolecular cycles (or rings) arise. Interacting with other polymers, an intermolecular reaction, causes the formation of branched chains. Each time an intermolecular reaction takes place the molecular mass (molecular weight) (M_w) increases. With time M_w will increase quicker and quicker as a consequence of an increase in future interaction between polymers until it eventually becomes "infinite" and this is the gel point. When M_w reaches infinite the longest relaxation time is also infinite and the sample will no longer flow like a polymer solution, it will be a gel. This means that given that intermolecular bonds are favored over intramolecular bonds the cross-linking of chains will lead to gelation for chemical gels (Kavanagh and Ross-Murphy (1998)).

1.7.4 Strain sweep

Many semi-solid materials are viscoelastic and their properties cannot solely be characterized by viscosity measurements (e.g. capillary viscometry). In order to understand viscoelastic materials two types of strain responses are investigated. Linear strain (low strain) is when the samples response is proportional to applied strain . Non-linear strain (high, fracture) is the region where the sample shows a strain dependence by a decrease in modulus (either G', G" or G*). In tests where low strain is applied data can be obtained without destroying or distorting the microstructure of the material. This non destructive region is called the linear viscoelastic regime (or region) (LVR) (Zhong and Daubert (2013)). The LVR is the region in which the material, with its moduli G', G" and G* as well as δ are independent upon shear strain (Yan and Pochan (2010)). The absolute value of the LVR limit can be as high as 25% or as low as 0.01% for a gel system (Djabourov et al. (2013c)). By exceeding the upper limit of the non-destructive deformation range information regarding breakdown of material can be obtained (Figure 1.17). The material is usually subjected to a strain or stress sweep by shearing the material at a fixed frequency (Zhong and Daubert (2013)).

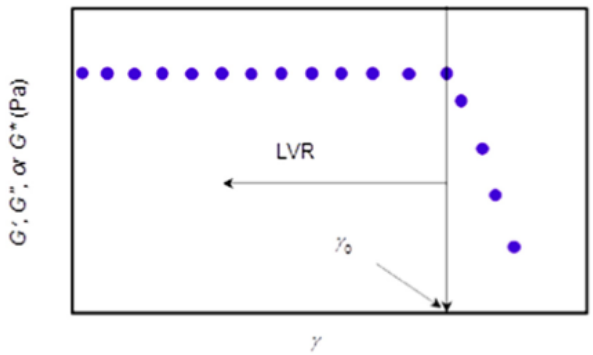

Figure 1.17: Example of a strain sweep (large strain span) that is performed in order to determine the limit of the linenar viscoelastic regime (LVR) of a material. γ is the applied strain. The moduli show strain dependence at larger strains, leading to the non-linear regime. Obtained from Zhong and Daubert (2013).

1.7.5 Frequency sweep

Frequency sweeps yields the mechanical spectra of a given material by oscillating said material within a wide frequency range at a fixed strain or stress that falls within (a pre-established) LVR (Zhong and Daubert (2013)). The reciprocal time it takes to complete one cycle of a sinusoidal

curve is called the frequency of oscillation (the time spent going from point A to B and back to A). Different materials will respond in different manners to a frequency sweep. Covalently cross linked networks will display a G'>G" relationship that is parallel and largely frequency insensitive at small deformation (Figure 1.18 b) (Kavanagh and Ross-Murphy (1998)). Dilute solutions will display a G" >G' relationship (Zhong and Daubert (2013)). Entangled networks will in contrast show a frequency dependence. At high frequencies G'>G" can be observed and if the frequency is reduced a cross-over can be observed between G' and G" in which the relationship changes to G">G'. At very low frequencies these entanglement solutions will flow as high viscosity liquids (Figure 1.18 a) (Kavanagh and Ross-Murphy (1998)). In addition to the behavior exhibited by covalently cross linked netwoeks, dilute soultions and entangled networks, there is the behavior of physical gels. Physical gels show a strong frequency dependence, meaning an increase in G' and G" as a function of increased frequency, but no cross-over as seen for the entagled networks (Stading and Hermansson (1990)).

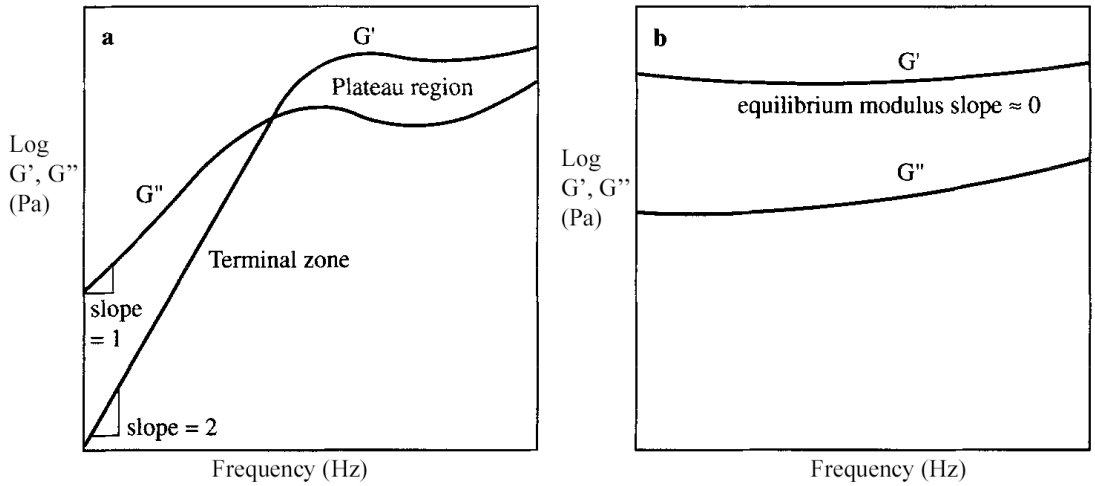

Figure 1.18: Example of frequency sweep results for an entangled network (pseudogel) (a) and a covalently cross linked network (b). Note that if the frequency range is not wide enough a crossover and plateau region for (a) will not be seen and if the gel is a strong gel it will maintain the G'<G" without any crossover even at large deformations. An example of a typical frequency sweep could be 0.01-100 Hz. Adapted from Kavanagh and Ross-Murphy (1998).

1.8 Aim of the thesis

The overall aim of the project in which this thesis is a part of is to investigate whether G-block technology can change the ECM of neoplastic tissue and possibly aid in better drug delivery.

The laboratory work planned for this thesis will be divided into two distinct parts. The first part involves a histological evaluation of a pancreatic tumor model where some of the mice have received certain doses of G-block and others have gotten saline as a control. Here the aim is to optimize protocols for immunohistochemical staining of proteins associated with tumor proliferation and survival, both treated with G-block and controls, for three extracellular components (collagen IV, fibronectin and α-SMA). Further, it is of interest to see if it is possible to quantify the optimized staining and interpret the results to investigate if there are any differences between control and treated tumor tissue and also evaluate whether or not there is a dose response.

The second part of the thesis moves from the world of tissue and a macroscopic look at the tumor and its environment to a smaller system where the rheological properties of collagen gel with and without of G-block are evaluated. First it is of importance to establish a good protocol for making a collagen solution that results in a collagen gel and to optimize the rheological parameters. Second, it is also of relevance here to see if the addition of G-block has an effect on the collagen gel. In addition, it is explored if or what effect different doses of G-block has on the rheological properties of collagen gel.

Chapter 2

Materials and methods

2.1 Immunohistochemistry

2.1.1 Tumor info

The cell line used in this experiment was the Capan-2 cell line. It was xenografted subcutaneously into BALB/c mice. The treatment conditions are displayed below (Table 2.1). The mice with number 3-9 received 4 doses of G-block and the mice with number 11-16 received 10 doses of G-block dissolved in physiological saline. The controls received 4 doses (mouse 1 and 2) and 10 doses (mouse 9 and 10) of injected physiological saline. Xenografting and medical administration of drugs and injections to the mice were not done by the author. The final formalin fixated paraffin embedded blocks were obtained from Dr. Shalini Rao.

Table 2.1: Overview of the tumor sections and the treatment given to them. Group 1 (number 3-8) received 4 doses of G-block while group 2 (number 11-16) received 10 doses of G-block dissolved in physiological saline. The controls received 4 doses (1 and 2) or 10 doses (9 and 10) of physiological saline.

#	Name	Treatment	Dose strength
1	TD214+432 A	saline, 4 doses, control	
2	TD214+433 A	saline, 4 doses, control	
3	TD214+434 A	0.5 mg/kg, 4 doses	Low
4	TD214+435 A	0.5 mg/kg, 4 doses	Low
5	TD214+436 A	25 mg/kg, 4 doses	Medium
6	TD214+437 A	25 mg/kg, 4 doses	Medium
7	TD214+438 A	560 mg/kg, 4 doses	High
8	TD214+439 A	560 mg/kg, 4 doses	High
9	TD214+523	saline, 10 doses, control	
10	TD214+524	saline, 10 doses, control	
11	TD214+525	0.5 mg/kg, 10 doses	Low
12	TD214+526	0.5 mg/kg, 10 doses	Low
13	TD214+527	25 mg/kg, 10 doses	Medium
14	TD214+528	25 mg/kg, 10 doses	Medium
15	TD214+529	560 mg/kg, 10 doses	High
16	TD214+530	561 mg/kg, 10 doses	High

2.1.2 Antibodies

The antibodies used in this thesis were obtained from Dr. Shalini Rao and ordered from Millipore, Abcam and DAKO. They were allocated upon arrival into 2 ml Eppendorf tubes and frozen (Table 2.2).

Table 2.2: Overview of the antibodies used in the immunohistochemistry procedures and the expected locations of staining within tissue.

	Anti-Collagen IV	Anti-Fibronectin	Anti-α SMA (Abcam)	Anti-α SMA (DAKO)	IgG control
[mg/ml]	1	5	0,2	70	0,2
Manufactured by	Millipore	Abcam	Abcam	DAKO	Abcam
CAT-number	AB8201	AB2413	AB5694	M0851	AB27478
Mono-/polyclonal	Polyclonal	Polyclonal	Polyclonal	Monoclonal	Polyclonal
Localization	Basal lamina	Extracellular matrix	Smooth muscle cells	Smooth muscle cells	-

The secondary antibody used here was a part of the DAKO EnVision HRP Anti-Rabbit kit (K4011).

2.1.3 Protocol

The formalin fixated paraffin embedded tissue samples were incubated at 60°C for 30 minutes, then deprarafinated in NeoClear® (CAS 64741-65-7, Merck) 2 x 10 minutes. The re-hydration process consisted of a decreasing percentage of alcohol in water and was done in the following way- rinse 2 times in absolute alcohol, then once in 96 % alcohol, then once in 80 % alcohol, then once in 70 % alcohol and then once in distilled H_2O. After the rehydration the sections were placed in hydrogen peroxide (H_2O_2) for 10 minutes to block endogen peroxidase. In order to perform demasking the sections were placed in a container with either tris (pH 9) or citrate (pH 6) buffer in a microwave oven for 15 minutes. The sections were then left on the bench in the container to cool down to room temperature for 15 - 20 minutes. Then the sections were rinsed in rinsing buffer for 5 minutes before primary antibody was applied to the sections (Table 2.2 shows detailed info about the antibodies and Table 2.4 shows optimal conditions) and left to incubate. 70 μL of primary antibody in a buffer solution at appropriate dilution was applied (Table 2.4). The incubation was either done at 1 hour in room temperature or over night (12-14 hours) in the fridge at 4°C. After the incubation period the sections were washed in rinsing buffer three times at 5 minutes each, then the sections were incubated with the secondary antibody (2 drops on each section) (Dako Envision HRP Anti-Rabbit) for 30 minutes before being rinsed twice in rinsing buffer for 5 minutes per rinse. After the rinsing process 80 μL of DAB^+ solution (DAKO) was applied while constantly evaluating the color development under a microscope. The DAB^+ solution consisted of 10μL of DAB+ chromogen and 500μL of substrate buffer from kit: K4011. The time it took for an appropriate color intensity to appear was recorded by a timer and then used as a standard when performing the optimized protocol (Table 2.4 shows the optimized amount of seconds the DAB^+ was on for each antibody.). After the staining with DAB^+ counterstaining with hematoxylin was performed (15 sec) then the sections were rinsed in running luke-warm water for 5 minutes before being mounted with Glycergel Mounting Medium (C0563) and coverslip. For a detailed overview of the protocol the reader is referred to appendix B.1 and appendix B.3 for an example of a protocol setup with controls. Appendix B.2 shows how the rinsing buffer and antibody diluent utilized here were made.

2.1.4 Initial parameters

The set up for the initial parameters for collagen IV and fibronectin (Table 2.3) were based on experiments done by Bugge et al. (2016) supervised by Dr. Rao. This optimization was done in a mouse breast cancer model. An article by Bailey et al. (2008) served as a starting point for α-smooth muscle actin. In this article the CAPAN-2 cell line was xenografted orthotopically into athymic nude mice.

Table 2.3: Overview of the initial parameters applied to the tissue sections in the optimization process. The values were obtained from previous work done in the lab for collagen IV and fibronectin, while some of the α smooth muscle actin parameters were obtained from Bailey et al. (2008).

	Anti-Collagen IV	**Anti-Fibronectin**	**Anti-α smooth muscle actin (DAKO)**
Antigen retrieval buffer	Tris buffer pH 9	Tris buffer pH 9	Citrate buffer pH 6 and Tris buffer pH 9
Rinsing buffer	TBS	TBS	TBS
Dilution primary antigen	1:50 and 1:100	1:100	1:400
Incubation time	O.N	1 h RT	1 h RT
Secondary antibody	goat anti-rabbit	goat anti-rabbit	goat anti-rabbit
DAB+ (sec)	90 ± 5	55 ± 5	55 ± 5
Positive control	Colon (human)	Kidney (mouse)	Colon (human)

2.1.5 Optimized parameters

The optimized parameters (Table 2.4) were determined by a series of trials in which various dilutions, antigen retrieval buffers, DAB+ times, controls and incubation times were tested (Appendix B.2, B.3 and B.4 shows the parameters varied in the optimization process).

Table 2.4: Overview of the antibodies used in the immunohistochemistry procedures with the optimized rinsing buffer, dilution of primary antibody, incubation time, amount of time DAB $^+$ was left on the sample and what the positive control was.

	Anti-Collagen IV	**Anti-Fibronectin**	**Anti-α smooth muscle actin (Abcam)**
Antigen retrieval buffer	Tris buffer pH 9	Tris buffer pH 9	Citrate buffer pH 6
Rinsing buffer	TBS	TBS	TBS
Dilution primary antibody	1:150	1:50	1:75
Incubation time	O.N	1 h RT	1 h RT
Secondary antibody	goat anti-rabbit	goat anti-rabbit	goat anti-rabbit
DAB+ (sec)	90 ± 5	55 ± 5	55 ± 5
Positive control	Colon (human)	Kidney (mouse)	Duodenum (mouse)

2.1.6 Image analysis

2.1.6.1 Image acquisition and image acquisition guidelines

The images shown in the results and discussion part of the thesis were acquired with a Nikon Eclipse Ci microscope, a Nikon DS-Fi1 camera and and the software NIS-Elements. The images used in the thesis to showcase the H&E staining and two images in the results and discussion section for fibronectin (Figure 3.7 C and D) were taken on a Nikon Eclipse TS100 microscope with a Nikon DS-Fi1 camera coupled with the software NIS-Elements. The images used in the data analysis were acquired with the Nikon Eclipse TS100 microscope with a Nikon DS-Fi1 camera coupled with the software NIS-Elements. The images used for the data analysis were taken after the thesis images and as a consequence of this the color of the stains had faded considerably. In order to ensure that the colors were intense enough to be detected and separated by the ImmunoRatio application all the images were color adjusted in Adobe Photoshop CS6 (version 13.0 x64) with the build in auto-color function. For photographing the tissue sections used in the quantification analysis the following guidelines were utilized:

- Avoid areas of necrosis
- Avoid edges of tissue
- Find a good average representation of staining within the section.
- Try to include both lightly and intensely stained areas if they are both representative.
- If the area (lightly or intensely stained) lies close to/overlaps with areas of necrosis, try to avoid it.
- Try to avoid sections that have dried out.

Images of tissue sections that met the criteria listed above were included in the data analysis (Figure 2.1 left image). Images with for instance necrotic areas will be displayed in the result and discussion section but these images will not a part of the image analysis (Figure 2.1 right image). They will only serve to showcase differences in tumor tissue morphology.

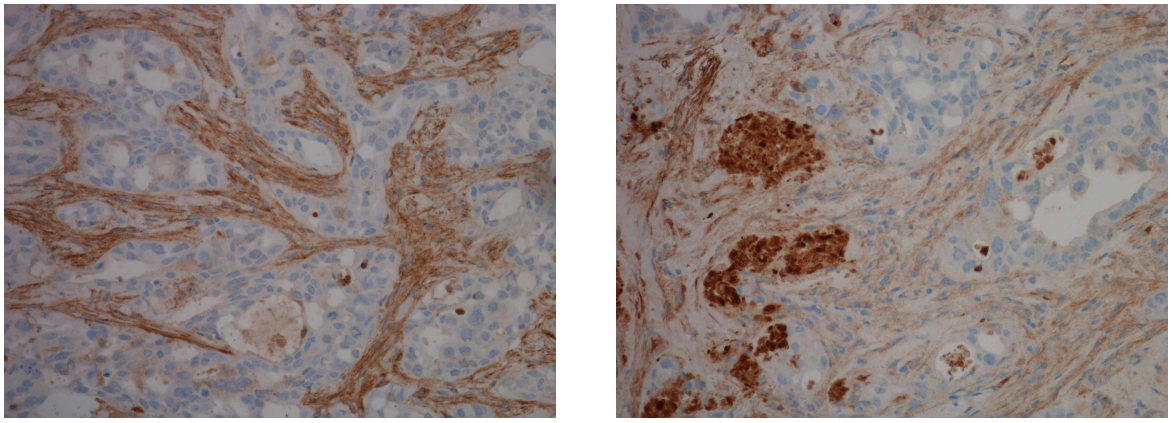

Figure 2.1: Image on the left meets the above mentioned criteria for image analysis as it is not taken close to the edge, it has not dried out and there is no necrotic tissue in the image. The image on the right does not meet the demands as there are clear regions of necrosis in this image (very darkly stained areas).

Before taking each photograph the white balance was adjusted by finding an empty area on the slide and selecting ”auto-white” in the menu within NIS-Elements.

2.1.6.2 ImmunoRatio

ImmunoRatio quantifies amount of DAB+ as a ratio of percentage DAB+ staining to nuclear staining (labeling index) by using an algorithm that separates the hematoxylin (blue) and the DAB+ (brown) (Figure 2.2) (Tuominen et al. (2010)). The result is displayed as two images where the top image is the original image and the bottom image is the analyzed image with the resulting DAB+ /nuclear area in percent displayed on top (Figure 2.3). In this quantification method there needs to be little to no DAB+ staining intracellularly. This is to enusre that the program is able to differentiate between nuclear staining and DAB+ staining.

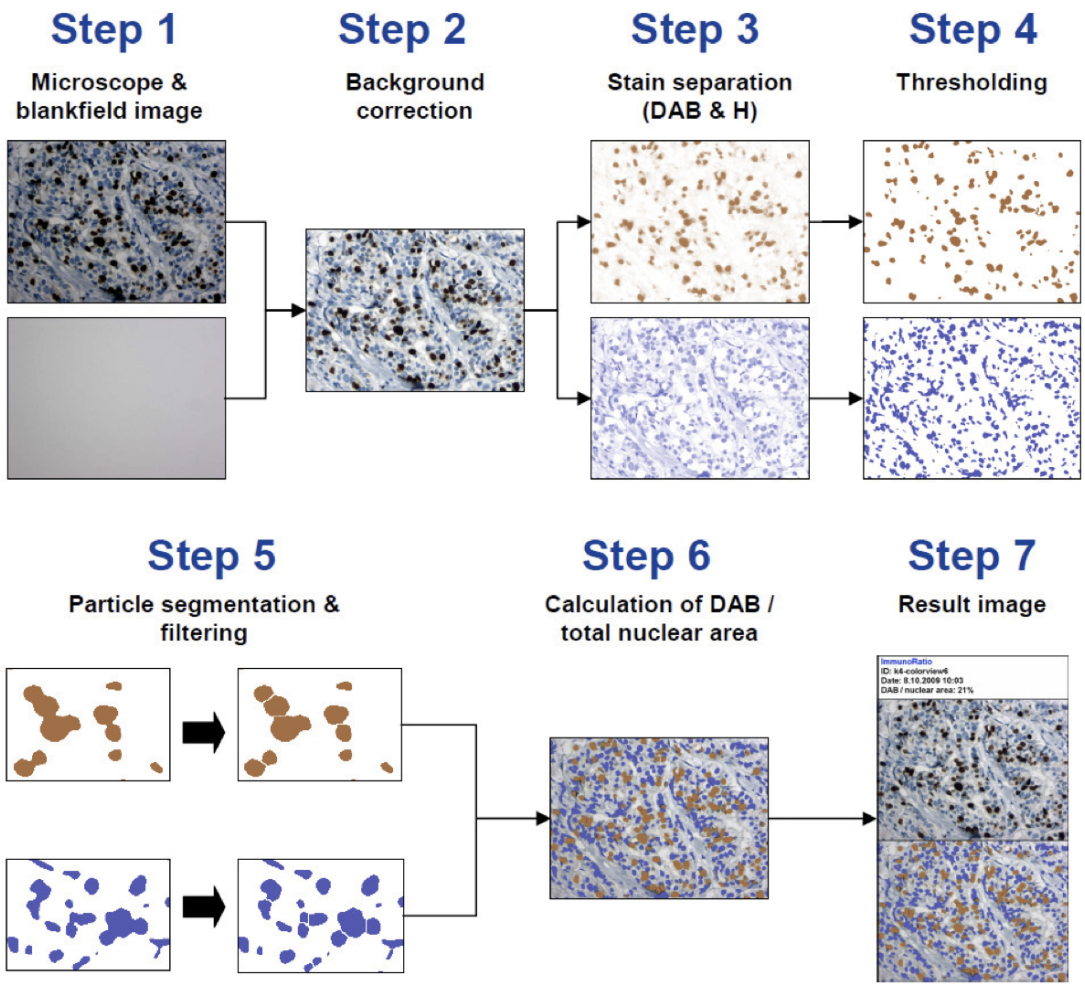

Figure 2.2: A flowchart that shows the ImmunoRatio analysis algorithm. Step 1) The image of interest is taken along with a blank-field image. The blankfield image is used to correct uneven lighting and color balance. Step 2) This results in a background corrected balanced image. Step 3) Separation of DAB and hematoxylin within the image. Step 4) Noise reduction witin the image by using adaptive IsoData thresholding. Step 5) Nucleus segmentation is performed on both of the separated images and small particles along with thin fibroblastic are discarded. Step 6) The DAB and hematoxylin images are overlaid on top of the original image and the percentage of DAB to total nuclear staining is calculated (labeling index). Step 7) The original image and the modified image are displayed with the labeling index. Obtained from Tuominen et al. (2010)

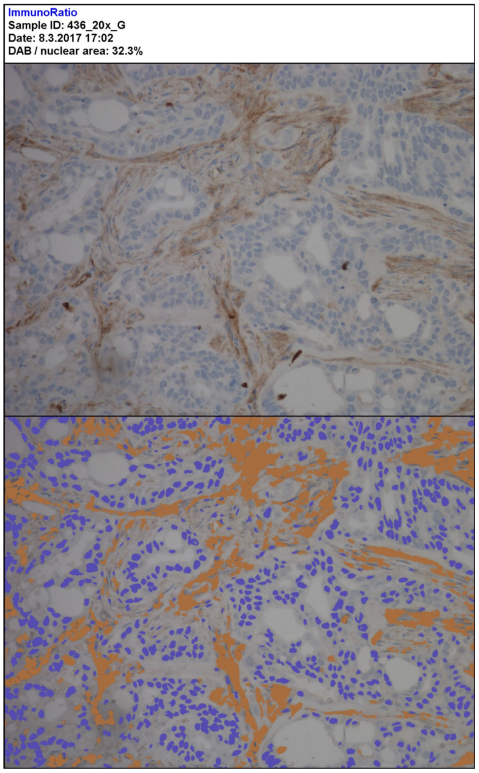

Figure 2.3: The resulting image and information obtained when using the ImmunoRatio web application on an image of a section stained for fibronectin. The DAB/ nuclear area percentage was used to compare different tissue sections. Obtained from Isola and Tuominen (2010)

2.1.6.3 Fiji/ImageJ

Fiji is an imaging processing package with a lot of plugins and as such is a modified version of ImageJ. ImageJ is a Java based software developed by the National Institutes of Health (Schindelin et al. (2012)). By separating an image into three channels (blue, brown/orange and green) (Figure 2.4) the intensity of the desired color channel can be measured. The blue image represents the hematoxylin stain of the image, the brown/orange image represents the brown color obtained from the DAB+ reaction and the green image is a so called 3rd component which is a complimentary image of the previous two. This image should ideally be white, if it is not this would imply that the color vectors applied by the program do not fit or that the image is not properly white balanced (Landini (2015)). After the image is color deconvoluted and the intensity determined (see below) the average DAB+ staining can be obtained and tissue sections can be compared.

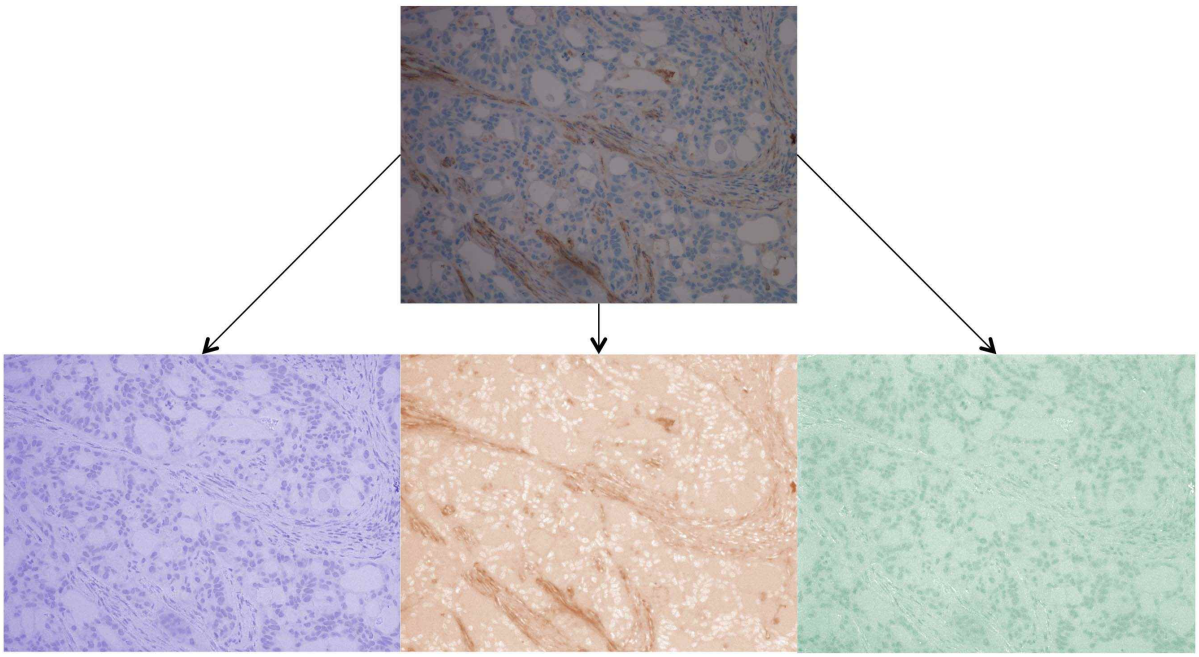

Figure 2.4: The process of color deconvolution in Fiji. Top image shown the source image which has been stained for fibronectin. Bottom left is the hematoxylin stain in the image, bottom middle is the DAB color in the image and the bottom left is the complimentary image.

Procedure for determining the intensity was obtained from (ResearchGate (2015)).

Run image - Color - Color deconvolution.

Choose H-DAB in the pull down menu. Then choose the image named "`Colour_2`".

Choose Run Analyze - Set Measurements and then check that "Mean gray value" and "Display label" are both on.

Then finally choose: Run Analyze - Measure. This will cause a new window to pop up which contains the measure of intensity (max, mean and min for each image analyzed). The intensity measurement must then be converted into optical density (Equation 2.1). This will quantify the average darkness of the image caused by the DAB staining.

$$OD = log \frac{max\ intensity}{mean\ intensity} \tag{2.1}$$

2.1.7 Statistical analysis

The results from ImmunoRatio were transferred to Microsoft Excel (version 14.4.8). The basic calculations of mean and standard deviation were performed in Excel. The graphs, t-tests, ANOVA and Tukeys HSD were done in RStudio (version 1.1.383). The t-test used was Welch Two Sample t-test and the significance level was set to $p<0.05$, it was used to check for differences between the control and G-block treated tumor tissue. The one way-analysis of variance was used to analyze differences between groups with regards to treatment response and the Tukey's post hoc test was used to determine where the differences between the groups were. The statistic analysis was performed on the ImmunoRatio results.

2.2 Rheology

All the rheological results obtained in this thesis were from a Kinexus Ultra + rheometer from Malvern, UK with a cone and plate geometry. The cone used in all of the experiments had a diameter of 40 mm, an angle of 1 degree. A solvent trap was used to prevent sample drying. The data was recorded on a computer using the program "rSpace". Before the experiments were run the instrument was automatically initialized and calibrated before the cone was lowered down onto the plate (gap = 0.000 mm) and both the plate and cone were chilled to 4°C and left to equilibriate for 15 minutes with a thermal cover on. After the equilibriation period the cone was elevated to its top stop point and the programmed sequence was initiated. 325 μl of sample was applied to the plate. Water (MilliQ water) was applied to the outer ring of the plate and oil (DowCorning 200/10cS fluid Silicone) was applied into the oil basin before the thermal cover was put back on. The programmed sequences used can be found in appendix C.2.1, C.2.2, C.2.3 C.2.4). For the main part of the thesis the collagen sequence I and II were used and they are describred below.

2.2.1 Temperature ramp and isothermal hold

After the initialization of the programmed sequence a temperature ramp was run. Here the temperature was increased from 4°C to 37°C with 1°C min^{-1} for the main programmed sequence- the collagen sequence (see appendix C.2.1). The strain was fixed at 0.1% and the frequency fixed at 1 Hz. When the temperature reached 37°C it was held there for five hours with the same fixed strain and frequency.

2.2.2 Frequency sweep

The frequency sweep was performed directly after the hold time of five hours. During the frequency sweep the strain was fixed at 0.1%, constant temperature of 37°C and the frequency was increased from 0.01 - 10 Hz.

2.2.3 Strain sweep

Immediately after the frequency sweep a strain sweep was preformed in the region of 0.01 - 100% to determine the viscoelastic region. The strain sweep was done with a fixed frequency at 1 Hz and constant temperature of 37°C.

2.2.4 Isothermal hold part II

For the samples with G-block added an additional temperature hold of 1 hour implemented with the same fixed temperature, strain and frequency (37°C, 0.1% and 1 Hz) as the 5 hour isothermal hold.

2.2.5 Preparation of reagents

2.2.5.1 DPBS, sodium bicarbonate, DPBS with G-block

The DPBS stock used is made from Hyclone DPBSx10 (Cat. No SH30378.02 from Thermo Scientific) and MilliQ water (measured conductance: 18.20 MΩcm), 1 part DPBSx10 and 9 parts MilliQ water. Sodium bicarbonate stock was made by weighing out 7.5 g of $NaHCO_3$ (from Merck) and added to 100 ml of MilliQ water. DPBS was made as described above and then in order to obtain a final concentration of G-block of 5 mg/ml, 9 mg of G-block was added to 1 ml of DPBS stock (Table 2.5 lists the different start and final concentrations). The final concentration is achieved when dissolved G-block is mixed with collagen and $NaHCO_3$. The G-block used had a DP_n of 13 and was prepared by Morten. J. Dille at NTNU, Trondheim. The stock for dissolved G-block was made one day in advance of the first parallel and was viable for one week.

Table 2.5: Concentrations of G-block used (start) to achieve a desired total G-block concentration within the final sample.

Start $[mg/ml]$	Final $[mg/ml]$
9	5
4.50	2.50
2.25	1.25
1.12	0.62

2.2.5.2 Collagen

2 ml of 0.1% acetic acid (HAc) was added to a vial of collagen from rat tail tendon (Cat. No. 11 179 179 001 from Roche, Appendix C.3). The vial contained 10 mg of collagen. The solution was then placed in a fridge (4°C) and allowed to swell for a minimum of 48 hours before being gently stirred.

2.2.5.3 Gelatin

2 g of gelatin powder (Gelita Bovine Gelatine, Batch: 631150, 150 Bloom, Appendix C.4) was added to 40 ml of MilliQ water on a hotplate set to 60°C and allowed to dissolve under constant stirring at 50 rpm.

2.2.6 Cool down procedure

In order to minimize the collagen samples exposure to heat all reagents and containers were kept in a fridge at about 4°C. A metal plate was placed in a freezer (-40°C) for a minimum of 24 hours before the experiment took place. The pipettes were cooled down in a fridge for approximately 20 minutes prior to use. The rheometer was initialized, an instrument check and a zero gap procedure was performed before the cone was lowered down onto the plate with a gap of 0.0 mm. The plate and cone with a solvent trap was cooled down to 4°C. The temperature was held for 15 minutes to ensure that the geometry was properly cooled down. A cold glass beaker was placed in a larger beaker filled with ice on top of a frozen metal plate placed on a scale and collagen was pipetted into the beaker by reverse pipetting. The amount of collagen pipetted

into the beaker was determined by the scale. The desired weight of acid dissolved collagen was 0.40 g ($\pm$ 0.02 g). The beaker was transferred to an ice filled container and here the rest of the reagents were added. Before the remaining reagents were added the cone was elevated to its top stop. 555 μl of DPBS stock and 47 μl $NaHCO_3$ or 555 μl of DPBS with added G-block (various concentrations) and 47 μl $NaHCO_3$ was added. The final solution was then applied to the rheometer (325 μl) and the cone was lowered as per instructed by the programmed sequences (Appendix C.2.1, C.2.2, C.2.3 C.2.4).

2.2.7 Statistical analysis

The basic calculations along with the graphs were made in Excel. The box and whiskers plot, t-tests, ANOVA and Tukeys HSD were done in RStudio (version 1.1.383). The t-test used was Welch Two Sample t-test and the significance level was set to $p<0.05$, it was used to check for differences between the collagen gel with and without G-block added. The one way-analysis of variance (ANOVA) was used to analyze differences between groups with regards to treatment response and the Tukey's post hoc test was used to determine where the differences between the groups were.

Chapter 3

Results and discussion

3.1 Immunohistochemistry

The expert pathological evaluation of the immunohistochemical staining as well as the H&E staining was kindly provided by dr. Patricia Mjønes at the department of cancer research and molecular medicine at Gastrosenteret at St. Olavs Hospital. She evaluated the tissue sections, the staining patterns and staining color. She concluded that the cancer cells were little to moderately differentiated and that the staining obtained in the fibronectin and SMA slides were true (i.e not false positive). The staining seen in the collagen IV slides was confirmed by her to be artefacts as staining was observed inside cell nuclei.

Dr. Mjønes did her initial evaluations without knowing which of the slides had received treatment or were controls. The information written on the slides were the 43x and 52x numbers (Table 3.1), what antibody was used, the time the DAB+ was on and the date of the experiment. She had no access to what treatment the 43x and 52x numbers corresponded to. Further, she did not know in advance what had been discussed between Dr. Rao and the author of this thesis with regards to the staining. All the information she got in advance was the antibodies used and their datasheets. This was all done to minimize potential interpretation bias. In the initial observations she was free to pick slides from the plate presented to her with all the slides for the relevant antibody. After her initial comments and remarks about the staining and tissue morphology she was then handed two controls and 2-3 treated tissue sections for a comparison of these. In this part of the evaluation she was informed whether it was a control or treated slide she received. This was done

to see if she could see any differences between the treated and control slides that could possibly be a consequence of the G-block treatment.

Table 3.1: Overview of the tumor sections and the treatment given to them. Group 1 (number 3-8) received 4 doses of G-block while group 2 (number 11-16) received 10 doses of G-block dissolved in physiological saline. The controls received 4 doses (1 and 2) or 10 doses (9 and 10) of physiological saline.

#	**Name**	**Treatment**	**Dose strength**
1	432	saline, 4 doses, control	
2	433	saline, 4 doses, control	
3	434	0.5 mg/kg, 4 doses	Low
4	435	0.5 mg/kg, 4 doses	Low
5	436	25 mg/kg, 4 doses	Medium
6	437	25 mg/kg, 4 doses	Medium
7	438	560 mg/kg, 4 doses	High
8	439	560 mg/kg, 4 doses	High
9	523	saline, 10 doses, control	
10	524	saline, 10 doses, control	
11	525	0.5 mg/kg, 10 doses	Low
12	526	0.5 mg/kg, 10 doses	Low
13	527	25 mg/kg, 10 doses	Medium
14	528	25 mg/kg, 10 doses	Medium
15	529	560 mg/kg, 10 doses	High
16	530	561 mg/kg, 10 doses	High

3.1.1 General challenges with immunohistochemistry

IHC is a staining procedure where thin sections of tissue are stained through various steps involving heat, rehydration, and rinsing- to name a few. Interpreting IHC results is generally qualitative and subjective (de Matos et al. (2010)). Even though it is a relatively simple procedure it is at the same time a tricky procedure where the outcome can depend on a variety of factors. If for instance the tissue section on a slide does not stain for the given antibody it is not necessarily the case that the protein or marker of interest is absent, it can be that the tissue section on the slide is too old, that there was a conformational change in the epitope of an antigen caused by the process of either fixation, embedding or the IHC steps. Further it could be caused by tissue dehydration during incubation in which the tissue is exposed to air over a period of time. The latter was a big problem here even though great care was taken to minimize the chances of the tissue drying out when incubating over night.

The skill of the person performing the reactions and the eyes that interpret the resulting stain are also worth noting (de Matos et al. (2010)). Here, the final interpretation of the stains produced by the three antibodies was done by a skilled pathologist, Dr. Mjønes. During the optimization the decisions about appropriate antibody dilution, pH and DAB+ reaction time were made by the author and Dr. Rao. Dr. Rao was also well versed with IHC and as such served as a good mentor for the author, allowing for a very quick and steep learning curve in interpreting the resulting stains. With regards to the final evaluation done by Dr. Mjønes she was as previously mentioned not informed in advance whether she looked at a control or treated slide in the first round of evaluation. This was done to hopefully reduce the chance of interpretation bias.

3.1.2 H&E staining

The H&E stainings were obtained from dr. Shalini Rao at the department of cancer research and molecular medicine at St. Olavs Hospital. H&E stains allow for a clear visualisation of the tissue morphology when viewed by a skilled pathologist. Here the H&E stain is used to identify stroma cells, tumor cells and desmplastic tissue. The more pink stain in the images (Figure 3.1) shows the desmoplastic tissue, the small blue dots are tumor cells and the enlarged blue dots are stroma cells. The bigger open empty areas are thought to possibly be gland like structures created by the cancer and the smaller open areas could possibly be fat. An intensely pink stained area can be observed in one of the images below (Figure 3.1 D, arrow), this might, according to Dr. Mjønes, be an example of smooth muscle. As the tumor tissue here was cultured from a cancer strain and xenografted subcutaneously into immunosuppressed mice it is expected that there are no normal pancreatic cells or cell structures like Islets of Langerhans, nerves and the like present in the tumor model.

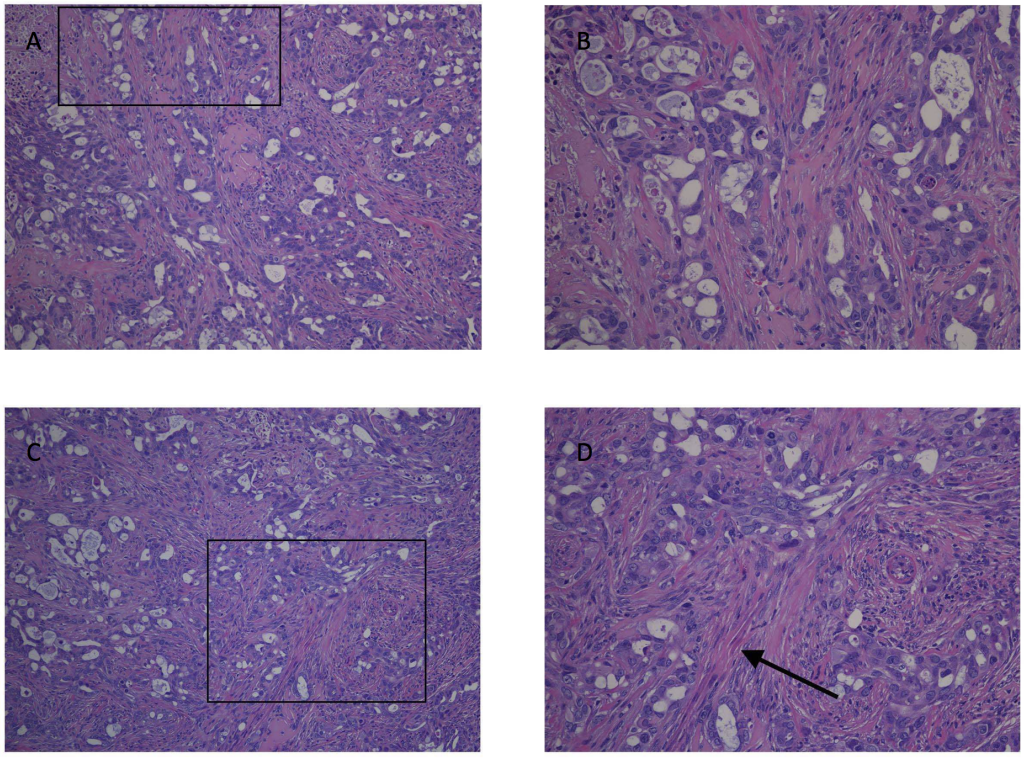

Figure 3.1: H & E staining of: A) Control 432A at 10x magnification, B) Control 432A at 20x magnification, C) Treated 435A at 10x magnification, D) Treated 435A at 20x magnification. The black rectangles show where the B and D images were taken in the A and B images. In image B the pink areas are desmoplastic tissue while the bigger purple spots are stromal cells and the smaller and slightly more oval purple spots within the desmoplastic tissue are cancer cells. The arrow on image D shows potential smooth muscle staining. All of the white areas are thought to be either gland-like structures or possibly adipose tissue.

Within the IHC part of this thesis the images presented on the following pages will have circles with a letter attached to them. This is shown to point out different structures of the tumor environment. In order to properly showcase how these cells/cell clusters look like when viewing the sections in a microscope a larger H & E stain image is shown here (Figure 3.2). As is evident the difference in size between the stroma cells and tumor cells makes it fairly easy to distinguish them when viewing an enlarged image. This difference is less evident in the images presented for the different antibodies due to the smaller size of each image. However, this is what is observed when the images are displayed individually and at a much higher resolution (Figure 3.2).

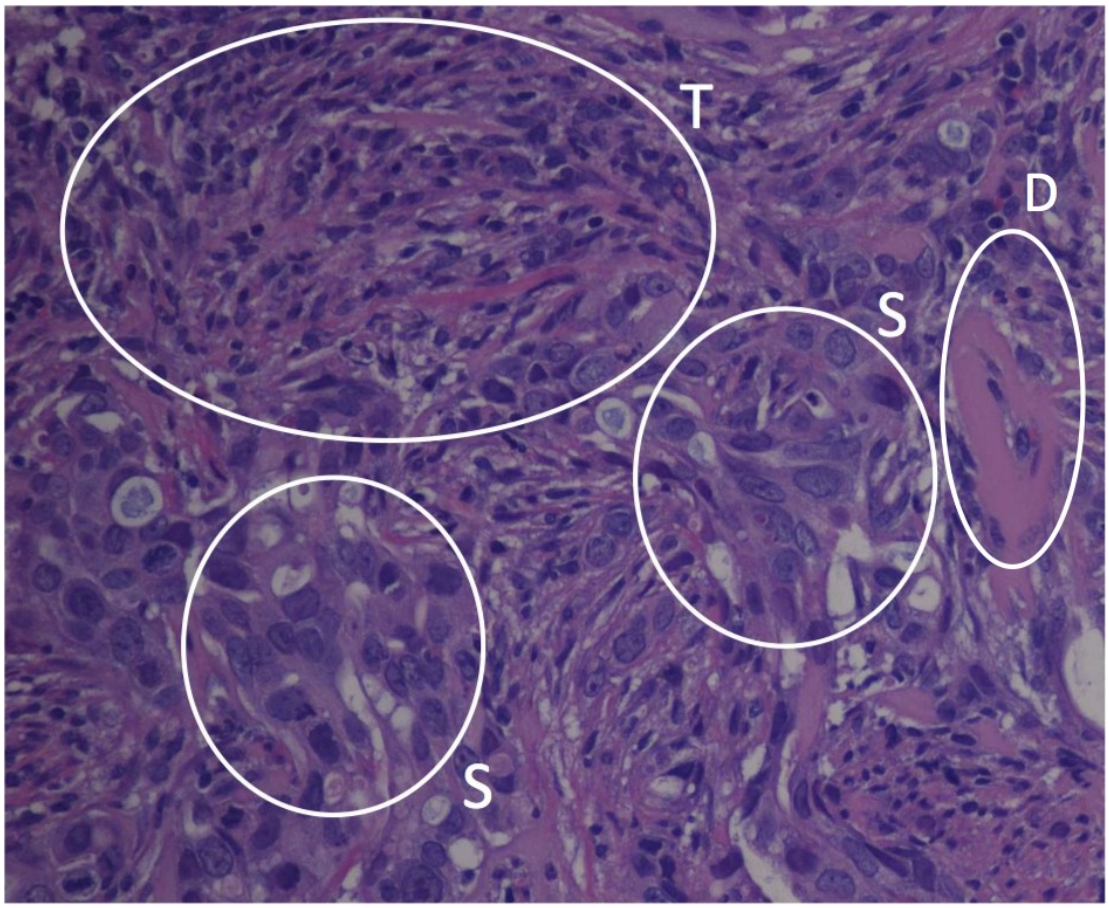

Figure 3.2: H & E staining- Tumor and desmoplasia hallmarks of one of the control tumors (432) at a 20x magnification. When evaluating the tumor tissue sections the shape and size of cells reveal their potential type. As this is a subcutaneously xenografted Capan-2 tumor model it is expected that only tumor related cells will be present. The image shows examples of a cluster of tumor cells (marked by a T) that appear as very small and often with a slight oval shape with surrounding desmoplastic cells (or stroma cells) (marked by an S). The stroma cells are bigger and come in a variety of shapes but they are all characterized by their greater size relative to that of tumor cells. The area in the oval with a D attached an area with only desmoplastic tissue.

3.1.3 Collagen IV

Collagen IV is an extracellular protein that is responsible for creating and maintaining the basement membrane. This membrane causes a separation between different types of tissue within the body. In healthy tissue, collagen IV is only found in the basement membrane, however, in tumor afflicted tissue it can be associated with organ or tumor fibrosis and accumulates in the microenvironment surrounding the tumor (Kalluri (2003)). Collagen IV is reported to be self-aggregating when the non-collagenous-1 domain (NC1) on three α-chains interact (Kalluri and Cosgroves (2000)). The formation of collagen fibrils occurs intracellularly in the rough endoplasmatic reticulum and Golgi complex before the fibrils assemblies into collagen fibers extracellularly (Lodish et al. (2000)).

The images display (Figure 3.3 A, B, C, D and 3.4 A, B, C, D) brown staining inside of the cells (characterized by darker brown DAB+ stain) in a large amount of the stroma cells. This type of staining is most likely not true staining as there appear to be a high amount of background noise as well as intracellular staining. Further, collagen IV should not be found within the nucleus it self, however, in a lot of the stroma cells it appear as if it has stained inside the nucleus. This observation of false-positive/artefact staining was also verified and supported by dr. Mjønes. The IgG control shows the expected non-specific staining. The negative control shows no staining, which is also as expected. The positive control (Figure 3.3 G-H and 3.4 G-H) shows staining of collagen outside and between the cells. The scalebar in each image represents 500 μm at the given magnification. The magnification was either 10x or 20x. See table 3.1 for information about tumor numbers and the doses received.

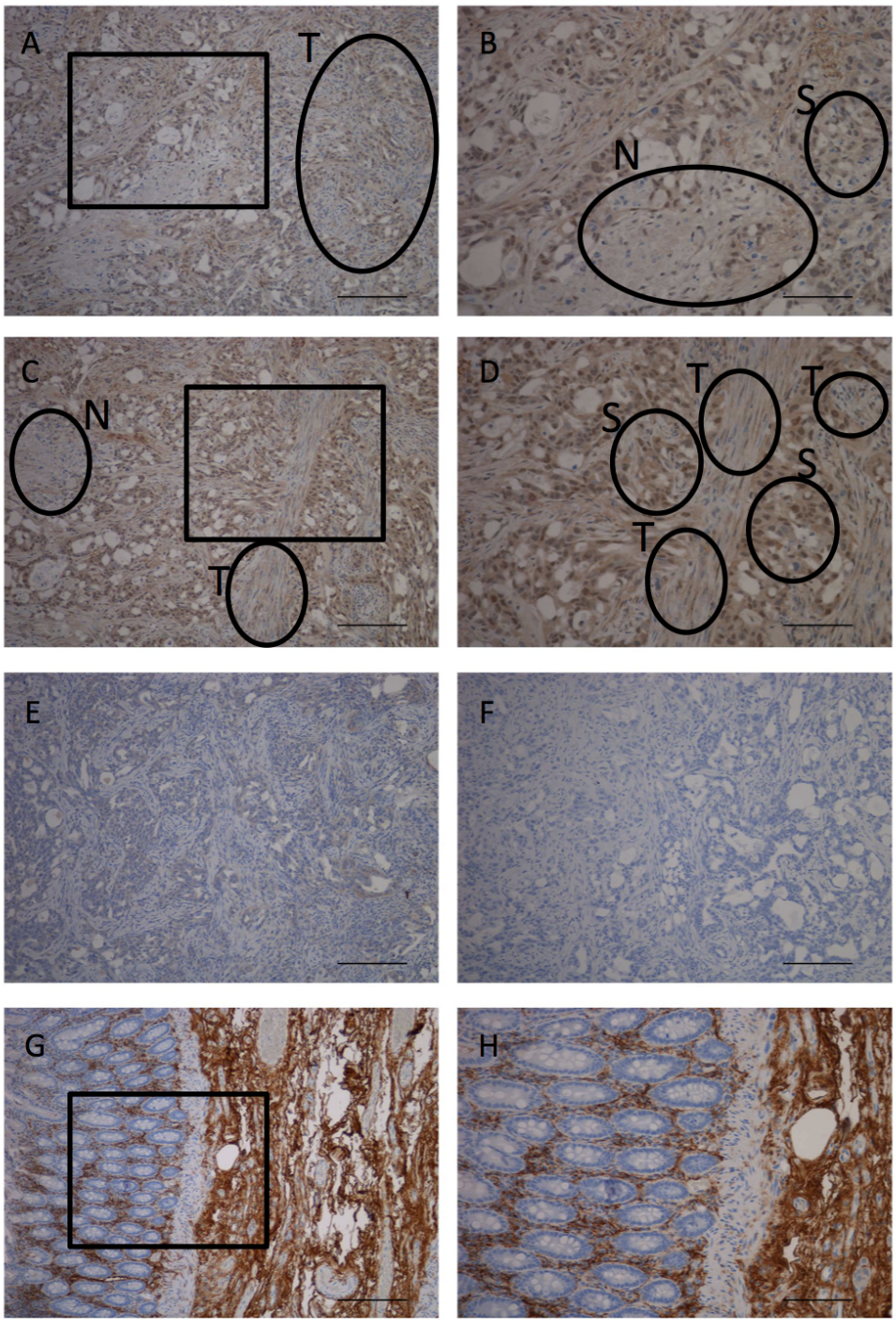

Figure 3.3: Results from IHC staining of collagen 43x. A) Control tumor 433 at 10x magnification, B) Control tumor 433 at 20x magnification, C) G-block treated tumor 435 at 10x magnification, D) G-block treated tumor 435 at 20x magnification, E) IgG negative control of G-block treated tumor 526 at 10x magnification, F) Negative control G-block treated tumor 526 at 10x magnification, G) Positive control (human colon) at 10x magnification, H) Positive control at 20x magnification. The rectangles show where in the 10x magnification the 20x image is taken. The letters outside the black circles denotes various structures of interest. N is necrotic area, S is stroma cells and T is for tumor cells.

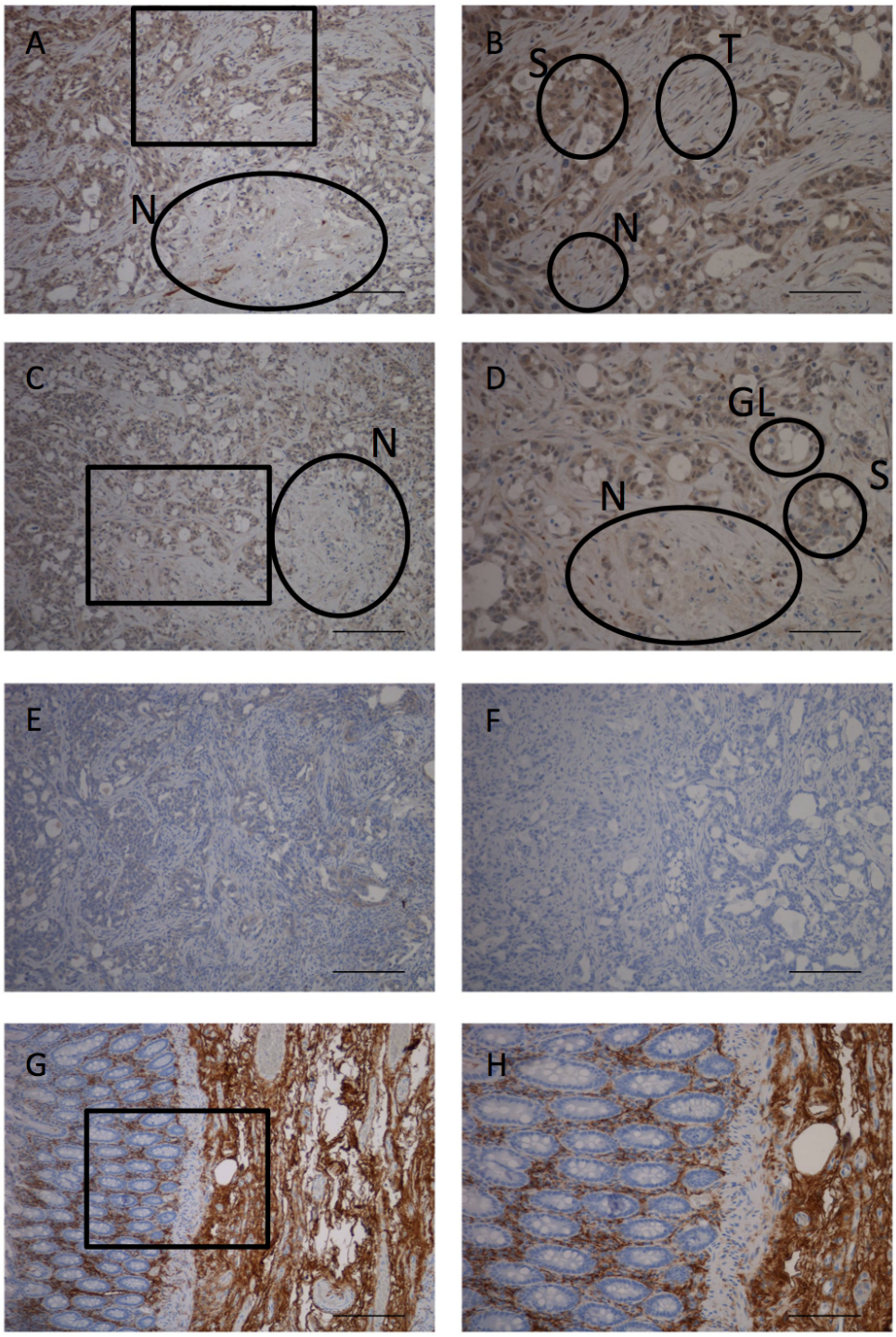

Figure 3.4: Results from IHC staining of collagen 52x. A) Control tumor 524 at 10x magnification, B) Control tumor 524 at 20x magnification, C) G-block treated tumor 528 at 10x magnification, D) G-block treated tumor 528 at 20x magnification, E) IgG negative control of G-block treated tumor 526 at 10x magnification, F) Negative control G-block treated tumor 526 at 10x magnification, G) Positive control (human colon) at 10x magnification, H) Positive control at 20x magnification. The rectangles show where in the 10x magnification the 20x image is taken. The letters outside the black circles denotes various structures of interest. N is necrotic area, S is stroma cells, T is for tumor cells and GL is for gland like structures that appear like open areas.

ImmunoRatio was the analysis tool chosen for the staining analysis of the tissue (Figure 3.5). The algorithm within the web page had trouble differentiating between DAB+ staining and hematoxylin staining in the collagen IV stained tissue. As the pathologist had deemed the staining to be untrue the tissue sections were photographed and the DAB+/Nuclear staining was recorded but not analyzed further as the nuclei stain (hematoxylin) could not be properly separated from the antibody stain. Appendix A.1 shows the raw data from ImmunoRatio for collagen IV.

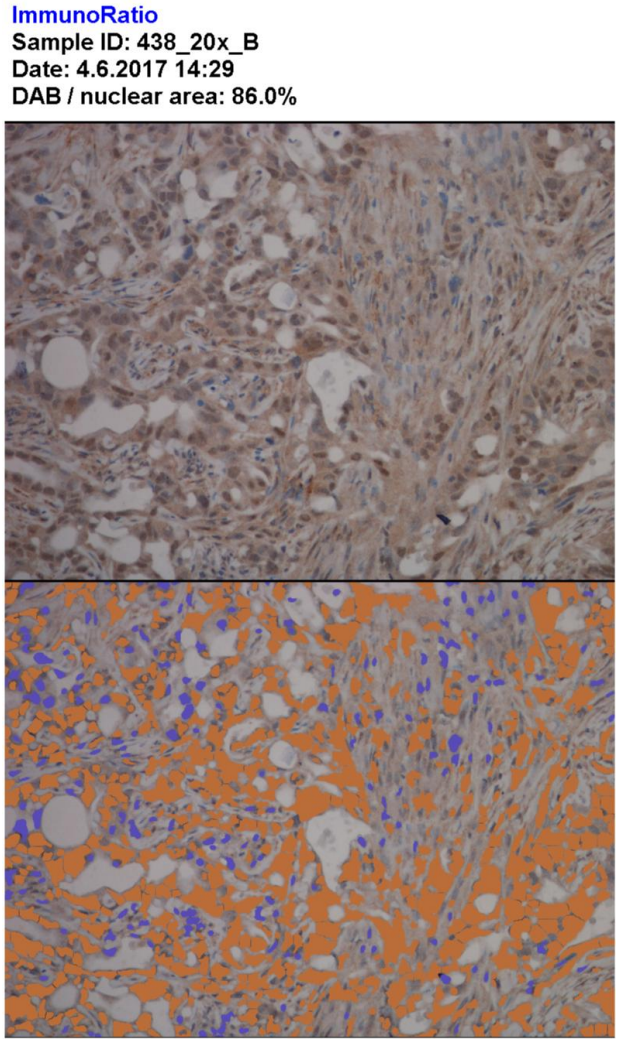

Figure 3.5: The top image shows a collagen IV stained tumor treated with G-block in ImmunoRatio. The small areas of darker brown hues are cells where the collagen antibody has given stain to cells, this type of staining is not expected to happen with collagen IV antibodies as collagen IV should not be found inside cells. These cells should have been tinted blue. The bottom picture shows the problem with the unwanted cellular and nuclear staining that skews the result image and DAB+/nuclear area ratio. ImmunoRatio was not able to differentiate between nuclei that should have been blue (by the hemotoxylin) and surrounding tissue that should have been brown (by DAB+).

The immunohistochemical staining of collagen IV did not stain in expected areas. The antibody appeared to stain inside cells, on top of cells and inside the nucleus. Further, it also appeared to stain inconsistently for tumor cells. It did however appear to stain the majority of stroma cells ((Figure 3.3 A-D and 3.4 A-D). This type of staining for collagen IV is not supposed to occur if the antibody is optimized properly and if it is a fitting antibody. As mentioned in the first section for this protein, collagen IV can in tumor afflicted tissue accumulate in the microenvironment surrounding the tumor (Kalluri (2003)). It is however not probable that collagen IV should stain in nuclei as this protein should not be present there. The problem with intracellular staining persisted though out the entire optimization period. Different dilutions were tested, both pH 6 and 9 were tested and amount of time the primary antibody was left on for (1 h RT vs O.N 4°C) were also explored. None of the changes yielded any dramatic difference in reducing the intracellular staining in the cells.

The antibody did however successfully stained expected areas in the control tissue (Figure 3.3 G, H and 3.4 G, H). The pathologist agreed that the staining seen in the positive control was as expected and the staining on the tumor slides was atypical. The reason governing the unexpected staining in the pancreatic model is not fully understood. It was hypothesized that the antibody chosen was not optimal for the chosen tissue. Ideally more optimizing should have been performed and different antibodies should have been tested.

The amount of time booked in the lab for this experiment was relatively short. In an effort to be as efficient as possible the choice to go with an antibody with a working protocol for a breast cancer model in mouse (Bugge et al. (2016)) was used as a starting point. This antibody had proven to work well in that mouse model and the preexisting protocol had also been optimized in the same lab with the same brands of reagents and with buffers prepared by the same personnel.

As the pancreatic and breast tissues were different with regard to for instance composition, cells and proteins it was clear from the start that rounds of optimizing were needed but it was theorized that with this antibody some of the parameters like dilution range and amount of time to leave DAB+ on were already narrowed down a bit and could be used, as previously mentioned, as an initial guide.

A problem that arose fairly late in the optimization process concerned the fact that the specific antibody used was no longer available from Millipore. By the time of this discovery so much

time had been spent on optimizing for this specific antibody from that specific producer that it was too late to start over with an antibody from a different producer. Because of this it was decided to use the remaining volumes (μl) of the collagen IV antibody on a full trial of all the sections and go with the parameters that seemed to give the best staining.

Another problem that plagued the entire immunohistochemical part of the thesis was the tendency for the tissue to dry out when tissue was incubated over night at 4°C with an antibody in a buffer solution. As the collagen IV antibody full trial was the first of the three antibodies to undergo a full set up with incubation over night some of the sections did partially dry out. This was discovered during the optimization phase before the full trial commenced and as such a plastic cover was placed over the tissue after the antibody solution had been added in order to minimize the potential of drying out in the full trial. This method of preventing tissue drying did not work on all of the sections and some of the sections still dried out.

If time had not been such a constraining factor it would have been of great interest to order a monoclonal collagen IV antibody or another type of polyclonal collagen IV antibody from another producer and optimized for one of these. Dr. Mjønes recommended trying a monoclonal antibody to potentially reduce the artefact staining potentially caused by polyclonal cross-reactivity. Monoclonal antibodies are more specific and only recognize one epitope as opposed to polyclonal antibodies that can bind to multiple epitopes. Further, monoclonal antibodies have a lower background reactivitiy than polyclonal (Ramos-Vara and Miller (2014)). Because of that it would be interesting to see if the staining appeared different with a different antibody.

3.1.4 Fibronectin

The staining of the tissue show staining between and around the cells (Figure 3.6 A-D and 3.7 A-D). The overall staining patterns with fibronectin on the tumor tissue was approved by dr. Mjønes as true and appropriate staining. The IgG negative control (Figure 3.6 E and 3.7 E) showed expected unspecific binding that does not resemble the staining produced with the fibronectin antibody. The negative control (Figure 3.6 F and 3.7 F) with only buffer applied in stead of an antibody solution showed that the DAB+ staining did not produce any staining on its own. The positive control of a mouse kidney showed expected staining between and outside of cells (Figure 3.6 G-H and 3.7 G-H). The amount of staining seen in the positive control is expected as fibronectin-levels should be low in normal healthy tissue (Alberts et al. (2008b)). Note that in Figure 3.7 C and D the images were taken with a different microscope and camera and at a later date than the other images and as such the color displayed is slightly different.

The fibronectin antibody worked well with the cancer model and gave good staining in the expected extracellular areas. This antibody had also been explored in the breast cancer study and the protocol there was also used here as an initial guide of what pH, dilution and DAB+ time to use. Staining with the fibronectin antibody gave an instant and intense stain in areas of necrosis upon application of DAB+ (Figure 3.6 D and figure 3.7 B, D). Upon conferring with the pathologist it was stated that it was not possible to draw any conclusion concerning the contents of proteins in areas of necrosis when evaluating stained sections from biopsies. Even though the antibody is supposed to only bind to fibronectin in tissue it can not be ascertained if the content in necrotic tissue has a higher occurrence of fibronectin than the surrounding tissue or if it is fibronectin at all. True (2008) states that the content of necrotic tissue with regards to immunoreactive epitopes is unpredictable and that false positive reactions can occur in necrotic tissue. So even though the content of the necrotic regions cannot be ascertained with certainty it is interesting to note that the fibronectin antibody stained very quickly and intensely in necrotic regions. The same quick and intense staining did not occur with the collagen IV or α-smooth muscle actin antibody. In both of those the necrotic areas remained mainly unstained by both DAB+ and hematoxylin and as such they almost appear as white areas. Because of the uncertainty regarding actual fibronectin contents within areas of necrosis these areas were excluded in the image analysis.

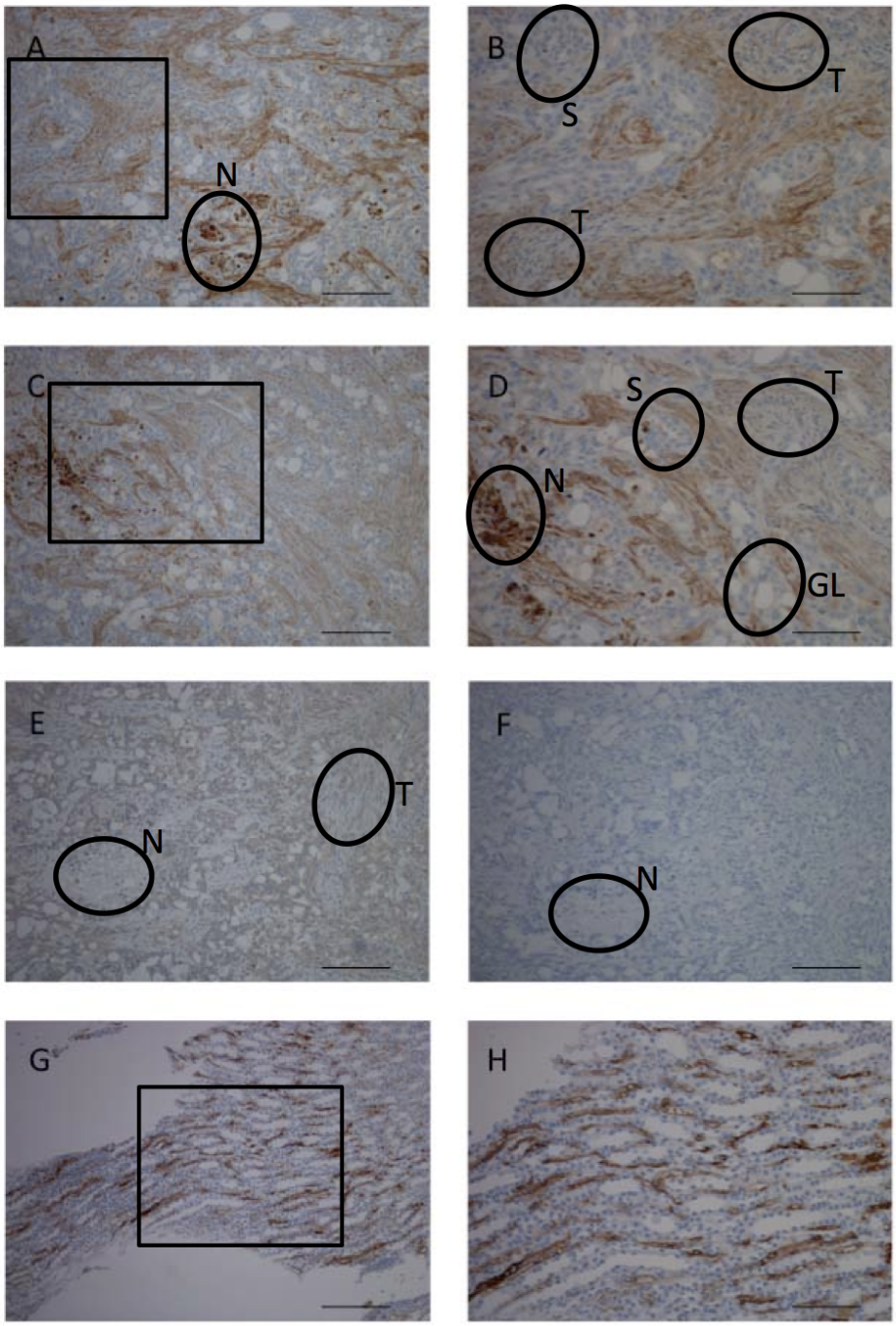

Figure 3.6: Results from IHC staining of fibronectin for treatment group 1 (4 doses). A) Control tumor 432 at 10x magnification, B) Control tumor 432 at 20x magnification, C) G-block treated tumor 435 at 10x magnification, D) G-block treated tumor 435 at 20x magnification, E) IgG negative control of G-block treated tumor 435 at 10x magnification, F) Negative control G-block treated tumor 435 at 10x magnification, G) Positive control (mouse kidney) at 10x magnification, H) Positive control (mouse kidney) at 20x magnification. The rectangles show where in the 10x magnification the 20x image is taken. The letters outside the black circles denotes various structures of interest. N is necrotic area, S is stroma cells, T is for tumor cells and GL is for gland like structures that appear like open areas.

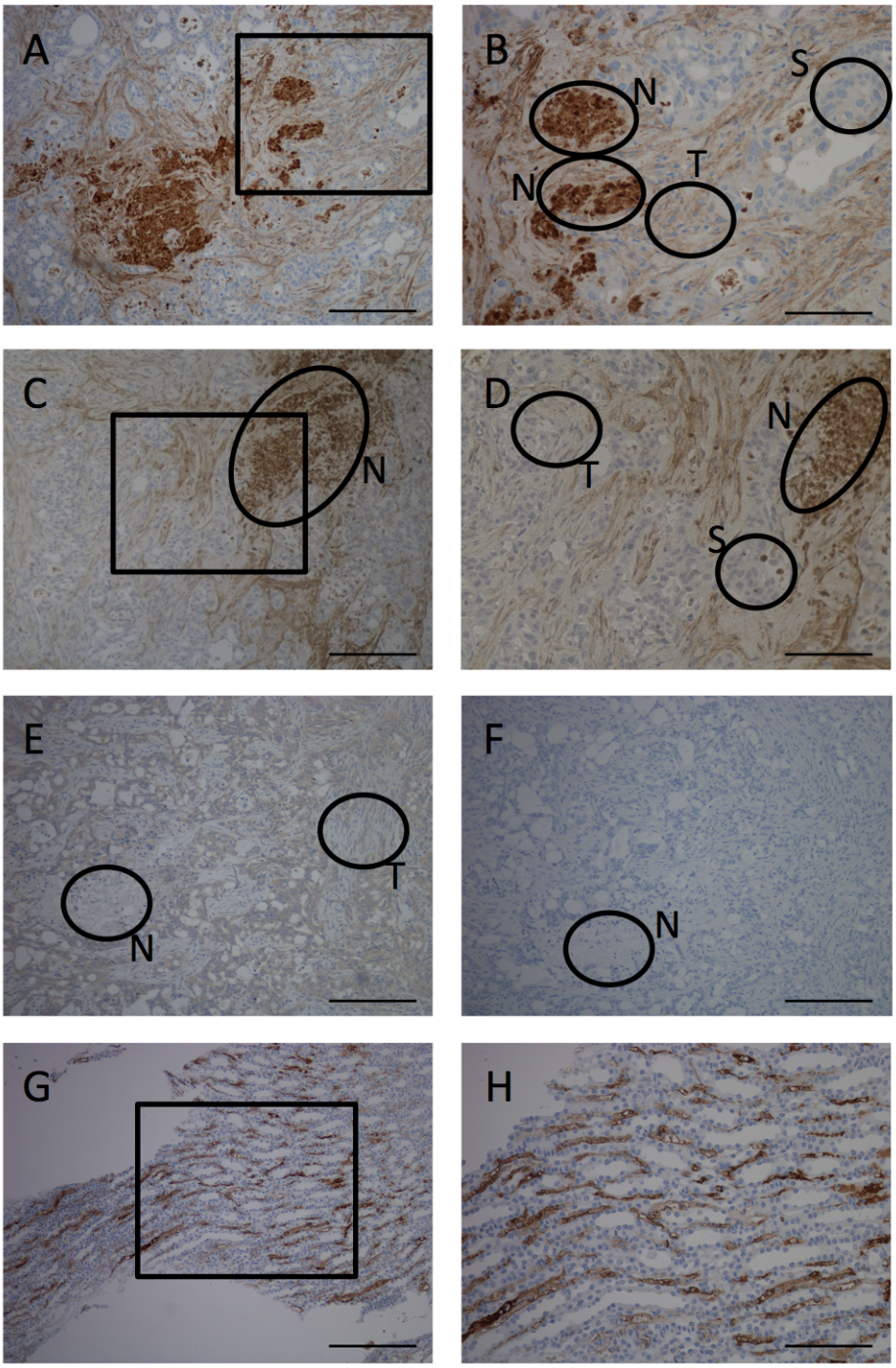

Figure 3.7: Results from IHC staining of fibronectin for treatment group 2 (10 doses). A) Control tumor 523 at 10x magnification, B) Control tumor 523 at 20x magnification, C) G-block treated tumor 529 at 10x magnification, D) G-block treated tumor 529 at 20x magnification, E) IgG negative control of G-block treated tumor 435 at 10x magnification, F) Negative control G-block treated tumor 435 at 10x magnification, G) Positive control (mouse kidney) at 10x magnification, H) Positive control (mouse kidney) at 20x magnification. The rectangles show where in the 10x magnification the 20x image is taken. The letters outside the black circles denotes various structures of interest. N is necrotic area, S is stroma cells and T is for tumor cells.

A two-way t-test was conducted and there was a significant difference in the mean of the treated

tissue and control tissue at $p < 0.05$ level in treatment group 2 where the mice had received 10 doses of G-block in physiological saline [$t(23) = 2.99$, $p = 0.006$] (Appendix D.1 shows an example of the R-script used to analyse the data from immunoRatio). The group that received 4 doses had no significant difference between control and treated ($p > 0.05$). The number of samples within each category are quite small (control and treatment). In the control group the $n = 2$ and in the treatment group $n = 6$ in the staining process but for the image process $n = 3$ as some of the tissue sections had faded too much thus making it very difficult to detect both the DAB+ and hematoxylin stain. There were taken 6 images of each slide in order to potentially capture as much of the tissue as possible while at the same time avoiding areas that did not meet the image acquisition guidelines. Due to the small sample size the significance of the results of the t-test is questionable as the power of the test (the ability to reject the null-hypothesis) is probably low (Dalgaard (2008)).

A one-way ANOVA was conducted to see if there was a difference between the amount of G-block received and the percentage of DAB+/Nuclear staining recorded (Appendix D.1 shows an example of the R-script used to analyse the data from immunoRatio). Group 1 that received 4 doses did not have any significant difference between groups with regards to amount of G-block received. Group 2 that received 10 doses of G-block had a significant difference between amount of G-block received at $p < 0.05$ level: [$F(2, 25) = 2.996$, $p = 0.0378$]. However, post hoc comparisons using the Tukey HSD test failed to find any significant differences between the different concentrations of G-block. This could be as a consequence of a low sample size and low test-power.

The staining patterns observed in the samples and also photographed did not appear uniform through out the tissue section. This is something that was also confirmed in the % DAB+/Nuclear stain recorded in ImmunoRatio. In some of the tissue sections there could be a high amount of DAB+ stain in some areas and a low amount of DAB+ stain in other areas. Both types of stains were photographed and analyzed in ImmunoRatio if they were deemed representative, based on an overall impression of the stain on the tissue section (Figure 3.8 and 3.9). This lack of uniform staining will influence the statistical tests as they will affect the mean values used to compare the different groups. The differences in amount of staining within a tissue section can be observed in both the control tumors and the treated tumors for both doses. Heterogeneity of gene expression might reflect tumor biology and Sklarew et al. (1990) reported that tumor

cells in breast carcinomas that varied in expression extent of estrogen receptor appeared to be more likely to fail systemic therapy than the tumors that exhibited a more uniform expression of the receptor. This could imply that the lack of staining uniformity in the tissue might possibly be linked to the gene expression. In addition, Sklarew et al. (1990) reported that the lack of uniformity could also possibly further complicate treatment. As previously mentioned, there was observed a degree of heterogeneity with regards to fibronectin expression in the tumor sections and this might possibly be linked to alterations in gene expression.

There was an observable distinct decrease in the overall amount of staining of fibronectin when evaluating the staining in the microscope for the 10 dose group that received 25 mg/kg and 561 mg/kg of dissolved G-block. This is also reflected in figure 3.9 for number 527 and 530. The treatment of 10 doses of 0.5 mg/kg dissolved G-block (Figure 3.9 525) did exhibit a low mean value but it was observed that the tissue section was non-uniform in staining amount. This non-uniformity is also apparent in the distribution of values in figure 3.9 for 525 relative to the other samples.

For the group that received 4 doeses of G-block there was also an observable decrease in the amount of fibronectin stained between the controls and the treated tissue sections when performing a microscopic evaluation. However, the statistical tests reported no significant differences. There does seem to be a bigger overlap between the controls and treated tissue section for the 4 does group (Figure 3.8) than between the controls and treated in the 10 dose group (Figure 3.9). That could explain why there were no significant results for the 4 dose group.

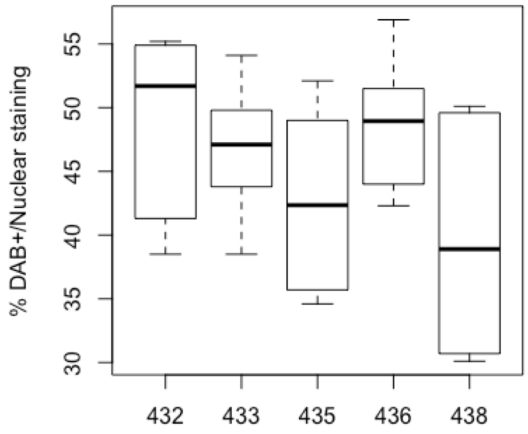

Figure 3.8: Descriptive statistics of the results obtained from the ImmunoRatio analysis for fibronectin where the mice were in treatment group 1 and received 4 doses of dissolved G-block (treatment) in physiological saline or 4 doses of physiological saline alone (control). The controls are 432 and 433, number 435 received 0.5 mg/kg of G-block, number 436 received 25 mg/kg G-block and 438 received 560 mg/kg G-block. The individual box and whiskers show the median (thick band inside box), the first and third quantile (boundaries of the box where 25-75% of the data is located) and the maximum value and minimum value (whiskers).

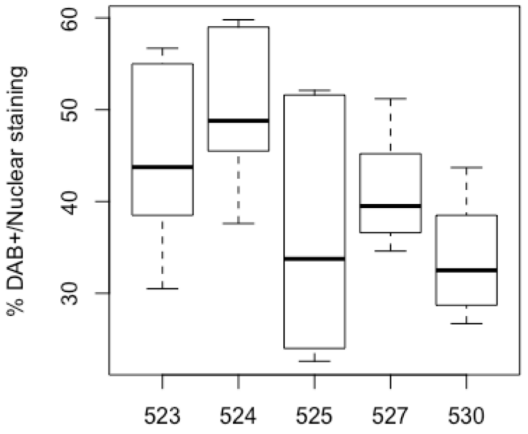

Figure 3.9: Descriptive statistics of the results obtained from the ImmunoRatio analysis for fibronectin where the mice were in treatment group 2 and received 10 doses of dissolved G-block (treatment) in physiological saline or 10 doses of physiological saline alone (control). The controls are 523 and 524, number 525 received 0.5 mg/kg of G-block, number 527 received 25 mg/kg G-block and 530 received 561 mg/kg G-block. The individual box and whiskers show the median (thick band inside box), the first and third quantile (boundaries of the box where 25-75% of the data is located) and the maximum value and minimum value (whiskers).

The G-block drug is still in its early stages of mechanism discovery and its exact mechanisms of action are still being elucidated. The apparent decrease in fibronectin seen in treatment goup 2 (10 doeses) might not be explained by the already known function of G-block (e.g. its binding of divalent cations like calcium). It is important to note that decrease in fibronectin does not necessarily mean an increased in breakdown of it. It might indicate that there is a reduction in production of fibronectin in this specific model. A reduction of production could indicate that there is a potential nuclear response- in the sense that the gene transcription is downregulated for fibronectin.

What is established regarding fibronectin is that the ECM contains little fibronectin in normal healthy tissue and as such a decrease in fibronectin in a cancer model that has received some sort of treatment could be promising. This is because fibronectin promotes tumor growth, metas-

tasis and resistance to drugs (Wang and Hielscher (2017)). Further, upregulation of fibronectin is correlated with poor patient prognosis and a fibronectin upregulation is one of the earliest events taking place in metastatic sites (Han and Lu (2017)). Fibronectin was also found to confer resistance to chemotherapy and adjuvant treatments in breast cancer tissue. Pontiggia et al. (2012) co-incubated human and mouse breast tumor cells with fibronectin and measured tumor cell sensitivity to tamoxifen. Tamoxifen is a selective estrogen receptor modulator and it has been the main adjuvant treatment for estrogen receptor (ER) positive breast cancer patients for around 30 years. The addition of fibronectin in the breast cancer tissue lead to tamoxifen resistance by fibronectin-mediated activation of $\beta 1$-integrin which in turn activates various signaling pathways. By disrupting the fibronectin and $\beta 1$-integrin interaction the conferred resistance was reversed, this lead to drug-induced apoptosis of the tumor cells. As such, the observed and measured decrease in amount of fibronectin for treatment group 2 (10 doses) could be encouraging as a decrease in fibronectin could possibly imply better responsiveness to treatment, at least with regards to the results from the breast cancer study. However, it is important to note that the tissue in the pancreas will differ from the tissue found in the breast. In order to draw any parallels between the results found by Pontiggia et al. (2012) in the breast cancer study and the decrease in fibronectin here relative to potential treatment responsiveness would require further extensive testing.

Secreted fibronectin presents as a dimer and each of the two monomer contain three types of repeating units: FN-I, FN-II and FN-III (Takahashi et al. (2007)). Fibronectin has a RGD motif which is located in the FN III_{10} repeat of fibronectin (Pankov and Yamada (2002). The RGD motif consists of the amino acids Arg-Gly-Asp and is an adhesion motif. Alginate (e.g G-block) do not have cell adhesion motifs but can be conjugated with RGD motifs (Gasperini et al. (2014)). It might be that G-block could potentially bind to fibronectin on FN III_{10} and as a consequence of this alter some potential interactions between FN III_{10} and other molecules. This could potentially have an effect on signaling from or to the microenvironment which in turn could potentially affect fibronectin. At this stage however, the abovementioned potential interactions are unverified and the exact mechanisms of G-block are still unknown.

G-blocks are known to bind to divalent cations, as previously mentioned. An group of enzymes found in the body that are important in terms of breaking down ECM components are the MMPs. MMPs are dependent on both zinc and calcium to maintain the expression of enzymatic activity

(Nagase and Woessner (1999)). If MMPs are deprived of calcium, e.g. by G-blocks in this instance, they might loose some of their enzymatic ability to break down ECM components like fibronectin. Following that logic, the decreased breakdown of fibronectin would in theory lead to a possible increase in amount of free fibronectin. That could in turn lead to a higher DAB+/nuclear staining if there is a higher amount of available fibronectin present extracellularly. However, that is the exact opposite of what was found here which is interesting and serves to highlight the need to further elucidate the effect G-block has on the tumor microenvironment.

3.1.5 α-SMA

Staining with α-smooth muscle actin antibody showed expected staining between cells (Figure 3.10 A-D and 3.11 A-D). The staining with α-smooth muscle actin was confirmed by Dr. Mjønes as true and expected staining patterns. The IgG negative control (Figure 3.10 E and 3.11 E) showed expected unspecific staining that did not resemble the α-smooth muscle actin antibody staining. The negative control (Figure 3.10 F and 3.11 F) to which only buffer was applied showed that the DAB+ substrate did not bind to any epitopes in the tissue. The positive control of mouse duodenum (Figure 3.10 G-H and 3.11 G-H) showed expected staining in the smooth muscle in the walls of the duodenum.

The α-smooth muscle actin antibody stained well with the antibody finally chosen. This final antibody was a polyclonal antibody like the antibodies used in the collagen IV and fibronectin staining. The risk with all three of the antibodies is the potential of cross-reaction, but this was checked with the IgG negative control and deemed to be negligible. The optimizing process did take a while as the parameters used in Bailey et al. (2008) which served as a guide here needed to be adjusted (see Table 2.3 for α-smooth muscle actin for parameters from Bailey et al. (2008)).

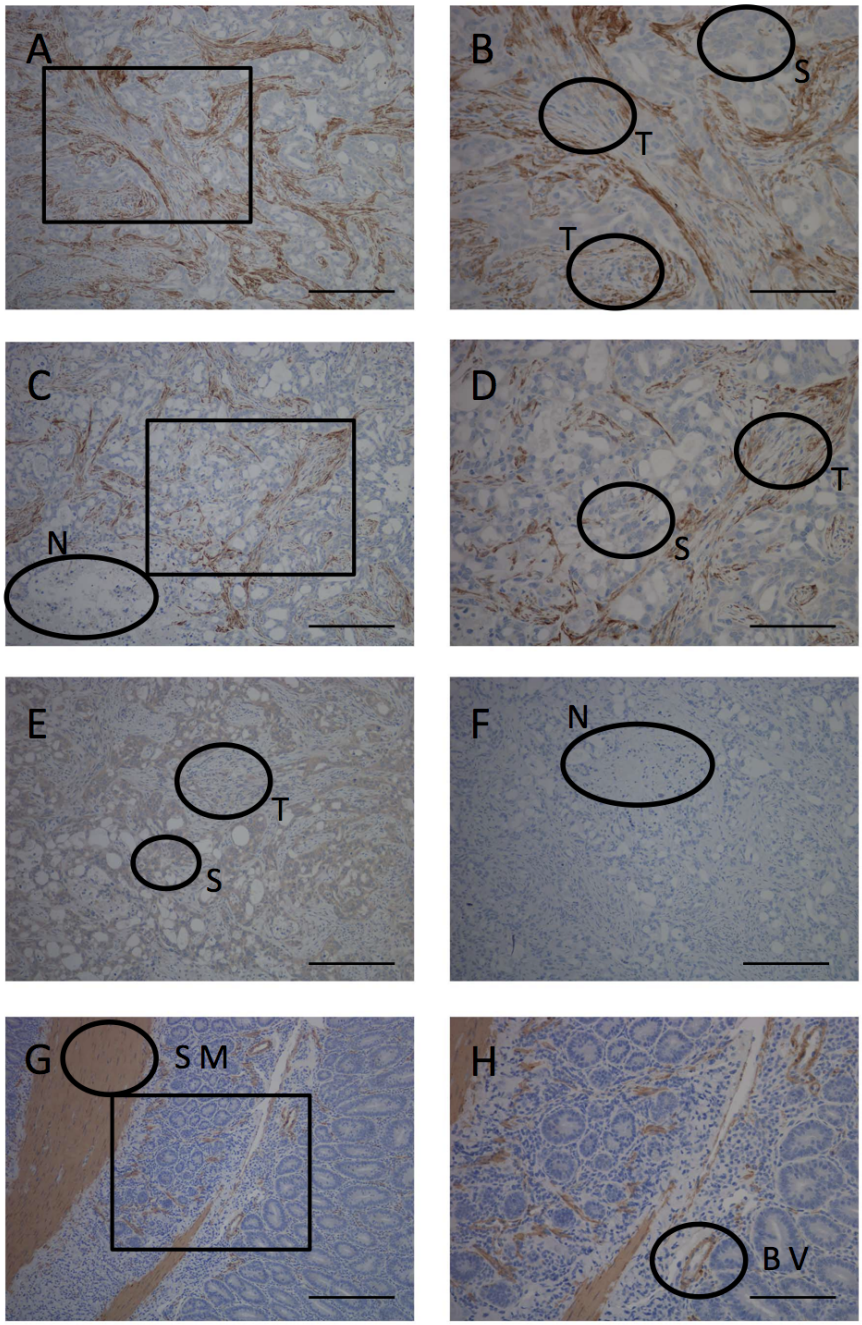

Figure 3.10: Results from IHC staining of α-smooth muscle actin treatment group 1. A) Control tumor 432 at 10x magnification, B) Control tumor 432 at 20x magnification, C) G-block treated tumor 437 at 10x magnification, D) G-block treated tumor 437 at 20x magnification, E) IgG negative control of G-block treated tumor 435 at 10x magnification, F) Negative control G-block treated tumor 435 at 10x magnification, G) Positive control (mouse duodenum) at 10x magnification, H) Positive control (mouse duodenum) at 20x magnification. The rectangles show where in the 10x magnification the 20x image is taken. The letters outside the black circles denotes various structures of interest. N is necrotic area, S is stroma cell cluster, T is for tumor cell cluster, SM is for smooth muscle in the duodenum wall, B V denotes a potential blood vessel with smooth muscle in the vessel wall.

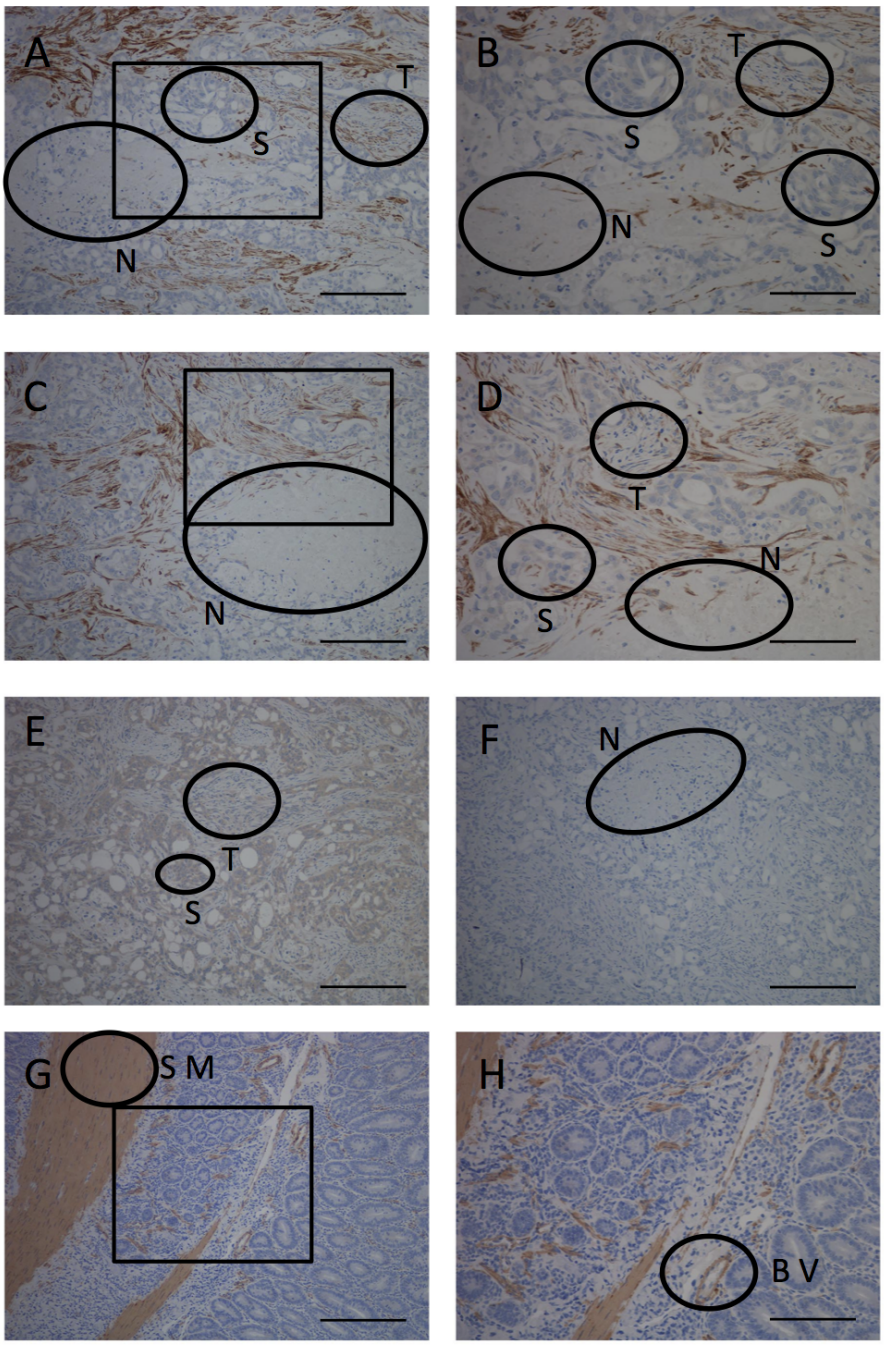

Figure 3.11: Results from IHC staining of α-smooth muscle actin treatment group 2. A) Control tumor 523 at 10x magnification, B) Control tumor 523 at 20x magnification, C) G-block treated tumor 529 at 10x magnification, D) G-block treated tumor 529 at 20x magnification, E) IgG negative control of G-block treated tumor 435 at 10x magnification, F) Negative control G-block treated tumor 435 at 10x magnification, G) Positive control (mouse duodenum) at 10x magnification, H) Positive control (mouse duodenum) at 20x magnification.The rectangles show where in the 10x magnification the 20x image is taken. The letters outside the black circles denotes various structures of interest. N is necrotic area, S is stroma cell cluster, T is for tumor cell cluster, SM is for smooth muscle in the duodenum wall, B V denotes a blood vessel with smooth muscle in the vessel wall.

The initial α-smooth muscle actin antibody was a monoclonal antibody from DAKO (M0851). This antibody was initially chosen as it had been used an article (Bailey et al. (2008)) in which the same tumor cell line (Capan-2) had been used and as such it already had a working protocol. The antibody was diluted 1:400 with antibody diluent and it gave a very faint stain at this dilution. The impression was that it seemed to stain next to nothing at the center of the tissue whilst the antibody stained more at some areas of of the outer part of the tissue (Figure 3.12). Other areas of the outer part of the tissue section showed no antibody staining at all. Further, the faint staining resembled to some extent that of an IgG negative control (e.g. Figure 3.10 E and 3.11 E). IgG negative controls exhibit unspecific staining and as seen in figure 3.10 E and 3.11 E the stain apperas to be more of a general tint to the ECM and stroma cells. This tint was also seen in the tissue treated with 1:400 anti-α-SMA from DAKO (Figure 3.12 left). As the monoclonal antibody proved to not preform in a satisfactory manner another α-SMA antibody was acquired from a colleague of dr. Rao.

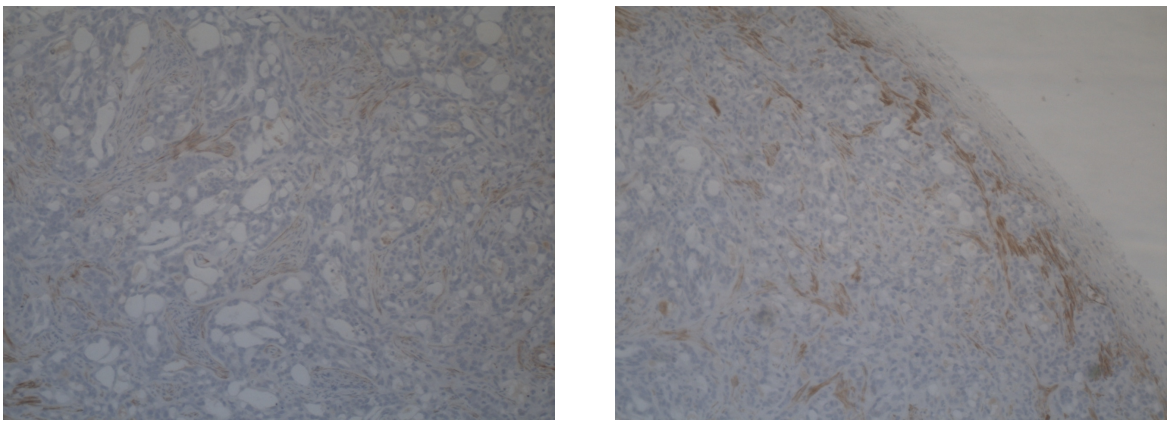

Figure 3.12: Results from IHC staining of α-smooth muscle actin from DAKO with a 1:400 dilution at 10x magnification. Left image shows the staining obtained in the center of the tissue and the right image shows staining on the edge of the tissue section. Note that there is very little staining closer to the center and the only staining achieved closer to the edge of the section is at the very edge it self.

The polyclonal α-smooth muscle actin antibody from Abcam gave a more satisfactory staining overall compared to the monoclonal α-smooth muscle actin antibody from DAKO. This antibody was the antibody optimized for and used in the full trial. The dilution had to be adjusted from 1:400 to 1:75 in a series of dilution tests in order to get what was deemed as a more appropriate staining (Appendix B.4). Further, the adjustment from 1:400 to 1:75 for the Abcam α-SMA was most likely necessary as the antibody concentration for the Abcam α-SMA was much lower than for the DAKO α-SMA. The antibody from DAKO was also tested at the 1:75 dilution in order to compare the two at a higher concentration and the impression was that the Abcam

polyclonal antibody still gave a better staining, even with the risk of potential cross-reactivity and background staining.

There was a slight, albeit non-significant, difference between the controls and treatment groups with this antibody (Figure 3.13 and 3.14). The control tissues in both group 1 (4 doses) and group 2 (10 doses) appeared to have weaker staining than the treatment groups when performing the qualitative microscopic evaluation. As both lightly and intensely stained areas had to be included if one or both were representative for overall staining within the tissue section the mean will be affected by this (along with the variance and standard deviation) and as such it can have an effect on the analysis. The difference between control and treated could indicate that there was an increase in α-SMA in the G-block treated tissue. In addition, Dr. Rao and Dr. Mjønes agreed that there was a slight visual observable increase in staining for the tissue that had received G-block treatment and this supported the impression that the author also was left with after performing staining of all of the tissue sections.

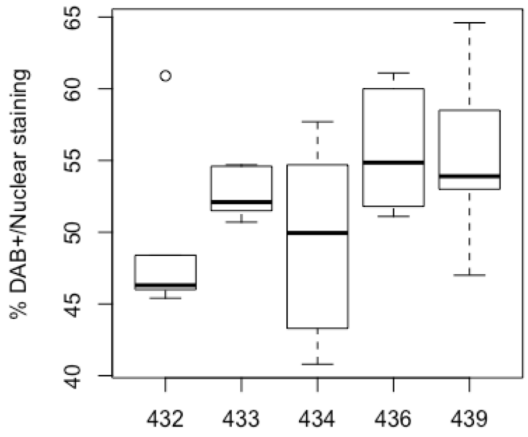

Figure 3.13: Descriptive statistics of the results obtained from the ImmunoRatio analysis for α-SMA where the mice were in treatment group 1 and received 4 doses of dissolved G-block (treatment) in physiological saline or 4 doses of physiological saline alone (control). The controls are 432 and 433, number 434 received 0.5 mg/kg of G-block, number 436 received 25 mg/kg G-block and 439 received 560 mg/kg G-block. The individual box and whiskers show the median (thick band inside box), the first and third quantile (boundaries of the box where 25-75% of the data is located) and the maximum value and minimum value (whiskers).

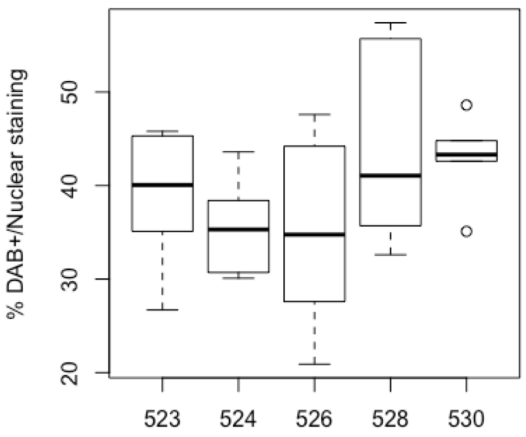

Figure 3.14: Descriptive statistics of the results obtained from the ImmunoRatio analysis for α-SMA where the mice were in treatment group 2 and received 10 doses of dissolved G-block (treatment) in physiological saline or 10 doses of physiological saline alone (control). The controls are 523 and 524, number 525 received 0.5 mg/kg of G-block, number 528 received 25 mg/kg G-block and 530 received 561 mg/kg G-block. The individual box and whiskers show the median (thick band inside box), the first and third quantile (boundaries of the box where 25-75% of the data is located) and the maximum value and minimum value (whiskers).

A Welch 2-sample T-test was conducted to see if there were any differences between the means of the control tissues and the treated tissue within each treatment group at a $p < 0.05$ level (Appendix D.1 shows an example of the R-script used to analyse the data from immunoRatio). Neither the group 1 with 4 doses nor group 2 with 10 doses had any significant difference between the control and treated tissue. However, when viewing the descriptive statistics for the control and treated tissues (Figure 3.13 and 3.14) there is a difference in means for the two controls within each of the groups. In group 1 that received 4 doses there is a percentage difference of about 8% between the means of the two controls and a percentage difference of about 5% between the means of the two controls in group 2 that received 10 doses. Because of the difference in means for the controls a one-way ANOVA was conducted to check for differences between the tissues. There was no significant difference between the different tissues in either group 1 or 2 at a p

<0.05 level. The sample size is the same here as for fibronectin and the same problem with low power in the statistical tests due to low sample size is also present here.

Non-uniform staining patterns were also present here as well as for fibronectin. For α-SMA the edges of the tissue seemed to stain more than the center of the tissue section. α-SMA seemed to be absent in necrotic areas and these areas appeared as completely blank when viewing the slide under a microscope (Figure 3.10 C and 3.11 C). This absence of α-SMA staining in necrotic regions is the polar opposite of what was observed for fibronectin. The absence of α-SMA stain in necrotic regions might indicate that the α-SMA epitopes were altered or destroyed. It is however interesting that the two antibodies (anti-fibronectin vs anti-α-SMA) produced such different results in necrotic regions.

Fujita et al. (2010) found that α-SMA was detected exclusively in the desmolastic stroma of PDAC. This finding seems to correspond well with the staining obtained here in which there was no staining on or inside turmor cells or stroma cells (Figure 3.10 B, D). Further, α-SMA also seemed to form a barrier between the tumor cell regions and the stroma cells (e.g. Figure 3.15 circled area). This could potentially be a protective mechanism from the cancer it self to further increase the density of its protective ECM to further hinder delivery of cancer treatment.

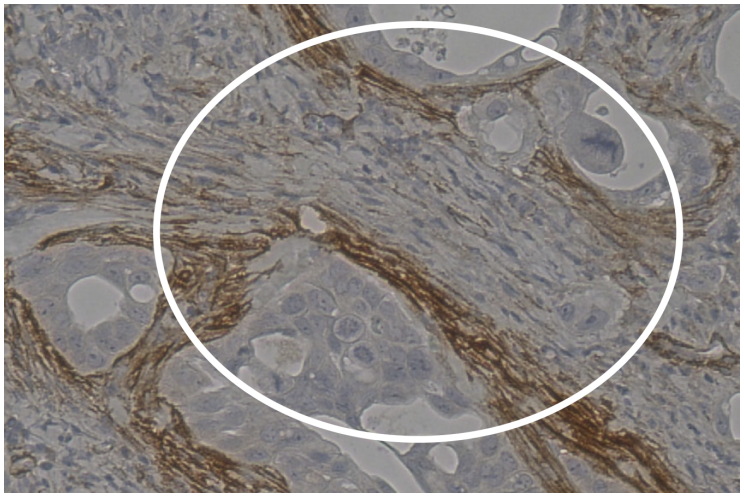

Figure 3.15: Separation of tumor cell area and stroma cells by α-SMA. The larger cells are stroma cells and the smaller, slightly oval cells are tumor cells. Image is taken at a 20x magnification.

Lee et al. (2013) found that patients with lung adenocarcinomas that had a high α-SMA expression in tumor cells showed significantly enhanced distal metastasis and unfavorable prognosis. Similar unfavorable prognosis outcome were found by Yamashita et al. (2012) in a study that focused on invasive breast cancer. The high α-SMA expression was in both studies linked to

poor patient survival. It is however unclear whether there is an upregulation of α-SMA or if there is a decrease in α-SMA breakdown in the tissue explored in this thesis. As touched upon in the fibronectin part of this chapter (Chapter 3.1.4) G-block is known to bind to divalent cations. Divalent cations are also used by MMPs and MMPs break down components of the ECM. So the G-block drug will possibly compete with MMPs for divalent cations and this could cause a potential decreased in breakdown of α-SMA and not an increase in production of α-SMA.

3.1.6 Fiji/ImageJ and ImmunoRatio

Fiji and ImmunoRatio were the two types of software explored in the imaging analysis in this thesis. Both of the softwares have strengths and weaknesses but in the end ImmunoRatio was the analysis tool chosen as it seemed to work the best with the tumor tissue.

ImageJ is a software with multiple plug ins, like Fiji, and this allows for great diversity of application. A downfall of the image deconvolution method within Fiji/ImageJ explored here was the presence of open empty spaces. The empty spaces and open areas were thought to be gland-like structures caused by the cancer but in this part of the discussion these areas will be referred to as empty spaces. The empty spaces did not stain either blue or brown in the staining procedure as there were no cells present there. However, when performing the color deconvolution the empty spaces appered to give some color in all of the three result images. Performing auto-white before taking an image should in theory cause the problem to be eliminated. This might hold true for images without many or large empty spaces but here the size and amount of these spaces caused problems as they skew the intensity results in the color deconvoluted images (Figure 2.4). Hence, the measuring of intensity in the image containing the DAB+ stain lead to trouble with the resulting output and this further complicated interpretation and subsequent analysis. The result was affected by how many and how big the open spaces were and the fact that they ended up being treated as DAB+ colored regions was problematic as this made it difficult to predict the staining intensity actually produced by the DAB+ in each image.

In ImmunoRatio there is no measure of the individual color channels intensity but the ratio of DAB+ staining to nuclear hematoxylin staining. This means that empty spaces do not have an effect on the results here in the same way as they do in Fiji/ImageJ. The empty spaces would decrease the amount of photographed cells and extracellular tissue but it would not affect the results in the same way as in Fiji/ImageJ. One weakness linked to both ImmunoRatio and also the color deconvolution method from Fiji/ImageJ pertains to the image acquisition guidelines. There it is stated that both faint and/or intensely stained areas are to be included if they appear to be representative for areas of the tissue, unless they are connected to areas of necrosis. This will have an effect on the variance and standard deviation within a tissue section and cause these values to be higher or lower than if these areas were excluded from the analysis. The decision not to exclude such areas was based on whether or not the intensity of the stain appeared to be representative of an overall stain in a certain area and true (for instance: if an area had a faint

stain and this was not caused by drying it was deemed true).

The moderate amount of empty spaces in the tissue sections lead to the decision of dropping the Fiji/ImageJ color deconvolution as an analysis tool. The ratio of DAB+ stain to nuclear staining as a method employed by ImmunoRatio proved to be problematic in the analysis for collage this is because the ImmunoRatio software was not able to properly distinguish between hematoxylin stained cell nuclei and collagen IV stained tissue (DAB+ stain) as the two stains appeared to stain on top of each other, as previously discussed (Chapter 3.1.3).

A problem encountered when using ImmunoRatio relates to color fading in the tissue as a consequence of late image-capturing. The sections had been mounted and kept in a closed box to minimize exposure to light. Never the less, the tissue slides had faded. In order to counteract this the images were color adjusted in Photoshop by using the auto-color adjust function. This could potentially have an effect on the DAB+/Nuclear staining ratio. However, since the DAB+ stain produced a brown-orange stain and the hematoxylin produced a blue stain it is not very likely that this adjustment would cause a dramatic change in the DAB+/Nuclear staining ratio. It is however a potential source of error and it is important to be aware that this could potentially influence the result of the analysis.

A drawback of using images and analyzing them through either Fiji/ImageJ or ImmunoRatio is that the tissue sections might fail to give an accurate representation of the entire tumor and each image will also only capture a part of the entire tissue section. Even when employing the guidelines used here there is a possibility that the analysis of the images will fail to, in a sense, see the full picture. As previously discussed, both weak and intense stains are to be included in the images and data analysis if deemed representative. The lack of uniformity of staining will as a consequence produce images that have a varying degree of DAB+/Nuclear staining. This will in turn have an effect on the values obtained in the statistical tests. As such, the need to verify the findings and explore the results for fibronectin and α-SMA further with techniques that are better at producing quantitative results is important. However, it has been shown here that it is possible to use certain softwares and plug-ins developed for IHC to either quantify the DAB+ staining intensity or the percentage DAB+/Nuclear staining ratio.

3.2 Rheology

The aim for this part of the thesis is to test the properties of collagen and determine how or if addition of G-block can affect the rheological properties of the collagen gel during its formation. In order to do this- optimization needed to take place to establish optimal temperature range, stability of collagen gel during a specific time frame, the LVR and the optimal frequency range. The increase or decrease in temperature done in this thesis is referred to as a temperature ramp. The details of all of the programmed sequences can be found in appendix C.2.1, C.2.2, C.2.3 and C.2.4.

3.2.1 The fault-tracking process

In this section of the thesis the primary focus will be on what went wrong with the initial tests of collagen gel. The measures taken to investigate how, what and which order different components and variables were checked and excluded are presented. This process has been included in the thesis as the problem was discovered in the end and as such the differences in the data in the various experiments could be explained and also replicated.

The process of optimizing the rheometer-system and parameters for the collagen gel initially produced high values for the elastic modulus (G') and the viscous modulus (G") during the first two parallels. The high viscoelastic moduli values were in the range of 1000- 100000 Pa. The viscoelastic moduli values recorded for the following two parallels were lower, in the value range of 0.1 - 100 Pa. This gave cause for concern as there was no visible overlap between the data sets for the two value ranges. As the parallels were all made with collagen from the same batch of dried collagen, the discrepancy was not likely to be caused by variations between the different vials of collagen. Due to the discrepancy in data the project needed to undergo a period of fault-tracking to ensure that the cause of the big spread in data values on different days could be explored, explained and replicated.

3.2.1.1 Initial observations and concerns

Before testing and comparing of collagen gel with and without G-block could commence the collagen gel it self needed to be optimized with regards to method of preparation, sample loading onto the rheometer and rheological parameters (strain and frequency). Collagen I is a protein that is capable of gelling with increasing temperature and pH is ≈ 7 (Djabourov et al. (1993) in aqueous systems.

Within the initial optimization period the first few parallels run on the rheometer with collagen alone gave unreasonable values for G' (elastic modulus), G" (viscous modulus) and δ (phase angle). The values for G' and G" were in the range of 1000- 100000 Pa (Table 3.2 "Collagen-Initial data"). Based on literature a more reasonable value range would be 0-1000 Pa. In an article by Zuidema et al. (2014) a collagen gel of 4 mg/ml did not exceed 200 Pa when subjected to a temperature hold of 30 minutes with temperature at 37°C, strain at 10% and frequency of 1 Hz. In Yang et al. (2009) a temperature ramp of 4- 37°C for 2 mg/ml collagen at constant stain and frequency (0.8% and 1 Hz respectively) yielded G' modulus values that did not surpass 100 Pa. It is therefor unlikely that a 2 mg/ml gel with a constant strain of 0.1% and constant frequency of 1 Hz should produce values in proximity of the 1000-100000 Pa range during a temperature ramp.

Table 3.2: Brief overview of rheological value range obtained during fault tracking process. The values listed are a general summary of the value range from the whole programmed sequence. The evaluation states if the results are reasonable or not reasonable based on previously known behavior of the sample, either via literature or previously recorded data in the lab.

	Value range (Pa)	Evaluation
Collagen- Initial data	10^3-10^5	Unreasonable
Collagen- Heat adjusted I	10^{-1}-10^2	Reasonable
Collagen- Heat adjusted II	10^3-10^5	Unreasonable
DPBS	10^{-2}-10^0	Reasonable
Glycerol	10^{-1}-10^2	Reasonable
Gelatin 5%	10^3-10^5	Unreasonable
Gelatin 5% with 4/40 cone	10^3-10^5	Unreasonable
Benecol (by author)	10^3-10^5	Unreasonable
Benecol (by Ulset)	10^2-10^4	Reasonable

The gels appeared to have already initiated the geling process before the rheometer could record the initial values for the G' modulus, G" modulus and phase angle. The absence of a recorded liquid to gel transition indicated that gelation either been initiated while the rheometer was in the process of stabilizing the temperature to 4°C after sample application, or before sample application to the rheometer. This temperature adjustment was instructed by the programmed sequence to take place before initial value recording could commence. Interestingly, the samples were observed as liquids upon application on the rheometer. This could point to gelling occurring while the rheometer was adjusting the temperature. Had there been a liquid to gel transition recorded there would have been a phase angle shift in which the phase angle would have gone from a high value (liquid-like) to a low value (elastic-like). The immediate high values for G' and G" gave cause for concern as this was clearly not a value range that was expected or reasonable of collagen gel. The first thing that was attempted was to evaluate potential heat sources and if an elimination of these would lead to lower viscoelastic moduli values and a detectable liquid to gel transition. The following measures were taken to minimize the samples exposure to heat:

1. Geometry was lowered down to the plate, the cone and plate were cooled down to 4° with a thermal cover and oil basin
2. Pipettes were placed in a fridge and cooled down for 15 minutes
3. Beaker and solutions for final mixture were cooled down well in advance
4. The metal cooling plate was chilled down to -40°C well in advance
5. The mixing beaker was placed on ice on top of the metal cooling plate during weighing
6. The solutions were kept on ice during the mixing process

By implementing those adjustments to the preparatory stage two successful parallels were run (Table 3.2 "Collagen- Heat adjusted I") and the viscoelastic moduli values were within a reasonable range. Following two successful parallels the high values reoccurred. The notion that potential added heat from the mixing process as the sole reason for the unusual results was discarded. It was evident that it was of importance to elucidate what the cause of the unreasonable viscoelastic moduli values were. However, it is worth emphasizing that this system proved to be very sensitive to heat and that attempting to maximize control over potential heat sources was important to ensure consistency between parallels.

3.2.1.2 Searching for the root cause

When embarking on a fault tracking process it is important to investigate one component at the time while attempting to keep the other components or parameters constant and undisturbed. After excluding heat addition as the sole reason for the unreasonable values the cone in the cone and plate geometry was the next component to be checked. Due to the viscoelastic moduli values varying from the reasonable range of 0.1-1000 Pa to the unreasonable range of 1000-100000 Pa, surface tension could be an influencing factor causing the recorded values to become distorted. The programmed sequenced used for the collagen gel (Appendix C.2.1) was utilized with both glycerol and DPBS as controls with the 1/40 cone. There was nothing pointing to surface tension causing any unwanted disturbances or elevated values with these two samples based on the recorded results. The G' and G" were low (0.01-1 Pa for DPBS and 0.1-100 Pa for glycerin) and the phase angle stayed at $\approx 90^\circ$ through the entire sequence for both samples. As such it was not probable that the high values recorded for the collagen gel could be attributed to surface tension.

Gelatin, which is a partially hydrolyzed version of collagen, was tested with the 1/40 geometry. A new sequence (Appendix C.2.2) was made to accommodate the different temperature needs required for gelatin. Collagen forms gel during increasing temperature and at pH = 7 while gelatin forms gel at a decreasing temperature (gelation for gelatin starts at $\approx 20^\circ$C) (Djabourov et al. (1993)).

The expectations for gelatin were for it to remain as a liquid (G">G', $\delta>45^\circ$) during the temperature ramp (60-20°C) and then during the temperature hold (1 hour at 20°C) a phase change was expected to occur (G'>G", $\delta<45^\circ$). There was no observed phase change during the temperature ramp or the temperature hold. Further, the rheometer recorded a G'>G" relationship and $\delta<45^\circ$ through out the entire sequence. The value range for G' and G" were located in the unreasonable range of 1000-100000 Pa. Interestingly, a 3.8% gelatin solution at 25°C, 10 rad s^{-1} ($\approx$ 1.6 Hz) and a strain of 5% should not exceed 500 Pa for G' in a two hours isothermal hold according to Ross-Murphy (1991). As such it is unlikely that a 5% gelatin solution should display values in the 1000-100000 Pa range for G' and G" at 0.1% strain and a frequency of 1 Hz in an isothermal (20°C) temperature hold of 1 hour.

The unreasonable values obtained were most likely not caused by the 1/40 cone. However,

this cone was in low demand at the lab and as such there was less data amassed with the 1/40 cone compared to the 4/40 cone in relation with gelatin. Because of this the 4/40 cone coupled with gelatin was opted for. This combination had proven to function well in previous projects. However, despite the change in cone, the values recorded for gelatin with the 4/40 cone were still high and in the 1000-100000 Pa range coupled with a low phase angle. This lead to the conclusion that the 1/40 cone was not likely to be the cause of the high G' and G" values (Table 3.2 "Gelatin 5% with 4/40 cone") as both the 1/40 and 4/40 cone gave unreasonably high values within the same value range.

A soft chewable cholesterol lowering tablet from Benecol (Raisio) (batch: 44000929), based on a patented delivery system called ConCordix (ConCordix), was used as a new control. The lab had extensive knowledge, established data and an optimized programmed sequence for the Benecol soft chew. It had been coupled with the 4/40 cone previously and as a consequence of that the 4/40 cone was utilized now in combination with the soft chew. As the 1/40 cone was not likely to be at fault and since the problem persisted when using two different programmed sequences it was of importance to check the data system and program to explore whether something was wrong with either the sequences (e.g. a bug) or the program that ran the tests. The need to check this was rooted in the fact that the collagen sequence set up was used as a template for the gelatin sequence. If there was something wrong with the collagen sequence it could potentially have been transferred over to the gelatin sequence.

The results for the Benecol soft chew were unreasonable and also devoid of any recorded liquid to gel transition with the 4/40 cone and the ConCordix sequence (Appendix C.2.3). The results for Benecol soft chew for a temperature ramp down (60-20°C) should show a G">G' at high temperatures, high δ and then a transition at around 35°C in which there should be a shift in the relationship between the moduli from G">G' over to G'>G" with a decrease in δ to below 45°. This outlined relationship did not occur. The rheometer documented instead high and stable values for the viscoelastic moduli in the 1000-100000 Pa range in all of the sections of the programmed sequence and displayed a complete temperature independence. In addition to this the recorded relationship between G' and G" were G'>G" through the entire programmed sequence. This would indicate that the sample was gel-like upon application meaning that it had the properties of a more solid-like material. This was in spite of the sample application to the pre-heated plate at 60°C and then subsequently ensuring that the soft chew melted to a high

viscous liquid on the plate. This range and reported recorded behavior were the same as seen in both the collagen and gelatin samples that exhibited unreasonable values.

The researcher who had extensive experience with the soft chews, Ann-Sissel T. Ulset, was involved after the soft chews exhibited unreasonable results. The researcher decided to run a new test on the soft chews to check if something had changed with the samples. The same amount of soft chew, the same geometry and the same sequence were used but on a different rheometer. The two rheometers were of the same make and model and as such the choice of rheometer used should in theory not have any impact on the data gathered given that both rheometers were functioning properly. However, when the researcher tested the soft chews the reasonable results outlined above were obtained. These results by Ulset raised the question of whether something was wrong with the rheometer utilized or if the procedure surrounding sample loading deviated between the author and Ulset. The loading procedure used by the author was described to Ulset. There were no apparent mistakes with the described procedure. Never the less, it was decided that both Dr. Nordgård and researcher Ulset should observe a sample loading of Benecol soft chew performed by the author. No mistakes were observed, but the program did record unreasonably high viscoelastic moduli values, low phase angle and a G'>G" relationship all through the sequence where loading was observed by Dr. Nordgård and researcher Ulset.

3.2.1.3 Identification and replication of root cause

The observation of the sample loading process yielded no further insight regarding the cause of the unreasonable values. Because of this it was decided that the researcher should test the gelatin sample on the rheometer primarily used in the fault tracking procedure. This was done in order to check if there was something wrong with the instrument itself or in the authors loading process that was yet undiscovered. The recorded results from the sample run by the researcher had lower G' and G" moduli values, higher δ values in the temperature ramp and a clear liquid to gel transition during the one hour temperature hold phase. This was in clear contrast to the data the author had recorded (outlined above). At this point the two data sets were compared. Certain values recorded by the rheometer were different between the data sets from the author relative to researcher Ulset. The first observation has already been presented, the differences in moduli and phase angle. The author got the 1000-100000 Pa value range while the values obtained by Ulset were below 100 Pa when testing the gelatin.

The error message K019 is a message that is reported when a sample has a low viscosity and it causes the machine to struggle with recording a correct response from the sample. This error code was absent in the authors data file. There was nothing in the data file that indicated that the gelatin sample tested by the author had a low viscosity at high temperatures. This error message was present in the beginning of the temperature ramp (60 -20 °C) for the data from Ulset. Further, the complex viscosity was at 10^{-2} for the test performed by Ulset and at 10^{1}-10^{3} for the authors test of gelatin. This further indicated that the sample by the author was more viscous than the sample from Ulset, which in turn was unreasonable as the gelatin used in both datasets were from the same stock.

The torque value represents the force the instrument has to use in order to move/rotate the cone. At the very beginning of the programmed sequence in the temperature ramp section when the temperature is at 60°C the torque of the rheometer for gelatin loaded by Ulset is at 5.6×10^{-10} Nm. At the same point for a gelatin sample loaded by the author the torque value is at 7.6×10^{-4} Nm. This would imply that something was causing the instrument to increase its applied torque to rotate the cone with the samples applied by the author. This could not be the sample placed between the cone and plate, as the gelatin samples were from the same stock and the Benecol soft chews were from the same batch. Furthermore, the samples all showed an unexplained temperature independence in the temperature ramps when applied by the author and the value range for the recorded viscoelastic moduli remained constant despite sample variation, except for DPBS and glycerin, which will be revised shortly. All potential causes of the unreasonable behavior had been checked and deemed to be unlikely to cause the unreasonable results. Since there was such a big difference in the recorded sample behavior between the author and the researcher something had to deviate between the two loading procedures.

The point in which the authors loading process deviated from the researcher was in the lowering of the oil basin. The oil basin is a part of the solvent trap, along with the thermal cover. The oil basin is placed on the neck of the cone and the thermal cover is placed around the neck of the cone onto the oil basin and it is used to minimize sample evaporation (Figure 3.16 shows a schematic drawing of the solvent trap). The unreasonable recorded values were caused by the improper lowering of oil basin.

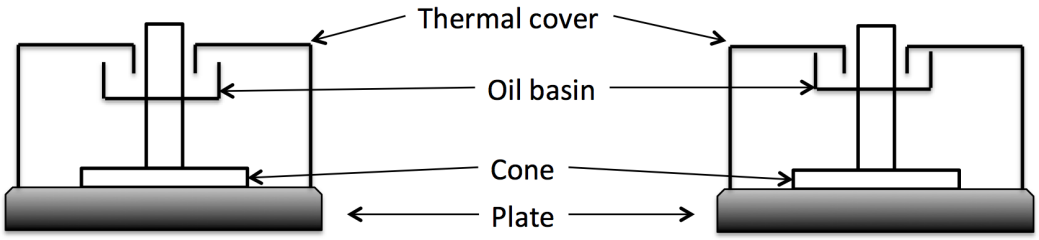

Figure 3.16: A schematic drawing of correct and incorrect positioning of the oil basin. Left image shows the correct position of the oil basin relative to the thermal cover. Right image shows the incorrect position of the oil basin relative to the thermal cover. Note the absence of a gap between the thermal cover and oil basin on the right image leading to contact between metal parts in the two objects.

The device used to lower the oil basin to ensure no contact between the basin and thermal covers was somewhat flexible. If the device was placed on top of the thermal cover (Figure 3.17 black lid) and the pressure applied was placed too far out on the sides of the device the device would not push the oil basin down (Figure 3.18 right image). Applying pressure too far out would in stead cause the center part of the device to rise. This failure to not lower the basin properly would in turn lead to the contact between oil basin and thermal cover (Figure 3.16 or 3.17, compare placement of oil basin in left and right image) and this would in turn would lead to the high values for G', G" and low δ. What was really recorded when the instrument reported high and stable G' and G" values was not the sample between the plate and the cone but the metal in the oil basin against metal in the thermal cover.

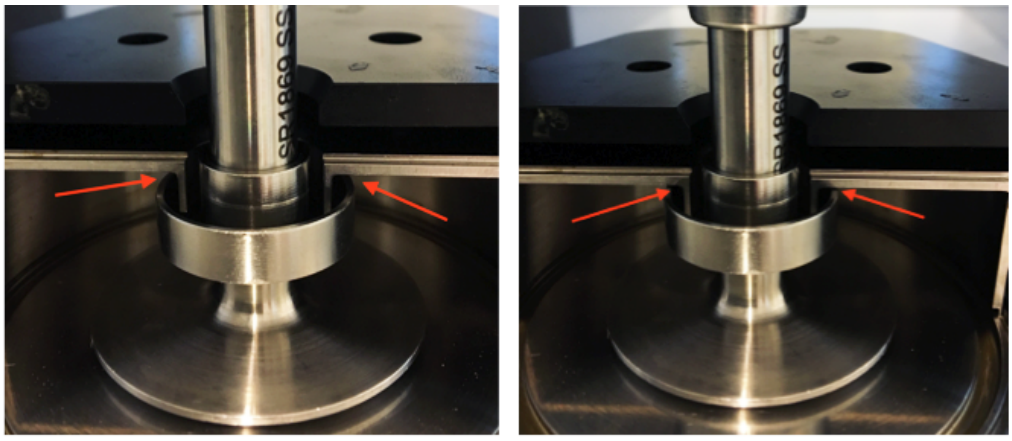

Figure 3.17: Left image shows the correct position of the oil basin relative to the thermal cover. Right image shows the incorrect position of the oil basin relative to the thermal cover. Note that there is an absence of a gap between the thermal cover and oil basin (arrows) on the right image leading to a contact between metal parts in the two objects.

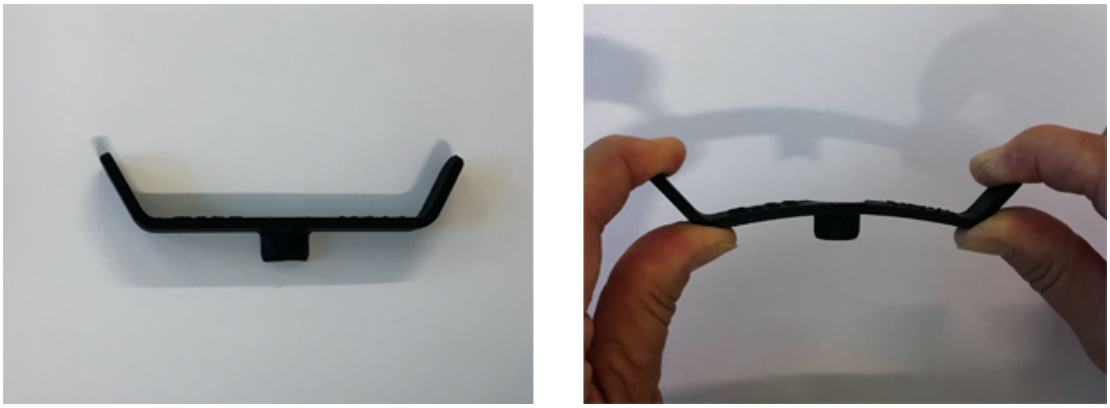

Figure 3.18: The instrument used to lower the oil basin slightly to ensure no contact between the thermal cover and oil basin occurs. The left image shows the device at rest and the right image shows the flexibility of the material the device is made of. The force needed to apply the bend illustrated here was rather small.

The discovery of the improper lowering causing there to be metal against metal between the oil basin and thermal cover made it possible to replicate the high values obtained initially. By deliberately ensuring that the oil basin and thermal chamber were in contact the same high viscoelastic moduli values and low δ, as outlined earlier, were obtained and the same high torque was reported by the instrument (Table 3.3). Interestingly, researcher Ulset did comment once during a strain sweep just before the fault-tracking was initiated that the machine produced some unusual noise. At that point, it was thought that it was just an artefact. It is now very likely that the sound was caused by the contact between the metal parts in the solvent trap.

Table 3.3: Brief comparison of the rheological values of collagen, gelatin and Benecol. The values listed are a general summary of the value range from the temperature ramp sequence of the collagen sequence, gelatin sequence and ConCordix sequence respectively. The results shown are from the data sets that reported the unexpectedly high values.

	Value range G' and G" (Pa)	Torque (Nm) value range
Initial data (collagen)	10^3 - 10^5	10^{-4} - 10^{-3}
Gelatin 5%	10^3 - 10^5	10^{-4} - 10^{-3}
Gelatin 5% with 4/40 cone	10^3 - 10^5	10^{-4} - 10^{-3}
Benecol (by author)	10^3 - 10^5	10^{-4} - 10^{-3}
Benecol (problem replication)	10^3 - 10^5	10^{-4} - 10^{-3}

Regarding the recorded values for DPBS and glycerin, the values were within a reasonable value range and the phase angle remained high through the entire sequence. It is likely that these samples as well as the two collagen samples that gave reasonable values were a direct cause of a proper lowering of the oil basin. Had glycerin and DPBS given the same high values as the rest

of the various samples the rest of the fault tracking process might have been different as these two liquids were supposed to be recorded as liquids within the parameters of the programmed sequence. However, the cause of the problem was discovered to be the improper lowering of the oil basin relative to the thermal cover in the end.

3.2.2 Rheological characterization of collagen gel

After discovering the cause behind the unreasonably high G' modulus values the testing of the effect of G-block added in collagen gel could begin. The programmed sequence for collagen consisted of a temperature ramp, temperature hold, frequency sweep and a strain sweep. In the temperature ramp the temperature was raised from 4 °C to 37 °C with an increase of 1 °C/min and a constant strain and frequency (0.1 % and 1 Hz respectively). Here the gelling kinetics were explored. In the temperature hold both temperature, strain and frequency were kept constant (37 °C, 0.1 % and 1 Hz respectively) for five hours. The temperature hold part allowed for recording of the development and setting of the gel over time. In the frequency sweep the frequency was no longer held constant at 1 Hz but increased from 0.01 to 10 Hz while the temperature and strain were kept constant (37 °C and 0.1 % respectively). If a gel is within the LVR the gel should display a G' >G" relationship (Zhong and Daubert (2013)). In the strain sweep the amount of strain was no longer held constant at 0.1% but instead increased from 0.01% to 100% while the temperature and frequency were kept constant (37 °C and 1 Hz). Strain sweeps yield information about the LVR of the sample and the non-LVR of the sample. In the non-LVR of the sample the sample will no longer gives a constant stress response to applied strain. Three parallels of collagen gel were run on three consecutive days, they are referred to as A1, A2 and A3.

It is reported by Djabourov et al. (1993) that the minimum collagen content in a solution to make a gel is 1.5 mg/ml and that the gelling starts above 4°C given that the pH >4. This means that gelation of collagen is achieved by modifying the thermodynamic conditions. Here the collagen concentration was at 2 mg/ml and the pH was ≈ 7.

3.2.2.1 Temperature ramp

The samples were observed to be liquid-like upon application and because of that it was expected that the following events were to occur: while the temperature was low (e.g. lower than 10-15°C) the phase angle >45° and G" >G'. When the temperature was high enough a transition phase would occur where the phase angle would be at 45° and the G' ≈ G". After the transition phase the phase angle would become <45° and G' >G" (Figure 3.19). The outlined relationships were seen in sample A3, but not A1 or A2 and will be discussed in greater detail below. It was also expected that all three parallels would exhibit a sigmoid shape when the G' modulus plotted on a logarithmic Y-axis. This occurred for sample A2 and A3 but not sample A1.

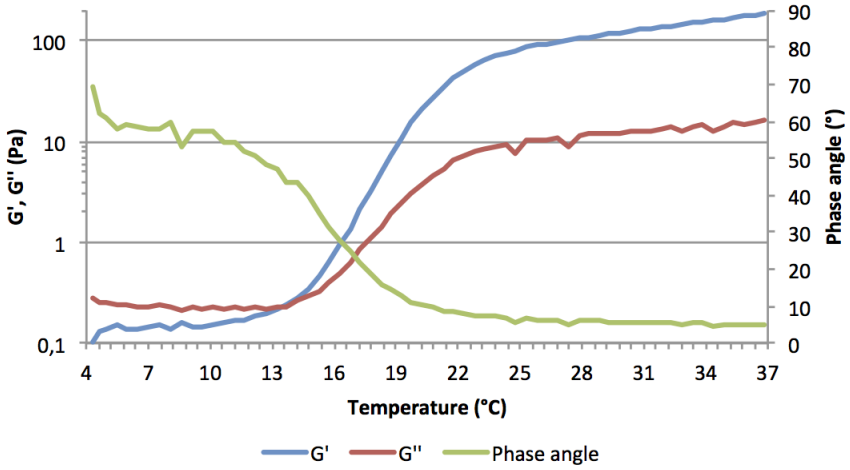

Figure 3.19: Expected behavior for collagen gel in a temperature ramp (4-37°). The expectations were for a transition point to occur where the phase angle (green line) goes from high to low as a function of increased temperature as well as a shift in the G' (red line) G" (blue line) relationship from G" >G' to G' >G". Strain and frequency were kept constant at 0.1% and 1 Hz respectively and the temperature was increased from 4-37°C with an increase of 1°C/min. The left Y-axis shows the elastic (G') and viscous (G") moduli values in Pa, the right Y-axis shows the phase angle in degrees (°) and the X-axis shows the temperature in Celsius (°C). Note that the left Y-axis is logarithmic. The sample shown is A3.

The temperature ramp (Figure 3.20) showed a low and similar G' for all three parallels from 4°C til 19°C. All three parallels showed an increase in G' modulus as the temperature was increased from 19°C up to 37°C. Interestingly, parallel A2 only reached 61 Pa at the end of the temperature ramp while parallel A3 was at 187 Pa and parallel A1 ended up at 112 Pa. This meant that G' for parallel A2 was only 32 % of parallel A3 while G' for parallel A1 was only 60% of parallel A3 at the end of temperature ramp (Table 3.4). This points to a big discrepancy, with regards to gel development as a consequence of increased temperature, between the parallels and it will be

revisited shortly.

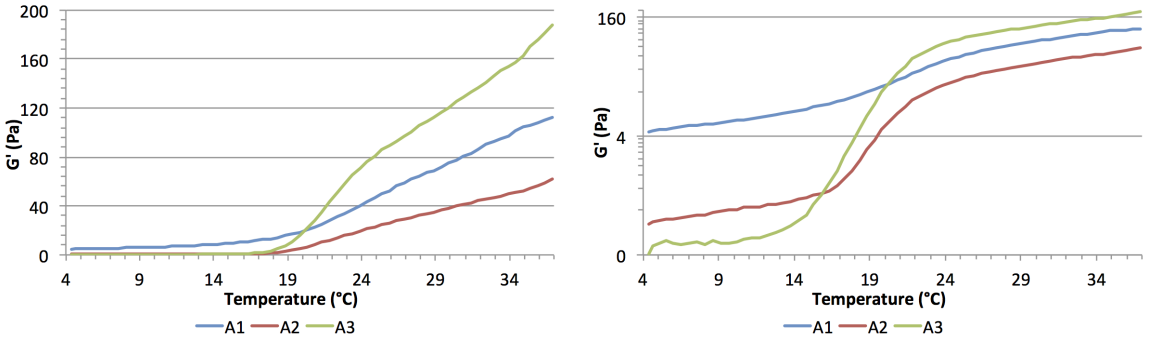

Figure 3.20: Temperature ramp for three parallels of collagen gel. Strain and frequency were kept constant at 0.1% and 1 Hz respectively and the temperature was increased from 4-37°C with an increase of 1°C/min. The X-axis shows the temperature in Celsius (°C) The Y-axis on the left graph is non-logarithmic and on the right graph the Y-axis is logarithmic.

Table 3.4: Overview of the start and end values of three parallels for collagen during temperature ramp (4-37°C (1 °C/min)) with regards to elastic modulus (G') and phase angle.

Parallel	Name	G' (start)	G' (end)	Phase angle (start)	Phase angle (end)
1	A1	4.5 Pa	112 Pa	21°	4°
2	A2	0.2 Pa	62 Pa	45°	5°
3	A3	0.1 Pa	187 Pa	69°	5°

At the start of the temperature ramp the phase angle for parallel A1 was at 21°, for A2 it was at 45° and for A3 it was at 69° (Table 3.4). If the phase angle is <45° at a given frequency then the sample has a solid-like behavior and if the phase angle is >45° at a given frequency the sample has a liquid-like behavior. At the end of the temperature hold the phase angle for A1 was at 4°, for A2 at 5° and for A3 at 5° indicating solid-like behavior. It is interesting to observe that the three parallels had very different phase angles at the start of the temperature ramp but ended up with phase angles of 4° and 5°. The difference in the initial recorded values for the phase angle versus the similarity of phase angle values recorded at the end of the temperature ramp could possibly be linked with differences in the development of the gel, possibly relative to time and temperature. During the temperature hold that followed the temperature ramp presented here the sample A2, which had the lowest G' modulus value at the end of the temperature ramp surpassed sample A1 in the temperature hold this could indicate a potential lag in the gel development (Figure 3.21).

Due to the low initial recorded values for the phase angle regarding samples A1 and A2 the

samples appeared to already have started the gelling process before the rheometer had initialized its recording of data hence, no recorded liquid to gel transition was observed. This could indicate that the gelling process had begun before either the instrument had started recording or before the sample was applied. In parallel A3 there was a phase change in which the G" was greater than G' and with a phase angle of 69° in the beginning. The liquid to gel transition could be observed at 17-20°C. At this temperature range G">G' becomes G' >G" and the phase angle drops dramatically until it reaches 5° at 30°C (Figure 3.19).

A potential reason regarding the absence of recorded liquid to gel transition, why it was not observed in all three parallels and in addition, why there was a discrepancy between the parallels, could be because this particular system was very temperature sensitive. The volume of applied sample (325 μl) was relatively small, even when great precautions were taken to minimize heat sources, the sample would potentially only needed a small heat transfer to raise its temperature and initiate the gelling process before recording by the rheometer could commence. The large value span for both G' modulus value and phase angle between the parallels through out the entire programmed sequence could be a consequence of this heat sensitivity.

Forgacs et al. (2003) reported that temperature sensitivity could affect the reproducibility of data when the same collagen stock was utilized on consecutive days and stored at 4°C. It is unclear whether the stock in the article was acidic or neutralized when stored as a stock solution, but if it was acidic the findings regarding the formation of microfibrils are very interesting and might offer a potential explanation regarding the discrepancy in recorded data between parallels within the same batch. In that paper it is mentioned that there could be a slow formation of microfibrils that accumulate over the course of several days. Forgacs et al. (2003) further reported that this would cause the viscoelatic moduli (G' and G") to increase with time. Further, they noted that measurements performed on the same day on the other hand resembled each other closely. It was observed here that the walk-in fridge where the collagen stock was kept would at certain times record a higher temperature than 4°C (highest noted down was 8°C) and this could possibly affect the formation of the above mentioned microfibrils.

Further, the difference could also be a consequence of potential heterogeneity in the dissolved acidic collagen solution as 2 ml of a 0.1% solution of acetic acid (HAc) was added to a vial of dried collagen. The acidic solution was left for minimum 48 hours at 4°C before the solution was very gently stirred, to avoid the formation of disturbing air bubbles, before the required amounts

of solution were extracted. It could be that the gentle stirring was not enough to ensure a uniform solution. By buying vials of pre-dissolved collagen in acid this potential problem could have been reduced. However, given that the findings reported by Forgacs et al. (2003) are relevant to acidic collagen stock this might pose a problem regarding the use of acidic pre-dissolved collagen and the potential of microfibril formation which could in turn affect the viscoelastic moduli unfavorably. Furthermore, a drawback of acidic pre-dissolved collagen is the lack of control over both the collagen concentration and environmental factors that the solution might have been exposed to (e.g. temperature, moisture and unwanted shaking causing air-bubbles). Utilizing collagen dissolved in-house the concentration and environmental factors are better controlled. However, it could be interesting to check if pre-dissolved collagen yielded any different results with regards to ensuring less spread between parallels.

3.2.2.2 Temperature hold

The temperature hold of 5 hours was initiated by the programmed sequence straight after the temperature ramp ended. The strain and frequency were kept constant at 0.1% and 1 Hz respectively and the temperature was kept isothermal at 37°C. As mentioned in the temperature ramp, the A2 sample was initially the sample with the lowest rate of increase in G' modulus value in the temperature ramp. In the temperature hold however (Figure 3.21) it is sample A1 that is the lowest while A2 shows a higher rate of increase in G' modulus value. The reason for this behavior and the reason for why A1 is here so much lower than A2 and A3 is unclear. A1 did have the lowest phase angle (21°, Table 3.4) at the start of the temperature ramp, indicative of solid-like behavior at the given frequency (1 Hz). Furthermore, the sample A1 exhibited noise between 80-130 minutes, these are thought to be artefacts. A possible explanation regarding the differences seen in the three gels during the 5 hour hold time could be caused by how the different gels develop, form and set at different rates. By prolonging the temperature hold the G' modulus values for the three parallels could possibly become more similar. However, these gels were made with the same reagents and prepared the same way by following the same steps in the same order. Because of this the gels should not show such differences in development and rate of development as recorded and shown here.

The sample A3 showed a higher rate of increase in G' than parallel A1 and A2. The peak recorded at 20-30 minutes was followed by a sharp decrease (Figure 3.21) before the G' modulus value

continued to rise almost linearly as a function of temperature hold time. This initial peak for A3 could have been caused by a slip between the geometry and sample as a consequence of for instance a water film forming on top of the sample or below it. This recorded slip and potential water film could in turn possibly be caused by a slight syneresis. It is however not certain as it could also just be a potential artefact since the G' modulus kept slowly increasing again after the sharp decrease. Syneresis is a spontaneous contraction of gel where an expulsion of solvent from the pores of the gel occurs without the evaporation of solvent (Scherer (1989)). When syneresis occurs the recording from the instrument will be distorted because of an absence of contact between the gel surface and the metal surface of the cone causing a sort of "slip" (Picout and Ross-Murphy (2003)). It is also likely that the instrument would then measure the values for the water film that would form between the geometry and the sample. This water film would most likely have low G' modulus values. This hypothesized slip and possible syneresis does however not fully explain the behavior of the samples as the G' modulus value keep increasing during the isothermal hold time after the slip caused by the potential syneresis.

The increase in G' observed for A1 and A2 in the beginning and also at 200 minutes in the temperature hold could possibly be a consequence of sample drying. Sample drying occurs at the exposed edge of the cone resulting in a film of polymer in stead of a gel (Picout and Ross-Murphy (2003)). This could cause the rheometer to record the polymer film values (Figure 3.21 e.g. large increase in G' for A2 at 190-220 min). The use of a solvent trap should ideally prevent sample drying. However, it was observed upon sample unloading that the oil basin had very little liquid left despite it having been completely filled with silicone (DowCorning 200/10cS fluid) at the beginning of the programmed sequence. This could potentially cause the air inside of the chamber to migrate out and air from outside of the chamber to leak in causing a drier environment inside of the chamber and allowing for sample drying to take place.

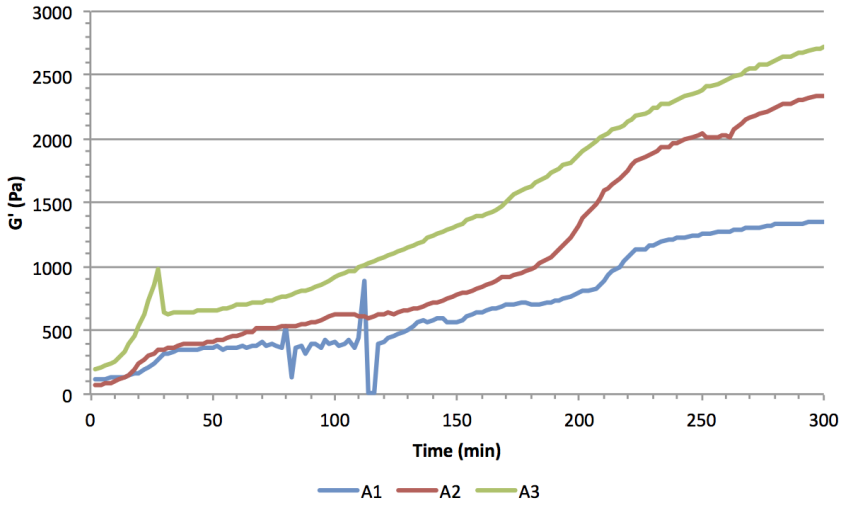

Figure 3.21: Temperature hold section (5 hours) for three parallels of collagen gel. The X-axis shows the time in minutes and the Y-axis shows the development of the elastic modulus (G') during the five hour isothermal hold time at 37 °C, 0.1% and 1 Hz.

Regarding the possibility of syneresis discussed previously, syneresis was visually observed in the vials containing the rest of the collagen solutions after rheometer application in all three samples. The remainder of the sample from A3 was left in an incubator at 40°C for three hours in a closed vial. When it was taken out again there was a separation of gel and solvent (Figure 3.22). The same observation was made when a sample (A2) was left undisturbed at room temperature for 4 hours in a closed vial. The degree of syneresis is estimated to be between 40-50%, meaning that it was observed almost an equal amount of solvent relative to the amount of gel. This degree of syneresis is unlikely to have occurred with the sample on the rheometer as such a high degree of syneresis would have caused the geometry to loose contact with the sample. This lack of contact would have caused the rheometer to measure low G' modulus values as it likely be measuring the G' modulus value of a liquid that would have been expulsed from the gel and not the gel it self. That liquid would also most likely have a low viscosity, at it would consist of a high degree of water. It is unclear why there was such a high degree of syneresis in the vial and further, it is unclear why this was not recorded in the sample on the rheometer. It is as mentioned unlikely that this degree of syneresis would have occurred between the cone and plate never the less, it is interesting to note that there was such a high degree of syneresis in the remaining gel in the vial. Had such a high degree of syneresis occurred on the rheometer it is unlikely that the G' modulus value would have kept increasing as it did for all three samples through out the 5 hour isothermal hold.

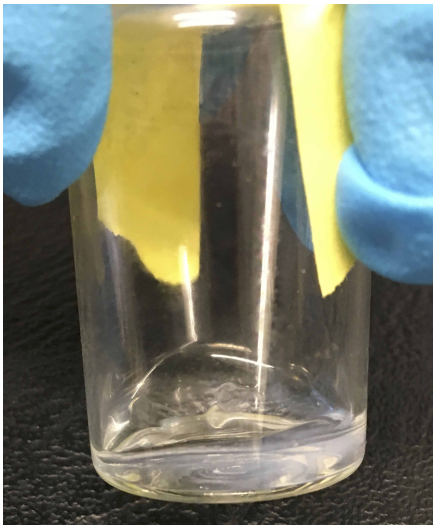

Figure 3.22: Observed changes in collagen gel sample A3 when left to incubate at 40 °C for three hours. The vial was placed at an approximate 30° angle and when taken out and placed on a bench there was a separation of gel and solvent. The gel (turbid) can be seen in the front of the vial and the solvent is seen in the back of the vial. It is estimated that the degree of syneresis is between 40-50% meaning that it was observed almost an equal amount of solvent relative to the amount of gel.

There was no apparent equilibrium reached or recorded during the 5 hour temperature hold (Figure 3.21). Had equilibrium been reached the values for G' would have leveled off and stayed stable through the remaining part of the temperature hold. It is mentioned in Picout and Ross-Murphy (2003) that for some gels there is no final value of G' modulus as log [G'] appears to increase indefinitely when plotted as a function of log (time).

During the subsequent frequency sweep and strain sweep the G' keep increasing slightly (Table 3.5). The value displayed from the frequency sweeps was obtained 15 minutes after the value for the temperature hold and the strain sweep value was obtained approximately 9 minutes (for A2 and A3) and 13 minutes (for A1) after the frequency sweep value. The values for the frequency sweep and strain sweep corresponded to a frequency of 1 Hz and 0.1% strain (Figure 3.23). Through the 24-28 minutes the G' modulus value for A1 increased with 2%, G' modulus value for A2 increased with 0.6% and the G' modulus value for A3 increased with 4.7% (Table 3.5). Since the three parallels were made with the same reagents and prepared following the same protocol the samples were expected to resemble each other closer than what they did. As A2 showed almost no increase in G' modulus during the 24 minute interval it could be that the gel was close to reaching an apparent equilibrium while parallel A3 had an increase of 4.7% during a 28 minute interval suggesting that this gel was further away from reaching an apparent equilibrium while A1 was located somewhere in between the two other parallels with regards to

increase in G' modulus over time. By increasing the isothermal hold time it the equilibrium could possibly been reached. It is however also possible that, as previously mentioned, this collagen gel is unable to reach a final G' modulus value.

Table 3.5: The G' modulus value at the end of the temperature hold, the G' modulus value in the frequency sweep at 0.1% and 1 Hz and the G' modulus value in the strain sweep at 0.1% and 1 Hz as well as the total increase (%) in G' modulus from the end of the temperature hold to the value obtained in the strain sweep.

Modulus	Name	Temperature hold end	Frequency sweep	Strain sweep	Overall increase (%)
G'	A1	1352 Pa	1370 Pa	1380 Pa	2.0
G'	A2	2328 Pa	2340 Pa	2342 Pa	0.6
G'	A3	2725 Pa	2804 Pa	2860 Pa	4.7

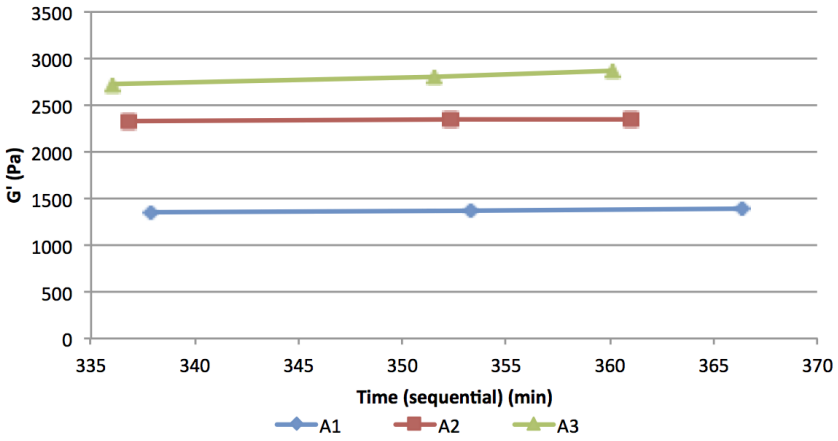

Figure 3.23: The G' modulus value for three parallels (A1, A2, A3) of collagen gel at the end of temp hold (first datapoint), in the frequency sweep at frequency of 1 Hz and 0.1% strain (second datapoint) and the G' modulus value in the strain sweep at a frequency of 1 Hz and 0.1% strain (third datapoint). The X-axis displays the time in minutes and it shows the time where the recorded values were obtained within the programmed sequence. The Y-axis shows the development of the elastic modulus (G') through three datapoints during temperature hold, frequency sweep and strain sweep.

3.2.2.3 Frequency sweep

The frequency sweeps were performed in the range of 0.01 to 10 Hz at constant temperature (37°C) and strain (0.1%). The strain was kept within the LVR of the sample. Performing frequency sweeps on a gel will ideally give a parallel relationship between G' and G" moduli with a G' >G" relationship and the gels response to frequency should be constant within the LVR (Kavanagh and Ross-Murphy (1998)).

All of the three samples showed unstable values at the lowest frequencies (0.01-0.1 Hz), these values were accompanied by a K019 error message that pointed to inertia effects (Figure 3.24). The K019 error code has been discussed in greater detail within the fault-tracking process part of this thesis (Chapter 3.2.1.3). Such a message is reported when the machine is unable to find and record a correct response from the sample. From 0.5 Hz til 10 Hz the samples displayed a parallel relationship between G' and G" with G' >G" and a low phase angle (<5°). The G' >G" relationship coupled with a low phase angle indicated that the samples had a more solid-like behavior than a liquid-like behavior in that range of the frequency sweep. The samples showed a slight increase in modulus during the frequency sweep, this could suggest some frequency dependence due to the presence of some dynamic elements.

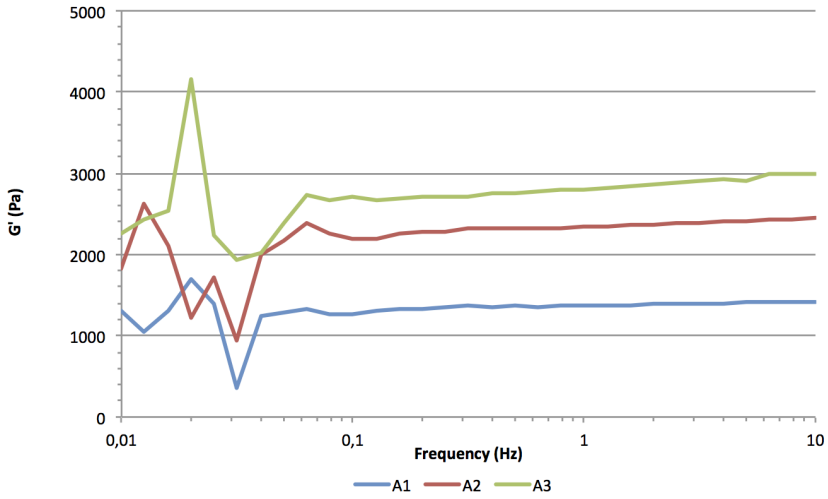

Figure 3.24: Frequency sweep (0.01 - 10 Hz) for three parallels of collagen. The X-axis shows the frequency in hertz and the Y-axis shows the development of the elastic modulus (G') during the sweep at constant temperature (37 °C) and strain (0.1 %). Note that the X-axis is logarithmic.

The system seems to exhibit some frequency dependence, as previously mentioned, due to an increase in G' modulus value in the frequency range of 1-10 Hz in the frequency sweep. In an article by Branco da Cunha et al. (2014) collagen I in a 1.5 mg/ml concentration appeared to also give a frequency dependent response when the strain was kept constant at 0.5% and the frequency sweep was from 0.01-10 Hz. This further strengthens the observation of potential frequency dependence in the collagen gels here. The increase for A1 was at 3.7%, for A2 it was a 4.5% increase and for A3 it was a 6.7% increase (Table 3.6, Figure 3.25). The time it took to record the 1-10 Hz range was approximately 4 minutes. The time between the frequency sweep measurement where the frequency was 1 Hz and the strain was at 0.1% and the strain sweep measurement where the frequency was 1 Hz and the strain was at 0.1% was approximately 8

minutes.

Table 3.6: The recorded G' value at 1 Hz and at 10 Hz as well as the increase in G' between 1 Hz and 10 Hz during the frequency sweep. The strain and temperature were kept constant (0.1% and 37°C). It took the program 4 minutes to go from 1 Hz to 10 Hz.

Name	G' at 1 Hz	G' at 10 Hz	Increase (%)
A1	1370 Pa	1422 Pa	3.7
A2	2340 Pa	2450 Pa	4.5
A3	2804 Pa	3004 Pa	6.7

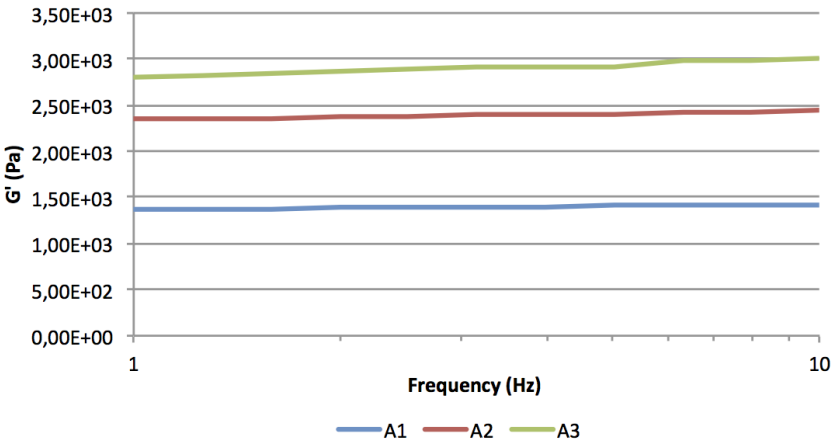

Figure 3.25: The development of G' modulus (Y-axis) for three parallels (A1, A2, A3) of collagen gel as a function of increasing frequency (1-10 Hz). The time it took to go from 1 Hz to 10 Hz was 4 minutes and the rheometer recorded responses at a 30 second interval. The X-axis shows the frequency in hertz and the Y-axis shows the development of the elastic modulus (G') during the sweep at constant temperature (37 °C) and strain (0.1%). Note that the X-axis is logarithmic.

By comparing the percentage increase between the G' modulus value at the end of the temperature hold at which the frequency was 1 Hz and the strain was 0.1% with the G' modulus value in the strain sweep where the frequency was at 1 Hz and the strain was at 0.1% the results show (Table 3.7) that the percentage increase in G' modulus value within the frequency sweep was much higher than the percentage increase in G' modulus value overall. Further, it is worth noting that the time span between the values used to calculate the overall percentage increase was approximately 25 minutes for parallel A2 and A3 and approximately 30 minutes for A1, as opposed to 4 minutes for the frequency sweep. The increase in 5 minutes for the A1 parallel relative to the A2 and A3 is most likely caused by the rheometer, the reason behind the 5 minute increase is unclear. It could be that the instrument had to do some calibrations that were not recorded in the data file.

By performing a linear regression on the graph in figure 3.23 and solving the trendline for the time interval 340-344 minutes the percentage increase is even lower (Table 3.7). Since both the full 25 and 30 minute interval as well as the arbitrary 4 minute interval within the 25 or 30 minute interval also proved to have a lower percentage increase than the percentage increase obtained in the frequency sweep it is highly likely that there is a frequency dependent response in the gel when it is exposed to a frequency sweep at a fixed strain that is within the LVR of the sample.

Table 3.7: The recorded G' value at 1 Hz and at 10 Hz as well as the increase in G' between 1 Hz and 10 Hz during the frequency sweep. The strain and temperature were kept constant (0.1% and 37°C). It took the program 4 minutes to go from 1 Hz to 10 Hz.

Name	Increase (%) frequency sweep	Increase (%) overall	Increase (%) 4 min.
A1	3.7	2.0	0.3
A2	4.5	0.6	0.1
A3	6.7	4.7	0.8

Given that the increase recorded for G' modulus value during the frequency sweep is a frequency dependent response from the sample this would indicate that the gel is a physical gel. A physical gel will display a frequency dependence, but no cross-over between the two moduli and G' modulus will remain greater than G" modulus (Stading and Hermansson (1990)). On the other hand, the frequency dependent behavior could also be a consequence of a response of entangled networks and that the transition from G' >G" to G" >G' was not seen because the frequency range was not wide enough. Because of that it could have been interesting to increase the frequency range from 10 Hz til 100 Hz and see how the material would react at higher frequencies and if the increase in the G' modulus would continue or if the relationship between G' and G" would change. As the instrument recorded K019 for all three parallels intermittently at the lowest frequencies (0.01-0.05 Hz) it is unlikely that there would be any benefit in lowering the start frequency. It is also worth noting that the samples did not reach an apparent equilibrium during the 5 hour hold period and it could also be a contributing factor to the increase in G' modulus recorded during the frequency sweep.

3.2.2.4 Strain sweep

Following the frequency sweep a strain sweep was initiated by the program in which the strain was increased from 0.01 to 100% while the frequency and temperature were kept constant at 1 Hz and 37°C. The samples showed a G' modulus that appeared to be strain independent from 0.01 to 0.3%, confirming that a constant strain at 0.1% for the rest of the programmed sequence was within LVR of the sample (Figure 3.26). At 0.5% the decrease in modulus is visible and at 5% strain the samples show signs of damage as the G' modulus is decreasing. At 10% strain the G' modulus for the samples is well outside of the LVR (Figure 3.26). A sample is within the LVR when the response of the sample (here G' modulus) remains constant to the applied strain (Zhong and Daubert (2013)). At 50-100% strain the recorded G' modulus values for all three samples show unstable values. The G' modulus values recorded in this strain range (50-100%) are thought to be artefacts caused by the rheometer as it is not able to correctly predict the response of the sample to the applied strain causing a fluctuation in recorded values. The phase angle did not rise any higher than 10° during the strain sweep for any of the parallels. Had the maximum applied strain been increased it could possibly have shown that the gels response to strain (G' modulus) would have been different, it could potentially show a catastrophic failure and this would cause the phase angle to give a quick increase in response that would possibly have exceeded 45° while the G' and G" moduli values would have exhibited a dramatic rate of decrease.

The destruction of a sample, the break, is indicative of a true or strong gel since such gels fail or break at some point just beyond their maximum stress response (here G') causing the gel to be destroyed. A good example of such behavior is Jell-O. If deformed enough (e.g. hacked with a spoon or fork) the Jell-O will break into little pieces. These pieces need to be heated if the gel parts are to merge together into a larger gel again. Weak gels and polymer solutions on the other hand can flow if subjected to a large enough deformation and they are able to reform given sufficient time to recover without being reset (Ross-Murphy (1984)). In the frequency sweep the gels appeared to show a frequency dependent response. This could imply that the gels were physical gels as physical gels show a frequency dependent response (Stading and Hermansson (1990)). The weak and strong gels mentioned above both fall within the category of physical gels. Because of this it is quite possible that the samples are physical gels. Whether these gels are strong or weak gels could potentially be determined by the following conditions: 1) how the

samples respond to strain sweeps that included applied strains well outside of the LVR of the sample, 2) whether or not the samples underwent a catastrophic break in the strain sweep and 3) whether the samples showed signs of reforming if an additional temperature hold had been added to the programmed sequence. If the G' modulus for collagen gel had increased over time that would have been indicative of a weak gel. Had it not shown any increase in G' modulus it could have been indicative of a strong gel.

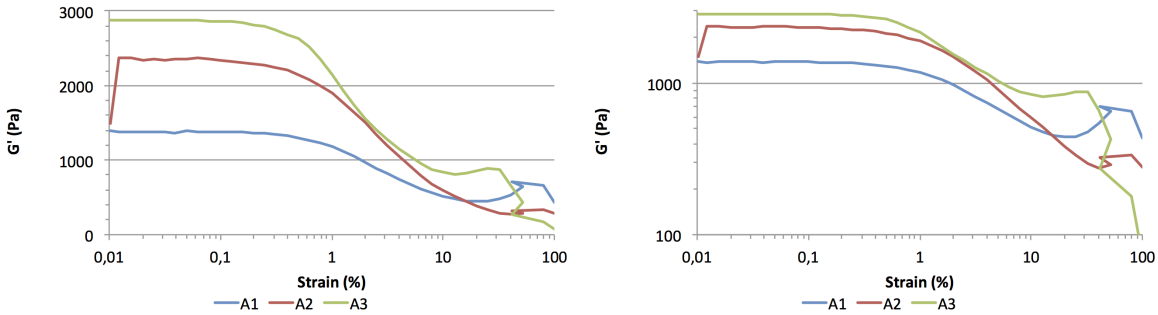

Figure 3.26: Strain sweep (0.01-100%) for three parallels of collagen gel. Temperature and frequency were kept constant at 37°C and 1 Hz respectively and the strain was increased from 0.01 to 100%. The Y-axis for the left graph is non-logarithmic and on the right graph the Y-axis is logarithmic. Both left and right graph shows the development of G' modulus value as a function of increased applied strain. The X-axis on both graphs is logarithmic and shows the amount of applied strain.

When unloading the sample there could be observed some turbid pieces, these were likely to be parts of the collagen gel (Figure 3.27, circle with G attached). Some of the sample left on the cone was slightly sticky when touching it with a Q-tip and after carefully running a Q-tip over the plate a few bits of gel were visible while the rest of the liquid was easily absorbed by the Q-tip. All of this hinted to the gel breaking apart during the strain sweep.

Figure 3.27: Observation upon sample unloading after a finished programmed sequence. The absence of an intact gel confirms the destruction recorded in the strain sweep. The circles with the G shows pieces of gel. A Q-tip has been gently moved around to absorb some of the liquid to make it easier to see the gel pieces.

3.2.3 Rheology- characterization of collagen gel with G-block

The rheological characterization of collagen gel with added G-block was performed in the same manner as the rheological characterization of collagen gel alone, except for an additional temperature hold after the strain sweep was added (see Appendix C.2.1 and C.2.4 for a comparison of the programmed sequences). The programmed sequence thus consisted of a temperature ramp, a temperature hold (5 hours), a frequency sweep, a strain sweep and a temperature hold (1 hour). This additional added temperature hold of 1 hour pertained to 3 of the 4 parallels within the 2.50, 1.25 and 0.62 mg/ml of G-block added. In the temperature ramp the temperature was raised from 4 °C to 37 °C with an increase of 1 °C/min and a constant strain and frequency (0.1 % and 1 Hz respectively). Here the gelling kinetics were explored. In the temperature hold both temperature, strain and frequency were kept constant (37 °C, 0.1 % and 1 Hz respectively) for five hours. The temperature hold part allowed for recording of the development and setting of the gel over time. In the frequency sweep the frequency was no longer held constant at 1 Hz but increased from 0.01 to 10 Hz, temperature and strain were kept constant (37 °C and 0.1 % respectively). If a gel is within the LVR the gel should display a G' >G" relationship (Zhong and Daubert (2013)). In

the strain sweep the amount of strain was no longer held constant at 0.1% but instead increased from 0.01% to 100%. Strain sweeps yield information about the LVR of the sample and the non-LVR of the sample. In the non-LVR of the sample the sample will no longer gives a constant stress response to applied strain. The last part of the sequence was an additional temperature hold of 1 hour. By implementing this the potential reformation of the gel could be documented. A weak gel or a polymer solution is able to reform given sufficient time whilst a strong gel needs to be reset (e.g. by reheating) in order to potentially be reformed (Ross-Murphy (1984)).

The concentration of G-block in the solution was at either 5.00, 2.50, 1.25 or 0.62 mg/ml and the G-block powder was dissolved in DPBS. For the 5.00 mg/ml concentration of G-block there were 3 parallels and for the rest of the concentrations there were 4 parallels. The first parallel for 2.50, 1.25 and 0.62 mg/ml G-block had collagen taken from another batch than the rest of the samples within that concentration (Table 3.8 parallel names with asterisk). These parallels did not have the additional temperature hold incorporated into the programmed sequence (Appendix C.2.1 was without additional temperature hold). Within each concentration of G-block there were large variations between each parallel with regards to recorded G' modulus values, because of this each parallel is shown in this section of the results and discussion. Some of the potential variations between parallels have been addressed in the section pertaining to collagen gel without G-block, and it is very likely that the previously discussed reasons e.g. heat sensitivity, potential sample-heterogeneity and possible microaggregates are valid here as well.

Table 3.8: Overview of the various parallels within the 4 concentrations of dissolved G-block. The G-block was dissolved in DPBS stock and then added in the collagen gel during the making of the gel. The asterisk (*) denotes that the sample was from another batch than the rest of the parallels within a given concentration.

[G-block] (mg/ml)	Parallel	Parallel name
5.00	1	B1
5.00	2	B2
5.00	3	B3
2.50	1	C1*
2.50	2	C2
2.50	3	C3
2.50	4	C4
1.25	1	D1*
1.25	2	D2
1.25	3	D3
1.25	4	D4
0.62	1	E1*
0.62	2	E2
0.62	3	E3
0.62	4	E4

3.2.3.1 Temperature ramp

All parallels within the four concentrations (Table 3.8) show an increase in G' modulus value at around 24°C and none of the G' modulus max values are over 200 Pa (Figure 3.28). The majority of the samples appeared to have initiated the gelling process either before the sample was applied to the rheomter or before the instrument could record the transition. This meant that the rheometer would record a phase angle of less than 45° and a G'>G" relationship at the given frequency. As the initial stage of the gelling process was not captured it is difficult to pinpoint exactly at what time and temperature the gelling process was initiated at. The rheomter was set up to start recording at 4°C after sample application. However, there was also a temperature calibration programmed into the sequence. That meant that if the temperature was higher or lower than 4°C after sample application the rheometer would first strive to reach 4°C before commencing with recording of values. This could in turn lead to a delay in recording causing the system to potentially miss the initial stage of the gelling process.

The continuous increase in G' modulus values observed after 24°C (Figure 3.28) for all parallels in all concentrations is indicative of the gelling process progressing and that interactions between the different components in the solution are taking place and a network is continuously formed as a result. It is likely that if the gel had set during the temperature ramp there would be a plateau where the G' modulus value would become constant given that the sequence max temperature was low enough to avoid denaturation.

The 4 concentrations of G-block added to collagen gel gave some slightly different responses relative to one and other. Collagen with a 5.00 mg/ml concentration of G-block have higher G' modulus max than the other concentrations and it seems to have a more clearly defined point in which the G' growth begins (Figure 3.28 top left graph). Collagen with 2.50 mg/ml of G-block (Figure 3.28 top right graph) had lower G' modulus max values than collagen with 5.00 mg/ml G-block but it did seem to have a similar G' modulus max value as D3 and D4 as well as E2 and E3 (Figure 3.28 bottom left and bottom right). The C1 parallel within the 2.50 mg/ml concentration was made from another batch of collagen and this potential batch variation could possibly explain the slightly different and flatter curve exhibited by C1 when compared with C2, C3 and C4.

Collagen with 1.25 mg/ml G-block added had two data sets with high G' max (D3 and D4) and two data sets where G' max was low (D1 and D2) (Figure 3.28 bottom left graph). For the high G' max the values were close to 70 Pa and for the low G' modulus max the values were at 15 Pa and 27 Pa respectively. This means that D1 is only 21% of D3 and D2 is only 39% of D3. The D1 parallel was done in August while the D2, D3 and D4 were performed in October. As such it could be expected that there would be some slight variations between D1 and D2, D3, D4 as the samples were made from different batches of collagen. However, since D1 was only 21% of D3 it is unlikely that batch variation was the only cause. The recorded values for D2 were quite low with D2 at only 39% of D3. This can however not be explained by potential batch variation as D2, D3 and D4 were from the same batch. By looking at the graphs the growth of D2 follows the trend exhibited by D3 and D4 but with a lower G' value (Figure 3.28 bottom left graph). A potential explanation could be, as mentioned in an earlier part of the thesis, sample heterogeneity from the acid dissolved collagen leading to a lower concentration of collagen in sample D2. To check for this pre-dissolved collagen in acid could have been ordered and tested to see if it too exhibited large variations between parallels. If the pre-dissolved collagen in acid also exhibited

the same inter-concentration variation another potential explanation for the variation between D2, D3 and D4 could be the temperature sensitivity of the samples. On the other hand, it could be that D2 was in fact better temperature controlled than D3 and D4 causing the D2 to increase its G' modulus slower than D3 and D4. The program was able to record a liquid to gel transition for the D2 and D3 samples but not for the D1 and D4 samples, indicating that the D1 and D4 samples had the gelling process initiated before the rheometer could record it. As such there could possibly be several factors influencing the variations seen between the parallels, the above mentioned potential causes have been discussed in great detail previously (see Chapter 3.2.2.1 for more information).

Collagen with 0.62 mg/ml G-block did also exhibit 2 low and 2 high G' modulus max values. The E1 parallel had collagen from another batch than the rest of the parallels and along with E4 exhibited low G' max values. The potential of batch variations is something that could be relevant for E1 here (Figure 3.28 bottom right graph) as E1 does, together with C1 and D1, exhibit a flatter curve than the other parallels within the given G-block concentrations. None of the parallels within the 0.62 mg/ml G-block concentration exhibited any recorded liquid to gel transition, suggesting that the transition had already taken place prior to application and/or recording. The E4 parallel exhibited a lower value than E2 and E3 and all three were made from the same batch. Parallel E4 does however seem to follow the same shape as E2 and E3 but just at a low G' modulus value. It could be that what was discussed for parallel D2 with regards to temperature control is also relevant here for sample E4. It could also be that the issue of heterogeneity of amount of dissolved collagen in acid per sample is an issue here. A non-homogeneous sample could potentially have caused sample E4 to have a lower concentration of dissolved collagen relative to E2 and E3, leading to a lower G' modulus value as a consequence of less available collagen to form the gel and possibly leading to a weaker gel.

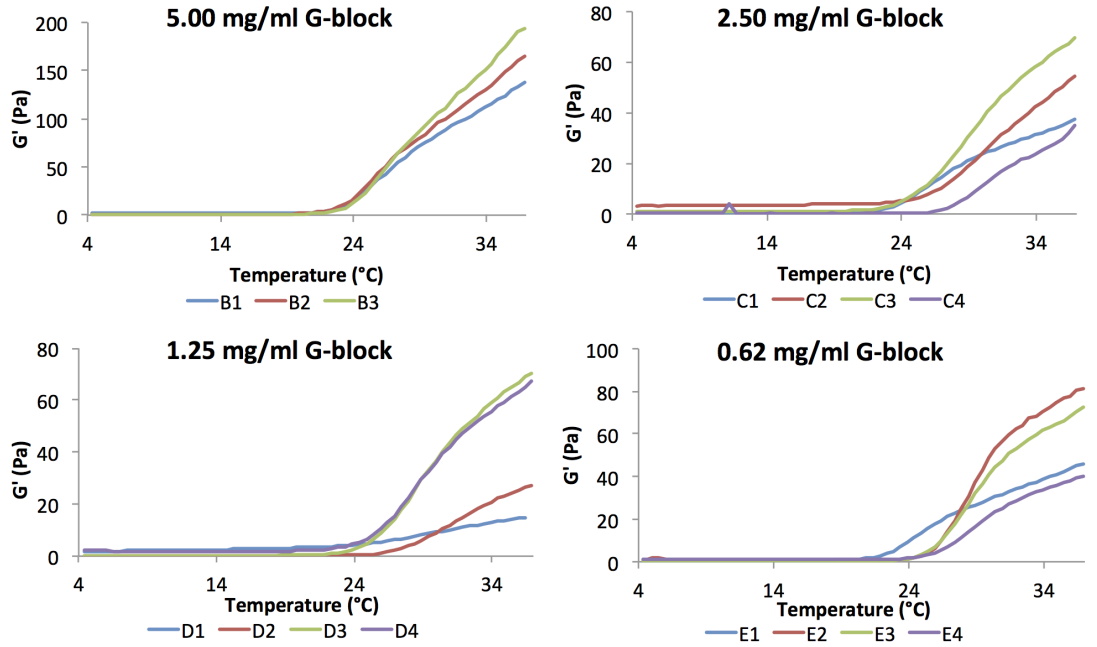

Figure 3.28: Temperature ramp for collagen with added G-block. The strain and frequency were kept constant at 0.1% and 1 Hz respectively and the temperature was increased from 4-37°C with an increase of 1°C/min. The graps show the development of the G' modulus value as a function of increased temeperature. The Y-axis displays the G' modulus value in Pascal (Pa) and the X-axis displays the temperature (in °C). The top left graph is for 3 parallels of 5.00 mg/ml G-block added in collagen gel and the top right graph is for 4 parallels of 2.50 mg/ml G-block in collagen gel. The bottom left graph is for 4 parallels of 1.25 mg/ml G-block added in collagen gel and the bottom right graph is for 4 parallels of 0.62 mg/ml G-block in collagen gel. Note that the C4 parallel had a K019 error recorded up until 24°C.

3.2.3.2 Temperature hold (5 hours)

The temperature hold lasted 5 hours (300 minutes) with temperature, strain and frequency kept constant at 37°C, 0.1% and 1 Hz respectively. None of the samples within the four G-block concentrations displayed any apparent equilibrium. The continuous increase in G' modulus value indicated that the samples were still undergoing a gelling process through the whole temperature hold of 5 hours. As mentioned previously, with regards to collagen gel alone, some gels never reach an apparent equilibrium and never fully set. Picout and Ross-Murphy (2003) mentions that for some gels there is no final G' modulus value as log [G'] appears to increase indefinitely when plotted as a function of log(time). In order to explore this the hold time could have been increased to see if a longer hold time would have allowed the gel to set.

Through the 5 hour temperature hold the phase angle for all of the samples stayed below 10° (Table 3.9 phase angle (start) and phase angle (end)) and the relationship between the viscoelastic

moduli remained G' >G" with G' having a much higher modulus for all concentrations and parallels. At the end of the 5 hour temperature hold all of the samples had a phase angle below 3° (Table 3.9 phase angle (end)). All of this indicated solid-like behavior of the samples at the given frequency and strain. It is interesting to note that there appears to not be a clear link between G' modulus value at the beginning of the hold time and the G' modulus value at the end of the hold time. It does not appear for instance that a high G' modulus value at the beginning is a clear indication of a high G' modulus value at the end of the hold time. This could possibly have something to do with intra-batch and inter-batch variations and also temperature sensitivity. The cause of this is however not clear at this point. However, by using the data for 5.00 mg/ml G-block (3.9) as an example the parallel with the lowest start value for G' modulus, B1, is the one with the highest G' modulus value at the end of the temperature hold. Parallel B3 had the highest G' modulus start value and ended up at a value that was 82% of B1 despite that the start value of B1 was 75.6% of the start value of B3.

Table 3.9: Overview of the various concentrations of dissolved G-block in DPBS stock added in the making of collagen gel. The asterisk (*) denotes that the sample was from another batch than the rest of the parallels within a given concentration. A dashed line (-) denotes that the value is coupled with an almost continuously K019 error code that surrounds the value of interest and is as such not an applicable value.

Parallel name	G' (start)	G' (end)	Phase angle (start)	Phase angle (end)
B1	140.3	2069	4.83	2.01
B2	157.3	908.2	4.85	1.95
B3	185.5	1696	4.60	1.86
C1*	39.52	987.9	4.99	2.9
C2	60.39	3131	5.55	1.68
C3	72.05	1406	7.65	2.34
C4	71.86	-	9.25	-
D1*	16.2	1670	4.03	2.01
D2	29.20	2482	6.24	1.61
D3	72.44	3328	6.28	2.00
D4	76.69	2645	5.92	2.12
E1*	49.01	4751	5.55	1.94
E2	79.64	1235	6.59	2.49
E3	75.15	2070	6.57	2.01
E4	41.48	620	5.85	2.66

Two of the samples showed signs of potential sample drying (B3 at 100 minutes and C2 at 150

minutes) in addition, there were indications of recorded slip in some of the samples. Parallel B1 (Figure 3.29) shows a sharp increase coupled with a sharp decrease at approximately 50 minutes into the temperature hold. The same trend is seen in C2 and E1 at 50 minutes as well (Figure 3.29). This could possibly be a slip caused by a potential water film between the geometry and the sample. For C3 a K019 error message was reported intermittently from 75 to 160 minutes and for C4 the error message was reported intermittently from 150 to 300 minutes. It is interesting to note that both the G' modulus values and the phase angle values just before and just after the values that have the K019 error message recorded are also affected by it in the sense that they too show unreasonable G' modulus and phase angle values relative to adjacent recorded values. As such the intermittent K019 error affects the values within the given intervals almost continuously. Within this part of the programmed sequence the stress controlled instrument was attempting to maintain a constant strain and to measure the resulting assumed stress response of the sample. If the rheometer fails to predict the correct response disturbances in the recording can occur in the form of sudden peaks and dips in the graph. These recordings are thought to possibly be artefacts caused by the instrument as it fails to predict the correct stress response from the sample to the applied constant strain.

There were observed some signs of drying out on sample C2 visually. When unloading the sample a white ring could be observed at the edge of where the cone had covered the plate. Further, there was noted a low amount of silicone in the oil basin at the end of the programmed sequence. This could indicate drying and could possibly lead to the elevated values seen in C2, relative to the rest of the parallels, from 150 minutes and through the remainder of the temperature hold section. If what was seen in sample C2 was sample drying the G' modulus values recorded could have been caused by a potential polymer film at the edge of the cone (Picout and Ross-Murphy (2003)). The use of a solvent trap should have prevented sample drying, however, as the level of silicone in the basin was low upon programmed sequence completion this could have caused the air inside the chamber of the solvent trap to migrate out and been replaced by air from the outside environment. This would lead to a drier environment inside of the chamber, leading to potential sample drying. A potential countermeasure could be to seal the section where the two parts of the thermal cover are coupled together with tape to ensure that the lid is secured tightly on both sides. Another potential countermeasure could have been to add fluid in the oil basin if the fluid level is low in an effort to maintain a high level of fluid in the basin to ensure that the environment inside the thermal covers remained saturated with damp air. A problem with this

however is that it could potentially interfere with the recording of data as the instrument would potentially be disturbed, because the thermal cover would most likely have to be removed to allow for visualization of oil basin before and during fluid addition to the basin.

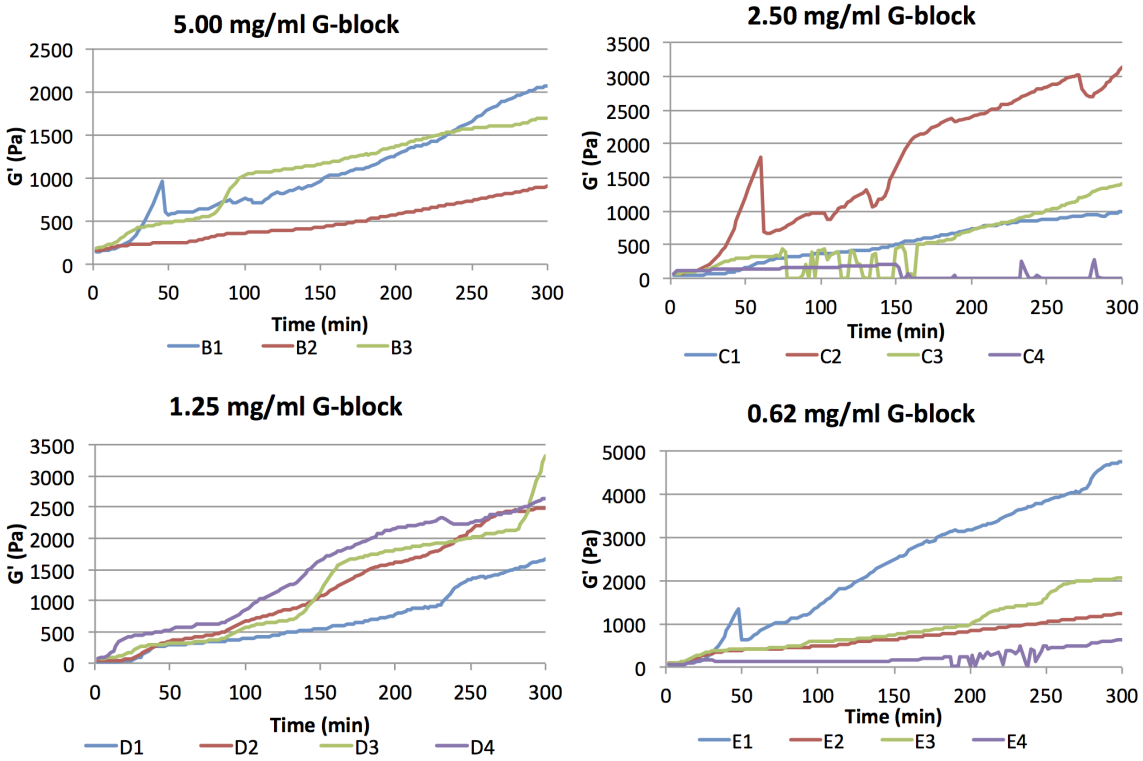

Figure 3.29: Temperature hold of 5 hours for collagen gel with G-block added. The temperature, strain and frequency were kept constant at 37°C, 0.1% and 1 Hz respectively. The top left graph is for 3 parallels of 5.00 mg/ml G-block added in collagen gel and the top right graph is for 4 parallels of 2.50 mg/ml G-block in collagen gel. The bottom left graph is for 4 parallels of 1.25 mg/ml G-block added in collagen gel and the bottom right graph is for 4 parallels of 0.62 mg/ml G-block in collagen gel.

For 1.25 and 0.62 mg/ml G-block in collagen gel there is as previously mentioned no apparent equilibrium or setting of gel during the 5 hour hold period (Figure 3.29 bottom right and bottom left graphs). The 0.62 mg/ml G-block E1 (Figure 3.29 bottom right, E1) shows signs of an elevated rate of increase in G' modulus when compared to the other G' values for parallels within the other three concentrations. However, there were no signs of the sample drying when unloading the sample. It is unclear why the E1 parallel had such an elevated rate of increase in G' modulus value compared to the other parallels within the 0.62 mg/ml concentration or compared to the parallels within the other 3 concentrations.

After sample application to the rheometer the remainder of the samples were kept in closed vials, the upper half of the vial and cap were wrapped in parafilm, in room temperature for 4 hours.

Upon inspection there appeared to be syneresis in all of the samples as well as a slight turbidity in the gel (Figure 3.30). This degree of syneresis (30-40%) means that the amount of solvent relative to the amount of gel was at 30-40% solvent and 60-70% gel in the vial. This degree of syneresis is unlikely to have occurred on the rheometer as such a high degree of syneresis would potentially have caused the rheometer to loose contact with the sample. This lack of contact would have lead the rheometer to measure low G' modulus values as it would probably be measuring the G' modulus of the solvent which in it self was very watery with a likely low viscosity. It is unclear why this high degree of syneresis was observed in the vial. It is also unclear why this degree of syneresis appeared to not happen in the rheometer as the recorded values do not suggest a clear syneresis response (Figure 3.29). Had there been a clear syneresis response there would have been recorded an elevated rate of increase then a sharp decrease in G' modulus value. The G' modulus value would then have remained relatively low as the rheometer would have been measuring the G' modulus value of the liquid that had been expulsed from the gel and not the gel it self. Here there were observed some peaks in the various parallels but after the peaks the G' modulus value kept increasing, indicating that other factors (e.g. drying) were possibly taking place.

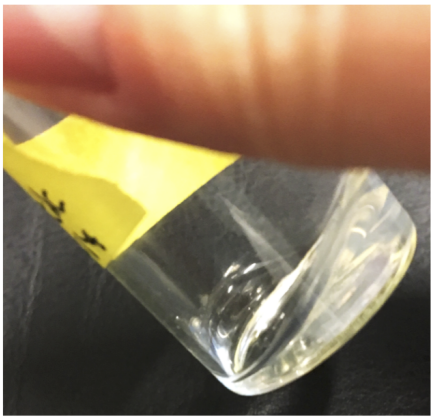

Figure 3.30: Observed changes in collagen gel with 5 mg/ml G-block when left undisturbed at the bench for 4 hours. A separation of gel and solvent can be observed. The gel (turbid) can be seen in the front slightly to the right of the vial and the solvent is seen in the back slightly to the left of the vial. It is estimated that the degree of syneresis is between 30-40% meaning that it was observed an amount of solvent of 30-40% relative to the 60-70% of gel.

3.2.3.3 Frequency sweep

A frequency sweep (0.01-10 Hz) was performed after the 5 hour temperature hold. All parallels at all concentrations showed instability from 0.01 til 0.1 Hz that is coupled with a K019 error

code which was recorded at an almost constant rate. As the instrument attempted to maintain a constant strain and measure the stress response through the frequency sweep it is likely that the instability is a consequence of a failure to accurately predict and record the response of the sample at such a low frequency. After 0.1 Hz and up to 10 Hz all of the parallels within each concentration show a slight increase in G' modulus value, this could be as a consequence of increased frequency (Figure 3.31) hinting at a potential frequency dependence. The phase angle stayed below 10° for all parallels in all concentrations at the 0.1-10 Hz interval indicating solid-like behavior in the given frequency range. This coupled with a G' >G" relationship further strengthens the impression of a solid-like behavior of the gel within the frequency range. The continuous increase in G' could possibly be caused by the gel still being in the process of setting as there was no apparent equilibrium reached during the temperature hold of 5 hours or it could be a consequence of a slight frequency dependence.

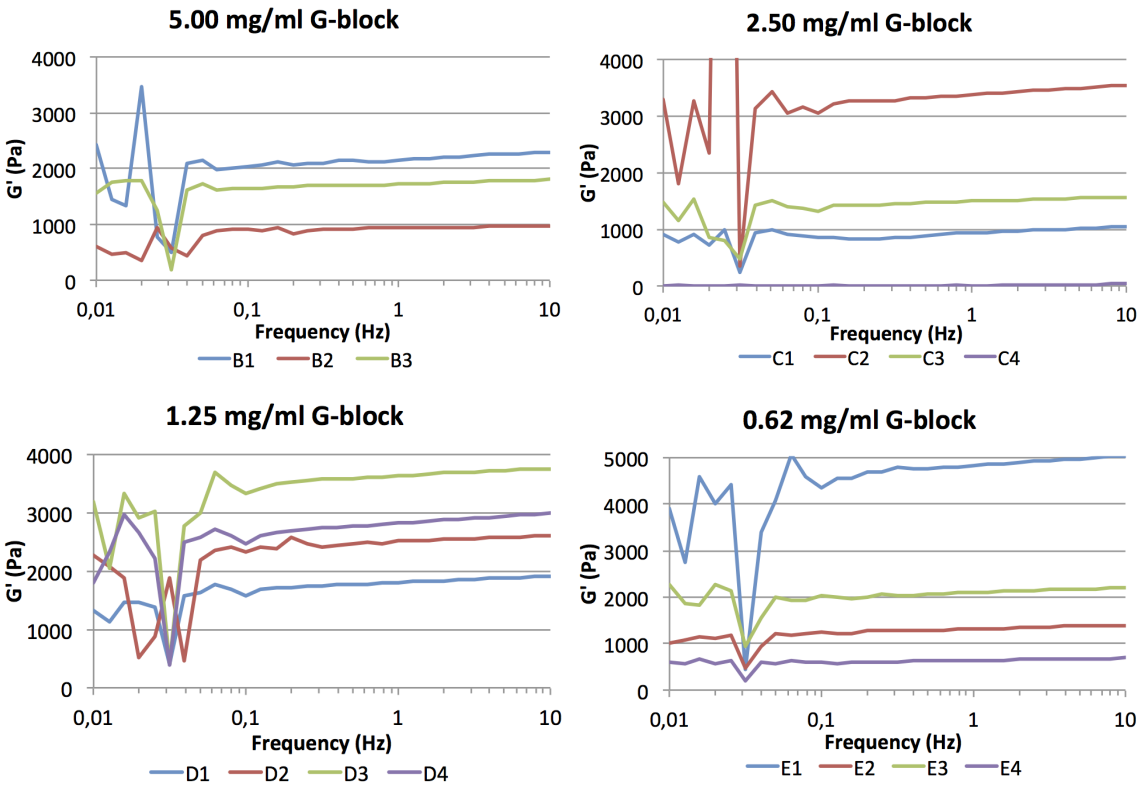

Figure 3.31: Frequency sweep for collagen gel with G-block added. The temperature and strain were kept constant at 37°C and 0.1% respectively. The graphs shows the development of the G' modulus value (in Pa) as a function of increased frequency. The frequency was increased from 0.01 to 10 Hz. The top left graph is for 3 parallels of 5.00 mg/ml G-block added in collagen gel and the top right graph is for 4 parallels of 2.50 mg/ml G-block in collagen gel. The left graph is for 4 parallels of 1.25 mg/ml G-block added in collagen gel and the right graph is for 4 parallels of 0.62 mg/ml G-block in collagen gel.The bottom left graph is for 4 parallels of 1.25 mg/ml G-block added in collagen gel and the bottom right graph is for 4 parallels of 0.62 mg/ml G-block in collagen gel.

As the samples all appear to show an increase in G' modulus value between 1-10 Hz in the frequency sweeps the percentage increase in this frequency interval has been calculated. The time it took for the rheometer to record the values in the 1-10 Hz interval was 4 minutes. For the most part the percentage increase is between 4-12% (Table 3.10 "Increase (%) freq. sweep"). If the sample is frequency insensitive it would be expected that the recorded values would remain fairly constant through at least the 1-10 Hz range in the frequency sweeps. However, a point can be made as to what percent increase is an acceptable range for the sample to be categorized as frequency independent versus frequency dependent. Since all of the samples except for D2 and D3 have an increase of over 4% in 4 minutes in the range of the 1-10 Hz in the frequency sweep it could be argued that this is a marked increase in such a short time span and that there is a potential frequency dependence.

In order to investigate this potential frequency dependence the samples appear to exhibit the same thing was done here as for collagen gel alone. The G' modulus value for the end of the temperature hold, in which both strain and frequency were held constant at 0.1% and 1 Hz respectively, was noted down. In the frequency sweep the G' modulus value at a frequency of 1 Hz and 0.1% stain was noted down and the same was done at a frequency of 1 Hz and 0.1% stain for the strain sweep (Figure 3.32). The time it took between the recording of the end value for the G' modulus in the temperature hold and the value in the strain sweep at 1 Hz and 0.1% strain was approximately 30 minutes. By using the same method as in Chapter 3.2.2.3 where the percentage increase was calculated for the full 30 minutes the results (Table 3.10 "Increase (%) overall) do not imply that the increase in G' modulus seen in the frequency range of 1-10 Hz in the frequency sweep is a consequence of frequency dependence. However, when performing a linear regression of all the graphs then using the trendline values obtained and solving for hypothetical values at 340 minutes and 344 minutes giving a 4 minute interval the percentage increase is below 2% for all the parallels within the different concentrations (Table 3.10 "Increase (%) 4 min"). The lower percentage increase obtained in the 4 minute interval from the trendline relative to the 4 minute interval in the frequency sweep does suggest that there is potentially some frequency dependence recorded in the sample for the frequency sweep at 1-10 Hz. This is because the increase seen in the 4 minute interval in the frequency sweep is greater than the calculated increase in a 4 minute interval based on the trendline for the 30 minute interval.

Table 3.10: Percentage increase in frequency sweep (1-10 Hz), overall percentage increase from the last recorded datapoint in temperature hold through to datapoint 1 Hz and 0.1% strain in both the frequency and strain sweep and a percentage increase in a 4 minute interval based on a linear regression with calculated values from 340-344 minutes. The time it took the program to go from 1 Hz to 10 Hz was 4 minutes. The asterisk (*) denotes that the sample was from a different batch relative to the other parallels within the given concentration.

Name	Increase (%) freq. sweep	Increase (%) overall	Increase (%) 4 min
B1	5.8	6.4	0.9
B2	4.6	4.4	0.6
B3	4.4	2.3	0.3
C1*	12.1	- 34.5	-3.7
C2	4.2	10.8	1.9
C3	4.3	6.0	0.9
C4	-	-	-
D1*	5.6	- 17.1	-1.9
D2	3.2	1.6	0.4
D3	1.1	7.6	1.1
D4	6.1	8.0	1.2
E1*	4.0	- 111.2	-7.5
E2	6.0	9.2	1.4
E3	5.0	2.4	0.4
E4	7.5	7.6	1.1

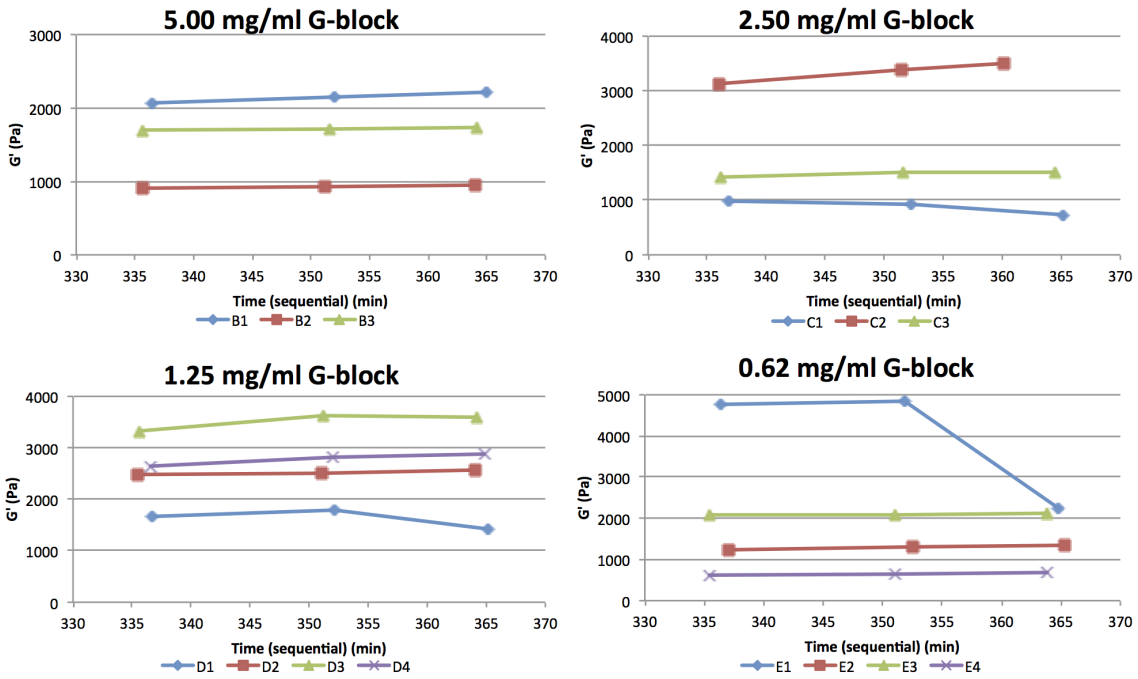

Figure 3.32: The graphs show how the G' modulus value develops over time from the end of the temperature hold (datapoint 1), via a datapoint the frequency sweep where the frequency is 1 Hz and the strain is 0.1% (datapoint 2) as well as a datapoint in the strain sweep where the frequency is 1 Hz and the strain is 0.1% (datapoint 3). The top left graph is for 3 parallels of 5.00 mg/ml G-block added in collagen gel and the top right graph is for 4 parallels of 2.50 mg/ml G-block in collagen gel. The left graph is for 4 parallels of 1.25 mg/ml G-block added in collagen gel and the right graph is for 4 parallels of 0.62 mg/ml G-block in collagen gel.The bottom left graph is for 4 parallels of 1.25 mg/ml G-block added in collagen gel and the bottom right graph is for 4 parallels of 0.62 mg/ml G-block in collagen gel. The X-axis shows the sequential time of the programmed sequence from the first to the third datapoint, and at what specific times the datapoints were taken at. The Y-axis shows the G' modulus values in Pascal.

Given that the increase recorded for the G' modulus value during the frequency sweep is a frequency dependent response from the sample this could indicate that the gel is a physical gel. A physical gel will display a frequency dependence, but no cross-over between the two moduli and the G' modulus will remain greater than the G" modulus (Stading and Hermansson (1990)). On the other hand, the frequency dependent behavior could also be a consequence of a response from entangled networks. It could be that the transition from G' >G" to G" >G' was not recorded because the frequency range was not wide enough. Because of that it could be interesting to increase the frequency range from 10 Hz til 100 Hz and record the response of the samples at higher frequencies. If the increase in the viscoelastic moduli continued and if the relationship between G' and G" changed that would imply an entangled solution. If the relationship between the viscoelastic modui remained the same and the moduli kept increasing that would imply that the samples were physical gels based on the frequency dependence. As the machine recorded

K019 for all three parallels intermittently at the lowest frequencies (0.01-0.05 Hz) it is unlikely that there would be any benefit in lowering the start frequency. It is also worth noting that the samples did not reach an apparent equilibrium during the 5 hour hold period and it could also be that the continued gel-process was a contributing factor to some of the increase in G' modulus recorded during the frequency sweep.

It is unclear why some of the samples showed a marked decrease between the datapoint obtained for the frequency sweep and strain sweep relative to the other parallels within the given concentration (Figure 3.32 C1, D1, E1). However, it is interesting to note that all the parallels with a marked decrease in G' modulus value were all from a different batch than the other parallels within the given concentration. Additionally, C1, D1 and E1 were in fact from the same vial of collagen gel. It is possible that something was different with this vial of dissolved collagen relative to the other vials. The collagen vial for C1, D1 and E1 was in addition from a different batch than the other vials used for the rest of the parallels within the given concentrations. This decrease in G' modulus value between the frequency sweep and strain sweep for C1, D1 and E1 relative to the other parallels could have been caused by some type of batch variation. It could also potentially be an artefact, it is however puzzling if this potential artefact occurred only for the samples C1, D1 and E1. Especially since C1, D1 and E1 were from a different batch than the rest of the parallels.

3.2.3.4 Strain sweep

A strain sweep immediately followed the frequency sweep. The temperature and frequency were kept constant at 37°C and 1 Hz respectively. The range for the strain sweep was from 0.01 to 100%. In the rest of the programmed sequence the strain was kept constant at 0.1% and it is here confirmed that the constant strain is within the LVR for this gel.

Increase in strain from 0.01 to 0.5% shows that the G' modulus has a constant response to strain for all parallels at various concentrations (excluding 3.33 top right, C4 and 3.33 bottom right, E1). For B1 and D2 an K019 error code was recorded at 0.01% while C4 had a constant K019 error code from 0.01 to 0.2%. After 0.5% strain the gels appear to begin to exhibit a reduction of the G' modulus value as a response to the applied strain. The variations with regards to G' modulus values between the parallels within the same concentrations are again thought to be

possibly caused by potential heat transfer before sample application and this is propagandized through the programmed sequence and affects the results for the entire programmed sequence. The increase and subsequent decrease recorded between 10-100% is most likely artefacts as the rheometer had problems with correctly predicting the samples response to applied strain as the applied strain was outside of the samples LVR (Figure 3.33).

The destruction of a sample, the break, is indicative of a strong gel. Such gels fail or break at some point just beyond their maximum stress response to applied strain (here G' modulus value), or strain response to applied stress. The break or fail causes the destruction of the gel. A weak gel or a polymer solution can respond with flow if subjected to a large deformation, and they can be reformed given sufficient time while a strong gel on the other hand needs to be reset (e.g. by reheating into a liquid solution) (Ross-Murphy (1984)).

In the frequency sweep the gels appeared to show a frequency dependent response. This could imply that the gels were physical gels as physical gels show a frequency dependent response (Stading and Hermansson (1990)). The weak and strong gels mentioned above both fall within the category of physical gels. Because of this it is quite possible that the gel samples here are physical gels. Whether these gels are strong or weak gels could potentially be determined by the following conditions: 1) how the samples respond to strain sweeps that include applied strains outside of the LVR of the sample, 2) whether or not the samples underwent a catastrophic break in the strain sweep and 3) whether the samples showed signs of reforming if an additional temperature hold had been added to the programmed sequence. If the G' modulus for the gel had increased over time during a temperature hold following a strain sweep that could have been indicative of a weak gel. Had it not shown any increase in G' modulus it could have been indicative of a strong gel.

The gels here show signs of damage at 0.5% as previously mentioned. The sample B1, B2, B3 and C2, show a dramatic increase in both phase angle and G" modulus and a dramatic decrease in G' modulus after 10%. This indicates that the sample exhibited a high viscoelastic liquid character at and after the point of the catastropic break and a probable destruction of the gel. The other samples within each concentration exhibited no increase in phase angle or G" modulus and no apparent change in the relationship between G' and G" (remained as G'>G"). By increasing the maximum strain the outlined behavior could potentially occur, as all the samples showed a marked decrease in G' modulus after 0.5%. In order to further investigate whether the gels were

weak gels or strong gels an additional temperature hold was implement for the 2.50, 1.25 and 0.62 concentrations of G-block added in collagen gel.

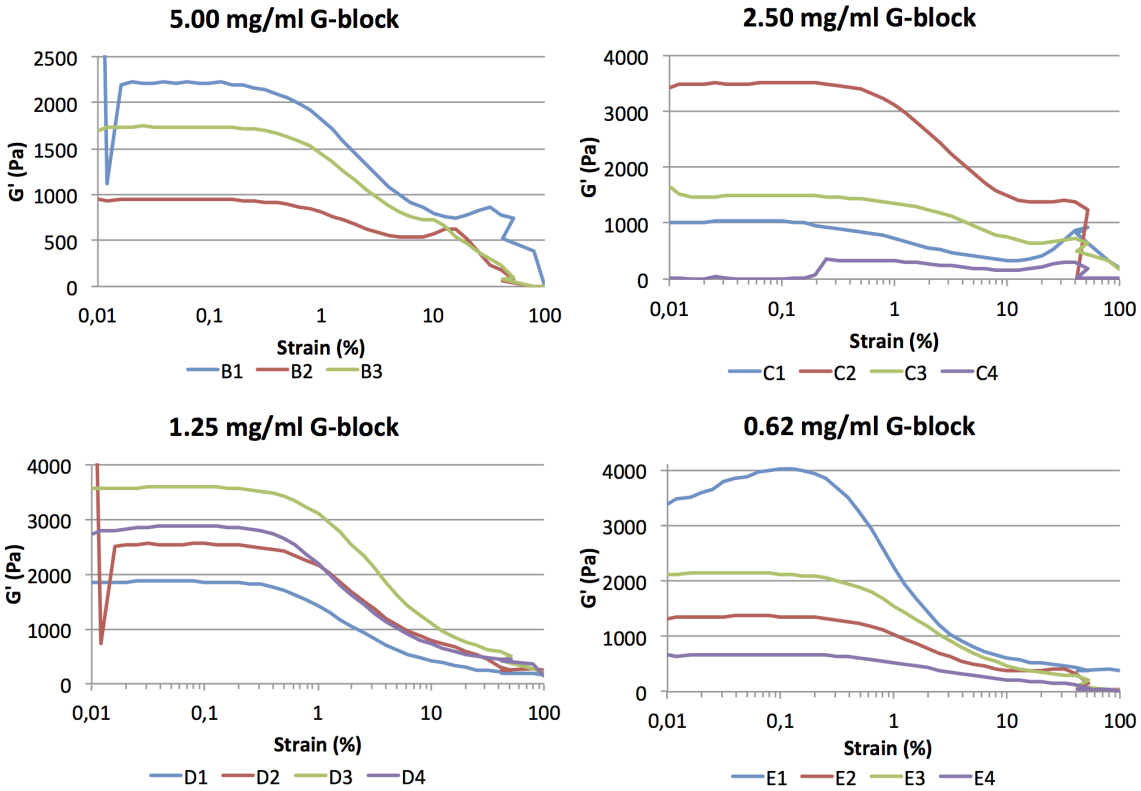

Figure 3.33: Strain sweep for collagen gel with added G-block. The temperature and frequency were kept constant at 37°C and 1 Hz respectively. The graphs show the G' modulus value as a function of increased strain. The strain was increased from 0.01 to 100%. The top left graph is for 3 parallels of 5.00 mg/ml G-block added in collagen gel and the top right graph is for 4 parallels of 2.50 mg/ml G-block in collagen gel. The bottom left graph is for 4 parallels of 1.25 mg/ml G-block added in collagen gel and the bottom right graph is for 4 parallels of 0.62 mg/ml G-block in collagen gel. The Y-axis displays the G' modulus value in Pascal (Pa) and the X-axis shows amount of strain (%).

3.2.3.5 Temperature hold (1 hour)

A temperature hold of 1 hour was initiated after the strain sweep. Here both temperature, frequency and strain were kept constant at 37°C, 1 Hz and 0.1% respectively. The addition of a temperature hold after the strain sweep was implemented after the three parallels of 5.00 mg/ml G-block in collagen gel were run, as well as after the first parallel for the 2.50, 1.25 and 0.62 mg/ml concentrations (C1, D1 and E1) were run. Because of this the mentioned parallels will not be shown as there are no data for them for the 1 hour temperature hold.

Implementing a temperature hold after subjecting a sample to a strain sweep can yield informa-

tion about the nature of a gel. It is possible that the collagen gel used here is a physical gel due to the frequency dependence exhibited by the gel. Physical gels can further be divided into two categories, strong and weak gels. If the gel shows signs of reformation during an isothermal hold period, it is highly likely that the gel is a weak physical gel. The reformation of a gel can here be interpreted as an increase in G' modulus. If it does not show an increase in G' during the isothermal hold time it is highly likely that the gel is a strong physical gel.

For the 2.50 mg/ml G-block in collagen the C3 parallel is omitted as it had a K019 error recorded for the majority of the hold time, leading to very unstable values that were likely artefacts. The C2 and C4 parallels show stable values at 1-2 Pa through the 1 hour hold period (Figure 3.34 top left). As the C2 gel did show signs of complete deformation in the strain sweep (Figure 3.33 top right, C2) the trend seen in this hold time could indicate that this collagen gel with 2.50 mg/ml of G-block (parallel D2) exhibits characteristics of a strong gel. These types of gel will not reform after a break as a weak gel will do if given sufficient time (Ross-Murphy (1995), Ross-Murphy (1984)).

The collagen gels with 1.25 mg/ml G-block (Figure 3.34 top right) added showed signs of reformation. The G' modulus showed an increase through the 1 hour hold time for all three parallels. This increase, especially for D2, could imply a reformation of the collagen gel which would be indicative of a weak physical gel. It is interesting to note that D3 and D4 seemed to have very similar curves and development through the hold time while the D2 parallel as mentioned had an elevated rate of increase in its G' modulus value from 10-20 minutes relative to D3 and D4.

The collagen gels with 0.62 mg/ml G-block (Figure 3.34 bottom center) had a parallel, E2, that showed a similar G' modulus value increase as D2 while the E3 showed a slight increase in G' modulus value through the 1 hour hold time and could also potentially be weak physical gels. The E4 parallel on the other hand showed no increase in G' modulus value through the hold time and this would imply that this gel was a strong physical gel. It is worth noting that the E4 parallel had consistently the lowest G' modulus values compared to the other parallels within the 0.62 mg/ml concentration. through the entire programmed sequence. It had the least amount of growth in G' modulus value in both the temperature ramp and temperature hold (5 hours). It is unlikely that gels made from the same vial of collagen with the same amount of solvent and G-block would fall into two different categories of physical gels. Because of this it is difficult to conclude that E2 and E3 are weak physical gels and that E4 is a strong physical gel. It is not clear

why E4 exhibited no signs of increase on G' modulus value while E2 and E3 did have increases in their G' modulus values.

Various types of collagen (collagen type I included) are known to undergo self-assembly *in vivo* (Kalluri (2003)). In a protocol by Plodinec et al. (2010) it is demonstrated, by using atomic force microscopy, that collagen type II fibrils can undergo reassembly after being exposed to mechanical disruption. Birk et al. (1990) states that: *in reassembly studies in vitro type I collagen forms thicker fibrils than type III collagen, while type II collagen fibrils generally have the smallest diameters.* Taken together this could imply that collagen is able to undergo reassembly of its fibrils both in vivo and in vitro. However, it is unclear whether or not collagen gel can be reformed after a catastrophic break without being reset in some way. The additional temperature hold here does however suggest that some of the gels have an increase in G' modulus value during the hold time and because of this recorded increase it could be that they can be categorized as weak physical gels, further, they were recorded to not undergo a catastrophic break. However, the increase in G' modulus observed in some of the samples (Figure 3.34 D2, D3, D4, E2 and E3) could be caused by something different, for instance drying of the remaining gel. Potential signs of drying were observed in the 5 hour temperature hold and it could be that sample drying could occur here as well. It could also possibly be that the remaining bits of the gel in samples D2, D3, D4, E2 and E3 increased in stiffness and this could have been recorded by the instrument. As there was no additional temperature hold after the strain sweep for collagen alone there is no "baseline" behavior available for how collagen gel alone would react to a temperature hold after being subjected to deformation of the gel.

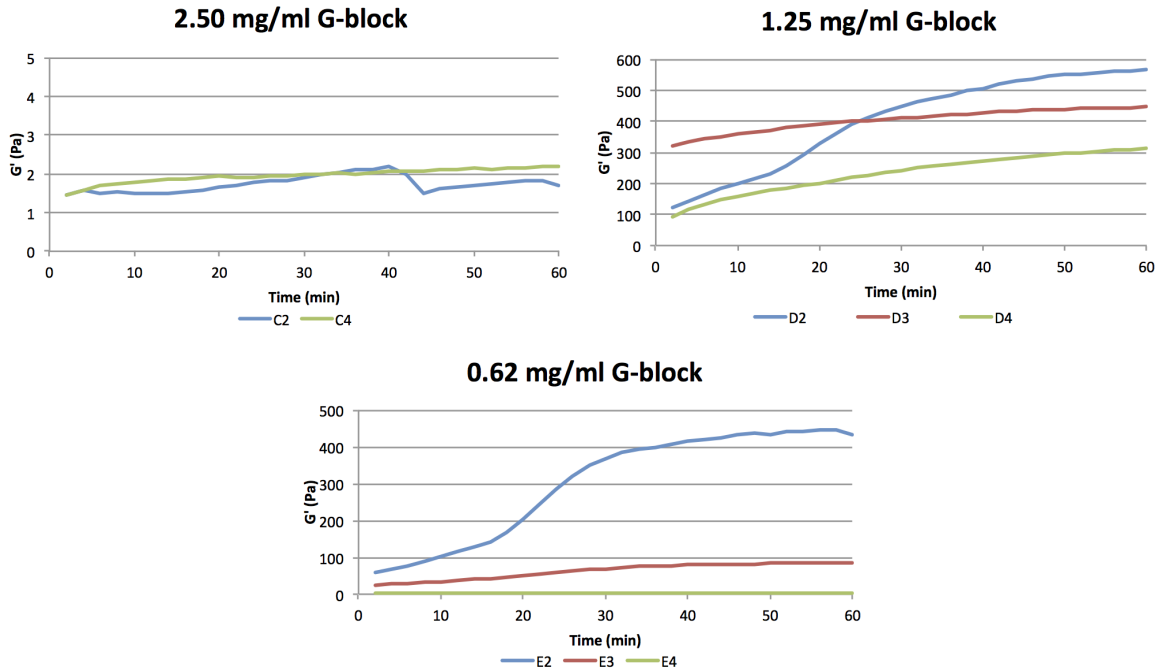

Figure 3.34: Temperature hold of 1 hour for collagen gel with G-block added. The graphs show the G' modulus value as a function of time in an isothermal temperature hold. The Y-axis displays the G' modulus value in Pascals (Pa) and the X-axis displays the time in minutes. The temperature, strain and frequency were kept constant at 37°C, 0.1% and 1 Hz respectively. The top left graph is for 2 parallels of 2.50 mg/ml G-block added in collagen gel, C3 has been omitted due to K019 error codes through out the hold time. The top right graph is for 3 parallels of 1.25 mg/ml G-block in collagen gel. The bottom graph is for 3 parallels of 0.62 mg/ml G-block.

3.2.3.6 The effect of batch variation

An article by Wu et al. (2005) found that results of shear tests and compression tests consistently indicated that the age of rats had a statistically significant effect on mechanical properties of hydrated collagen gels. The research showed that the viscoelastic moduli increased as a consequence of the age of the rats. The tests were done on rat tail collagen of 1 month, 4 months and 8 months old rats. The rat tail collagen used in this thesis was purchased from Roche and it is assumed that the producer has standardized protocols in which the rats are raised to a specific age before termination. However, since the issue of potential batch variation has been mentioned as a possible explanation for the variance seen between C1 and C2, C3, C4 as well as D1 and D2, D3, D4 and also between E1 and E2, E3, E4 this documented increase in viscoelastic moduli as a function of increasing age in the rats could potentially be relevant in relation to the variation seen between parallels from different batches. Furthermore, as the collagen is not made in-house and even if standardized protocols are followed by the manufacturer there will be less control

over how the collagen is extracted and what age the rats are at before being terminated and batch variation as a consequence of the age of the raised rats can not be completely dismissed.

3.2.4 Rheology- the effect of G-block addition in collagen gel

3.2.4.1 Gelling kinetics and temperature

The presence of G-block in collagen gel appears to affect the gelling kinetics of the gel within the temperature ramp (4-37°C, 1°C/min, strain constant at 0.1% and frequency constant at 1 Hz) by increasing the temperature threshold where the G' modulus beings to increase rapidly. In order to investigate this 20% of the G' max value was calculated. The G' max value (of the temperature ramp) was assumed to be the G' modulus value that corresponded to the temperature of 37°C. It is assumed that at 20% of G' max the temperature threshold required for an elevated rate of increase in G' should have been surpassed (e.g. Figure 3.28) and that the G' >G" relationship would be in place coupled with a phase angle lower than 45° indicating solid-like behavior at the given frequency (1 Hz). Based on the calculated $G'_{20\%}$ an approximate temperature in the temperature ramp could be found. The calculated $G'_{20\%}$ value was compared to the G' modulus values in the temperature ramp data sets and the value the $G'_{20\%}$ corresponded closest to was then checked against its corresponding temperature. If the calculated $G'_{20\%}$ value was between two values in the data set an average of the two temperature values was used.

There is a noticeable difference between collagen with and without G-block with regards to the location of the temperature linked to $G'_{20\%}$ within the temperature ramp data files. For collagen without G-block the temperature range for $G'_{20\%}$ is between 20 - 22°C while for collagen with 5.00, 2.50, 1.25 and 0.62 mg/ml G-block added the range is from 24-28°C (Appendix C.6, table C.4 lists the $G'_{20\%}$ and corresponding temperatures). The range for the 4 different concentrations of G-block in collagen gel is a bit wider than the range for collagen alone. This could be influenced by the amount of parallels and the fact that there were differences in G' modulus values between parallels within each concentration. The reason for the latter of the two has been discusses previously with relation to for instance temperature sensitivity and heterogeneity of collagen in parallels.

There is a significant difference ($p < 0.05$) when comparing the collagen gel without G-block to

each concentration of G-block added to the collagen gel (Table 3.11) (Appendix D.2 shows the R-script used to analyse the data from appendix C.6). The collagen gel with 1.25 mg/ml G-block had one (D1) parallel with a very low G' modulus in the temperature ramp. This resulted in a very low $G'_{20\%}$ and it is not certain what caused this but when excluding it from the analysis the variance and standard deviation decreases, leading to a smaller spread in the data. By excluding the D1 value the result from the t-test, comparing collagen gel with no G-block addition with collagen gel with 1.25 mg/ml G-block, becomes significant ($p < 0.05$). Both the non-adjusted and the adjusted results are presented. It is possible that the D1 sample is a potential outlier in the data set when comparing it to the three other parallels. The D2, D3 and D4 had $G'_{20\%}$ at approximately 28.5, 27 and 26.5°C respectively while D1 had $G'_{20\%}$ at approximately 18°C. This gives reason to suspect D1 to be an outlier.

Table 3.11: The p-values from a Welch Two-Sample T-test at $p < 0.05$ level. The asterisk (*) denotes here that a potential outlier has been excluded (parallel D1). See table C.4 in Appendix C.6 for an overview of the temperatures compared.

Conditions compared	p-value
No G-block vs. 5.00 mg/ml G-block	0.0025
No G-block vs. 2.50 mg/ml G-block	0.0026
No G-block vs. 1.25 mg/ml G-block	0.1767
No G-block vs. 1.25 mg/ml G-block adjusted	0.0014*
No G-block vs. 0.62 mg/ml G-block	0.0020

There is no significant difference between the 4 concentrations of collagen gel with G-block added with regards to changes in temperature for $G'_{20\%}$ as a consequence of increased or decreased concentration of G-block added to the collagen gel. This was confirmed by applying a one-way ANOVA with a Tukey HSD. It is important to note that the sample pool available is very small. There are only 3 or 4 parallels for each concentration. Further, the elastic modulus (G') did not show consistent values within each concentration. This means that there was a high variance. The result of the tests, particularly the significant results from the t-tests, must be read with caution. The validity as well as the power of the tests are likely low. This is a consequence of the low sample size. Had the parallels within each concentration given responses in which the G' modulus were closer between each parallel, causing a decrease in variance and standard deviation, the results would be more reliable. In order for that to take place the probable heat sensitivity issue of the system would have to be resolved.

In addition to potentially elevating the temperature threshold for $G'_{20\%}$, the mean max G' value for collagen without G-block added was higher than the mean max value for collagen with G-block added at 2.50, 1.25 and 0.62 mg/ml concentrations. For the 5.00 mg/ml G-block addition to collagen gel there was an increase in gel strength (Figure 3.35) relative to collagen gel alone. In addition, a single test was also done with 50 mg/ml of G-block added to collagen gel and this concentration also gave a higher G' modulus value when compared to the low concentrations of G-block (2.50, 1.25 and 0.62 mg/ml G-block) and collagen alone. Because higher doses of G-block (>5.00 mg/ml) might alter the strength of the gel it could be interesting to investigate the span between 2.50 and 5.00 mg/ml to see if this increase in gel strength at 5.00 mg/ml is the threshold and if the addition of higher concentrations of G-block (>5.00 mg/ml) increases the gel strength and lower concentrations of G-block (<5.00 mg/ml) decreases the gel strength. The lower concentrations (2.50, 1.25 and 0.62 mg/ml) appeared to give a decrease in gel strength when compared to collagen gel without G-block. It is worth noting that the values recorded by the rheometer between the parallels for each concentration were not consistently similar and the potential effect of increase and decrease on gel strength between the concentrations needs to be investigated further.

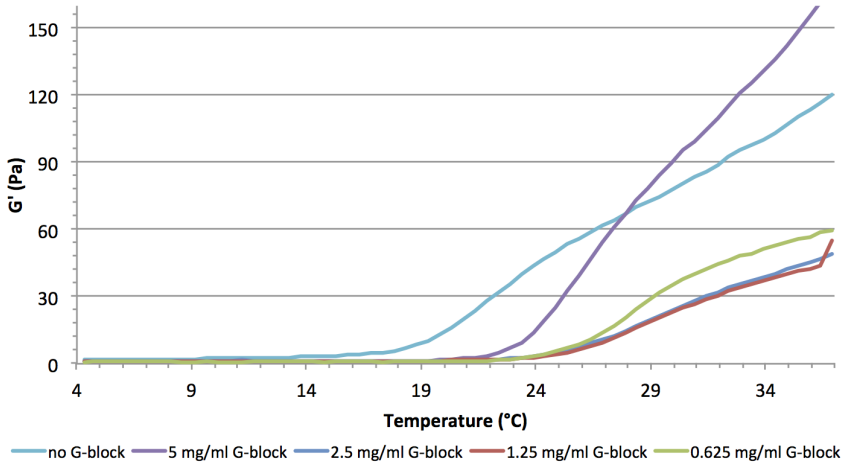

Figure 3.35: Mean values for collagen gel with and without G-block added in temperature ramps (4-37°C with an increase of 1°C/min) with strain and frequency held at 0.1% and 1 Hz. The Y-axis displays the mean G' modulus value for the given parallels within the 4 concentrations of G-block, as well as collagen without G-block, as a function of increasing temperature. Mean value for collagen without G-block consisted of 3 parallels, for 5 mg/ml G-block added there were 3 parallels, for 2.50, 1.25 and 0.62 mg/ml G-block added there were 4 parallels.

3.2.4.2 Setting of gel and frequency dependent behavior

The addition of G-block in the collagen gel does not appear to alter the setting of collagen gel during the 5 hour temperature hold. Neither collagen gel with or without G-block seem to not reach an apparent equilibrium during the 5 hour hold time. Picout and Ross-Murphy (2003) reports that some gels have no final G' modulus value. It is possible that this might be the case for the collagen gel utilized in this thesis. By modifying the programmed sequence and allowing for an overnight temperature hold of for instance 10 hours, this setting curve could have been explored further. Had the gel not showed an apparent equilibrium by the end of the 10 hour hold time it could very well be that it would not reach a final G' modulus value. The G' modulus values showed a degree of variation between parallels, both for collagen gel with and without G-block added. Because of this spread in G' modulus values it would be difficult to find any changes between collagen gel with and without G-block added in the 5 hour temperature hold and also to be able to attribute the changes to the addition of G-block.

The addition of G-block to collagen gels did not seem to alter the behavior of the gel when subjected to a frequency sweep (0.01-10 Hz). The gel seems to provide an increase in response as a consequence of increase in frequency in both collagen gel with and without G-block added from 1 Hz and up to 10 Hz. From 0.01 to 0.1 Hz all the samples exhibit noise. For collagen gel alone the increase seen in the frequency sweep is between 3.7-6.7% (Table 3.7) while for collagen gel with added G-block the percentage increase is between 1.1-12.1% (Table 3.10). It appears that the value range for the percentage increase in collagen gel with added G-block is greater than that of collagen alone. Since there is a variation recorded between parallels within concentrations it is not possible to attribute this to the addition of G-block alone at this point. Collagen, both with and without G-block added had a higher percentage increase in the frequency sweep relative to a calculated 4 minute interval (based on figure 3.23 and 3.32). This suggests that both collagen gel with and without G-block were frequency dependent at the given frequency range. This would in turn indicate that the gels were physical gels. If the max frequency had been increased and the gels had ended up reaching a plateau that could have been a potential indication of entangled networks.

3.2.4.3 Response to applied deformation

The response to applied strain by the collagen gel might be influenced by certain concentrations of G-block added to the collagen gel. For collagen gel alone the response given by the gel from 1-100% has a smaller decrease in G' modulus than for collagen gel with G-block. For collagen gel with added G-block all of the samples has G' modulus with a sharper decreases from 1-100% than collagen gel alone. For some samples there are indications of complete disruption of the gel (B1, B2, B3 and C2) when viewing the individual data sets. The phase angle increased greatly and the G' decreased greatly in the range of 40-60% strain. This implied that there was a marked change in the viscoelastic behavior of the sample with a change from elastic-like behavior to liquid-like behavior. This could be indicative of a catastrophic break (Figure 3.36 left). Given that there was a catastrophic break this could imply that the gels were strong physical gels. The remaining samples appeared to exhibit some of the same behavior as the collagen gel without G-block added. There was no sharp increase in phase angle ($<10°$) during the strain sweep indicating that the gel did not break completely (Figure 3.36 right). This could also be indicative of a more weak gel that would also potentially flow in stead of breaking.

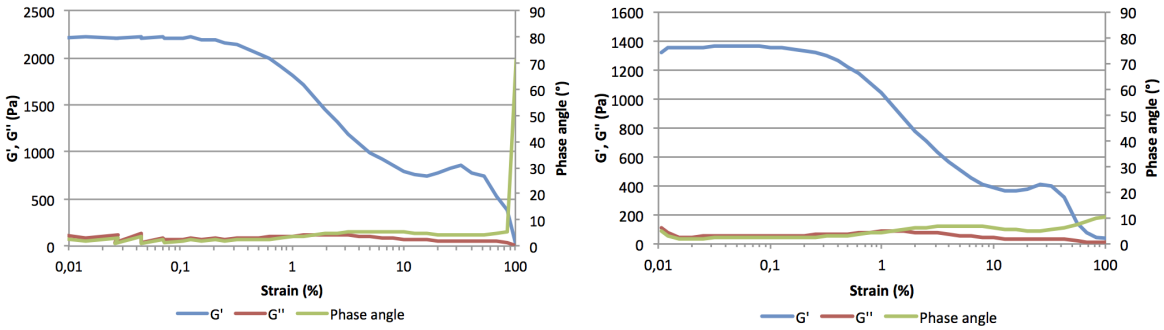

Figure 3.36: Examples of two responses from two samples to applied strain. Left graph shows the sample undergoing a catastrophic break where the phase angle shows a rapid rate of increase while the right graph shows an example of a sample that is not recorded to undergo a catastrophic break where the phase angle does not exhibit the same rapid rate of increase. The left Y-axis displays the G' and G" modulus values in Pascal (Pa) as a function of increasing strain (0.01-100 %) while the right Y-axis displays the phase angle in degrees (°) as a function of increasing strain.

In order to investigate a potential difference in the response to applied strain between the collagen gel with and without G-block with regard to at what point the samples began to show a response to applied strain the following was done: as 0.1% was used as a constant strain for the rest of the programmed sequence it was assumed that a potential G' max value could be found here. The 0.01% value was not opted for as some of the samples showed instability there (Figure 3.33

parallels B1, C3, C4, D2). The value G'$_{80\%}$ represents a 20% decrease in the G' max value. After calculating the G'$_{80\%}$ the closest corresponding G' modulus value in the data set was found. The corresponding percent of strain was then found within the data set and differences in this applied strain was analyzed. If the calculated G'$_{80\%}$ value was between two data points an average of the two corresponding applied strains was utilized.

There were no significant differences (at a $p<0.05$ level) found with regards to what applied strain gave a 20% decrease in G' modulus value when performing two-way T-tests on collagen gel alone versus collagen gel with G-block in various concentrations. This might suggest that G-block does not alter the collagen gels response to applied strain with regards to for instance the samples LVR region (Table 3.12). There does however seem to be a difference in response to applied strain with regards to recorded destruction of samples, as previously mentioned. Collagen without G-block added, as well as collagen with 1.25, 0.62 and possibly 2.50 mg/ml, appear to give the same type of response to applied strain at the end of the strain sweep. The response given by these samples appear to not undergo a catastrophic break as there is no transition phase and no dramatic increase in phase angle. Collagen with 5.00 mg/ml appear to have a catastrophic break where there is a steep decrease in both G' and G" coupled with a rapid rate of increase in phase angle. The same appears to occur for the single sample with 50 mg/ml of G-block added. This could suggest that doses at or above 5.00 mg/ml potentially alters the properties of collagen gel causing a shift from a weak physical gel to a strong physical gel.

Table 3.12: The p-values from a Welch Two-Sample T-test at $p < 0.05$ level. The applied strain in strain sweeps that corresponded to G'$_{80\%}$ of G' modulus max was compared.

Conditions compared	p-value
No G-block vs. 5.00 mg/ml G-block	0.6828
No G-block vs. 2.50 mg/ml G-block	0.5252
No G-block vs. 1.25 mg/ml G-block	0.8595
No G-block vs. 0.62 mg/ml G-block	0.1266

The implementation of an additional temperature hold of 1 hour after the strain sweep show that D2, D3, D4 and E2 did have an increase in G' modulus. It is however unclear precisely why this occurred. It might have something to do with the properties of the gel in which collagen gel alone is here a weak physical gel, collagen gel with 5.00 and possibly 2.50 mg/ml G-block added gives an increase in gel strength where as the lower doses (1.25 and 0.62 mg/ml) causes the gels

to remain as weak physical gels.

3.2.4.4 Potential effects of G-block on collagen

The following part will deal with hypothesized ways in which G-block might affect the collagen gel. Collagen undergoes self-assembly to form a hydrogel when a collagen solution is neutralized (e.g. with NaOH) and heated to physiological temperature (37°C). Furthermore, collagen contains various adhesion motifs, one being the RGD motif (consisting of the amino acids Arg-Gly-Asp). This is an important tripeptide that mediates an interaction between the ECM and a variety of cells. Alginate in contrast does not provide cell adhesion motifs, but it can be conjugated with RGD peptides to improve cell adhesion (Gasperini et al. (2014)). As collagen contains RGD motifs and alginate is capable of conjugating to RGD motifs it could be possible that G-blocks could bind to collagen and given a sufficiently high concentration of G-block it could potentially cause an increase gel strength or it could cause a decrease the gel strength by disrupting the collagen network.

The G-blocks of alginate have shown to provide rigidity to the polymeric structure of alginate, and the mechanical properties of alginate are influenced by the ratio of G- to M-blocks (Gasperini et al. (2014)). As such it is not impossible that G-blocks could potentially alter the rigidity and mechanical of other polymers when added to a solution. In addition, G-blocks are able to form hydrogels in the presence of divalent cations (Pawar and Edgar (2012)). There could potentially be traces of divalent cations such as calcium (Ca^{2+}) in the collagen solution. This might however be an unlikely scenario as the DPBS utilized here was without added calcium, which is a divalent cation. Hence, the only way divalent cations could have been present would be in the dried rat tail collagen. The rat tail collagen was not made in-house, because of this there could potentially be unaccounted traces of calcium. If there were traces of divalent cations such as calcium this could have contributed to gelation of G-block. This hypothesized gelation could in turn affect the recorded rheological properties of collagen gel with G-block as there could have been an increase in gel strength (here G' modulus) as a consequence of added gelation of G-block in addition to the gelation of the collagen gel.

The hypothesized binding between collagen and G-block could also potentially interfere with the self-aggregating nature of collagen after the collagen solution has been neutralized by occupying

or binding to certain areas of the helix slowing down the gelling process. This could potentially cause the shift recorded values in the temperature ramp where the rate of increase in G' modulus value is elevated after a certain temperature. Further, alginate, both G- and M-blocks are capable of forming acidic gels. Here the G-block was dissolved in DPBS and added to the acidic collagen solution before the resulting sample was neutralized. M-monomers and G-monomers of alginate have pKa values at 3.38 and 3.65 in 0.1 M NaCl respectively (Haug (1964)) and can form acidic gels if pH is lower than pKa (Draget et al. (1994)). Given that the acid-dissolved collagen had a pH lower than the pKa of G-monomers the G-block could have initiated a formation of an acidic gel. The time it took from the addition of G-block in DPBS to acidic-collagen and for the sample to be neutralized was between 1-2 minutes. This could potentially have been enough time for the G-blocks to initiate interactions, however these interactions would most likely be halted by adjusting the pH of the solution to over the pKa of G-monomers. Never the less, it could be enough to influence the strength of the collagen gel.

Chapter 4

Conclusion

4.1 Immunohistochemistry

Antibody staining by the way of immunohistochemistry is a relatively simple procedure. It is however simultaneously a procedure where the resulting quality of the stain can depend on a variety of factors. Some of those factors have been encountered and discussed in this thesis. Regarding collagen IV, the antibody used to stain for collagen IV appeared to give a high degree of artefact staining and background noise. The attempted optimization, by varying pH, dilution and incubation time, did not produce any viable results with the polyclonal collagen IV antibody from Millipore. For fibronectin the mice that received 10 doses of G-block had a significant difference in the amount of DAB+ relative to nuclear staining while the 4 dose category had no significant results. Since fibronectin is not present in high amounts in healthy tissue a potential decrease in the amount of fibronectin relative to nuclear staining, as a potential consequence of the G-block treatment, is an encouraging result. α-SMA staining did not have any significant differences in the amount of DAB+ relative to nuclear staining for either the 4 dose or 10 dose group.

There were no apparent differences with regards to what effect the three doses of G-block (0.5 25 and 560 mg/kg) had on the amount of fibronectin and α-SMA within the tumor tissue. This was confirmed with an ANOVA test. The potential lack of dose response was also present in a previous study done by Draget and Nordgård where the tumor sizes were evaluated (Figure 1.9). A decrease in tumor size for tumors treated with G-block relative to the control tumor was

apparent in their study (Figure 1.9). It does however not seem like there was an apparent dose response between the three concentrations of G-block used there. That ties in with the results found here concerning fibronectin.

4.2 Rheology

The improper lowering of the oil basin caused contact between the metal of the oil basin and the metal in the thermal cover which in turn caused unreasonable G' modulus value as well as a seemingly temperature insensitivity to the chosen temperature range, in which collagen should exhibit changes in both G' and G" moduli in addition to the phase angle. By resolving this the testing of collagen with and without G-block could commence. An addition of G-block to collagen gel appears to significantly shift the temperature in which G' modulus has a heightened rate of increase, from 20-22°C for collagen gel alone to 24-28°C for collagen gel with added G-block. A frequency dependent response was documented for both collagen with and without added G-block in the frequency sweep at the frequency range 1-10 Hz, the instrument used 4 minutes to measure the interval 1-10 Hz. The increase in G' modulus value was greater in the 1-10 Hz interval in the frequency sweep than for an arbitrary 4 minute interval, based on datapoints from the temperature hold, frequency sweep and strain sweep, calculated from a trendline. This serves to suggest that even though the gels did not show signs of reaching an apparent equilibrium during the temperature hold, the G' modulus increase seen in the frequency sweep was higher than the calculated expected increase in the same time interval. It is therefor plausible to believe that both the collagen gel with and without G-block added exhibit frequency dependence and that these gels are possibly physical gels.

The addition of higher doses of G-block might increase the elastic-like behavior of collagen gel by increasing the maximum value for the G' modulus and also by potentially altering the gels response to large scale deformation. Collagen gel with 1.25, 0.62 mg/ml and collagen gel alone appears to not exhibit a catastrophic break when subjected to a strain sweep (0.01-100%) indicating that these gels, remained as weak physical gels. Whilst collagen gel with 5.00 mg/ml and possibly 2.50 mg/ml appears to undergo a catastrophic break or is in the process of undergoing such a break (for 2.50 mg/ml G-block added), this might be indicative of strong physical gels. The variations between parallels with regard to recorded G' modulus values makes

it difficult to draw any clear conclusions concerning the effect of G-blocks on collagen. The G' modulus variations between parallels could potentially be caused by heat transference during sample preparation. The heat sensitivity of this system is an issue that needs to be resolved and by achieving that the parallels might exhibit more similar G' modulus values.

Chapter 5

Future work

5.1 Immunohistochemistry

It would be of great interest to do a series of western blots in order to potentially verify the findings from the fibronectin staining and also investigate α-SMA further. Western blot is a more quantitative method than IHC and as such it could allow for better data analysis. The software used to analyze the blots would be able to give quantitative data about the amount of protein within each band in the blot. Further, acquiring an other collagen IV antibody and optimizing for that in order to check whether the nuclear staining and intracellular staining obtained with the collagen IV antibody (from Millipore (AB8201)) was true or the product of artefact staining. If staining with the new collagen IV antibody showed different staining it would also be of interest to include this in a western blot trial.

A previous study on G-block (Draget and Nordgård (2015)) demonstrated a decrease in tumor growth when treating with RiXOVA in a pancreatic tumor model xenografted into mice. This was done with both RiXOVA as a single vehicle and in combination with Gemcitabine. Because of this decrease in tumor size it would be interesting to stain for Ki-67. Ki-67 is a protein strictly associated with cell proliferation (Scholzen and Gerdes (2000)) and as such it could be interesting to see if the addition of RiXOVA, RiXOVA with Gemcitabine and Gemcitabine alone had different impacts on cell proliferation by comparing the amount of Ki-67 staining obtained with the three variations mentioned above relative to a control tumor.

In Deer et al. (2010) the differences in phenotype and genotype between various tumor models for pancreatic cancers are discussed and it is stated that there exist some differences between the cell-lines with regards to cell adhesion in relation to ECM, cell migration and tumorigenicity (a cell lines ability to produce tumors *in vivo*). Because of this an evaluation of the tumor model could be beneficial as there exists differences between the tumor models that were investigated by Deer et al. (2010). Further, with respect to the briefly discussed potential of an upregulation of the expression of α-SMA versus a decrease in breakdown of α-SMA, performing an mRNA analysis of the gene expression of the α-SMA encoding gene could glean further insight into whether there is a decrease in breakdown or upregulation of gene expression with regards to α-SMA. This might in turn help to potentially further the understanding of whether G-block affects the MMPs which in turn would have an effect on the breakdown of α-SMA.

5.2 Rheology

In terms of continuing to explore the effect of G-block on collagen gel the first problem that needs to be resolved is the temperature sensitivity for this system in order to hopefully achieve parallels that display a greater consistently in G' modulus value. By achieving this the differences discovered will be less likely to be caused by a sub-optimal protocol. Additionally, the concentration of collagen relative to the solvent should could also benefit from an evaluation and optimization. The minimum concentration of collagen needed to form a gel is said to be at 1.5 mg/ml (Djabourov et al. (1993)), the collagen gel used here is at 2 mg/ml and it should be enough to form a gel, but it could be of interest to see if an increase or decrease in collagen concentration could potentially stabilize the system. Furthermore, the results regarding the increase in temperature relative to the $G'_{20\%}$ of the G'_{max} value needs to verified by performing several parallels. An evaluation of cone and plate geometry versus plate-plate serrated geometry might also be of interest as there were observed signs of slip in the temperature hold. However, serrated geometries might require more material as the serrated geometries are of the parallel plate type. Furthermore, a cone and plate as used here has a constant and uniform deformation rate within the gap whist parallel plates do not. As such, the benefits and drawbacks need to be further evaluated.

In addition to optimize for stability regarding heat sensitivity an evaluation concerning the type

of collagen used could be relevant. Here the dried collagen was dissolved in-house, ordering and comparing pre-dissolved collagen with the one dissolved in-house could reveal if there are some potential problems with solution uniformity.

Wøien (2015) performed diffusion studies on Matrigel with and without G-block and used IgG and tartrazine as markers. She found that the addition of G-block to Matrigel increased the diffusion rate of IgG and tartrazine. Because of that it could be relevant to explore whether or not an addition of G-block in collagen gel would increase the diffusion rate of IgG and a dye color. An increase in diffusion rate would impy an increased permeaibility, suggesting that G-blocks might alter the stucture of the collagen gel. Furthermore, investigating the structure of the collagen gel with and without G-block under a scanning electron microscope (SEM) would be interesting in order to explore if there are any apparent changes in the structure of the networks within the collagen gel and if these changes are caused by the addition of G-block.

Investigating what effect G-block has on pre-formed collagen gel by first making a collagen gel then soaking said gel in a solution of G-block (e.g. in DPBS) for a given period of time before performing compression studies on the G-block soaked gel by using a texture analyzer could be interesting. This is because preformed collagen gel soaked in a solution containing G-block could potentially better mimic how G-block would affect collagen in the body and it would allow for comparing the effect of various concentrations of G-block to see if various concentrations affect the gel in different ways like it was indicated that G-block did in this thesis. High concentration of G-block in collagen gel appeared to give a strengthening of the gel by increasing the recorded G' modulus value while low concentrations of G-block appeared to not increase the recorded G' modulus values. Lastly, further exploration of the effect G-block dosage has on the rheological viscoelastic moduli of collagen gel could yield some greater understanding regarding how the G-block works with collagen as it is demonstrated here that certain doses appear increases the gel strength and others appear to decrease it.

Bibliography

Aarstad, O. A., Tøndervik, A., Sletta, H., and Skjåk-Bræk, G. (2012). Alginate sequencing: An analysis of block distribution in alginates using specific alginate degrading enzymes. *Biomacromolecules*, 13(1):106–116.

Alberts, B., Johnson, A., Lewis, J., Raff, M., Roberts, K., and Walter, P. (2008a). Cancer. In Anderson, M. and Granum, S., editors, *Molecular Biology of the Cell*, chapter 20, pages 1205–1266. Garland Science, 5th edition.

Alberts, B., Johnson, A., Lewis, J., Raff, M., Roberts, K., and Walter, P. (2008b). Cell Junctions, Cell Adhesion, and the Extracellular Matrix. In Anderson, M. and Granum, S., editors, *Molecular Biology of the Cell*, volume 54, chapter 19, pages 1131–1203. Garland Science, 5th edition.

Avraamides, C. J. and Varner, J. A. (2010). Fibronectins and Their Receptors in Cancer. In Zent, R. and Pozzi, A., editors, *Cell-Extracellular Matrix Interactions in Cancer*, chapter 6, pages 111–137. Springer, London, 1st edition.

Bailey, J. M., Swanson, B. J., Hamada, T., Eggers, J. P., Singh, P. K., Caffery, T., Ouellette, M. M., and Hollingsworth, M. A. (2008). Sonic Hedgehog Promotes Desmoplasia in Pancreatic Cancer. *Clinical Cancer Research*, 14(19):5995–6004.

Birk, D. E., Fitch, J. M., Babiarz, J. P., Doane, K. J., and Linsenmayer, T. F. (1990). Collagen fibrillogenesis in vitro: interaction of types I and V collagen regulates fibril diameter. *Journal of Cell Science*, 95:649–657.

Braccini, I. and Pérez, S. (2001). Molecular basis of Ca^{2+}-induced gelation in alginates and pectins: The egg-box model revisited. *Biomacromolecules*, 2(4):1089–1096.

Branco da Cunha, C., Klumpers, D. D., Li, W. A., Koshy, S. T., Weaver, J. C., Chaudhuri, O., Granja, P. L., and Mooney, D. J. (2014). Influence of the stiffness of three-

dimensional alginate/collagen-I interpenetrating networks on fibroblast biology. *Biomaterials*, 35(32):8927–8936.

Bugge, E., Eide, I., and Gjersing, V. (2016). *Unravelling the mode of action of RiXOVA in breast cancer xenografts*. Bachelor thesis, Norwegian University of Science and Technology.

Christensen, B. (2016). *Compendium TBT4135 Biopolymers*. NTNU, Trondheim, third edition.

ConCordix. ConCordix- Benecol, accessed 20 September 2017. `https://www.concordix.com/benecol`.

Coons, A. H. (1958). Fluorescent antibody methods. *Gen Cytochem Methods*, 1:399–422.

Dalgaard, P. (2008). *Introductory Statistics with R*. Statistics and Computing. Springer New York, New York, NY, 2nd edition.

de Matos, L. L., Trufelli, D. C., de Matos, M. G. L., and Pinhal, M. A. d. S. (2010). Immunohistochemistry as an important tool in biomarkers detection and clinical practice. *Biomarker Insights*, 2010(5):9–20.

Decock, J., Thirkettle, S., Wagstaff, L., and Edwards, D. R. (2011). Matrix metalloproteinases: Protective roles in cancer. *Journal of Cellular and Molecular Medicine*, 15(6):1254–1265.

Deer, E. L., Gonzalez-Hernandez, J., Coursen, J. D., Shea, J. E., Ngatia, J., Scaife, C. L., Firpo, M. A., and Mulvihill, S. J. (2010). Phenotype and Genotype of Pancreatic Cancer Cell Lines. *Pancreas*, 39:425–435.

Desmoulière, A., Geinoz, A., Gabbiani, F., and Gabbiani, G. (1993). Transforming growth factor-beta 1 induces alpha-smooth muscle actin expression in granulation tissue myofibroblasts and in quiescent and growing cultured fibroblasts. *The Journal of Cell Biology*, 122(1):103–111.

Djabourov, M., Lechaire, J.-P., and Gaill, F. (1993). Structure and rheology of gelatin and collagen gels. *Biorheology*, 30:191–205.

Djabourov, M., Nishinari, K., and Ross-Murphy, S. B. (2013a). General properties of polymer networks. In *Physical Gels from Biological and Synthetic Polymers*, chapter 4, pages 97–123. Cambridge University Press, Cambridge, 1st edition.

Djabourov, M., Nishinari, K., and Ross-Murphy, S. B. (2013b). Helical structures from neutral biopolymers. In *Physical Gels from Biological and Synthetic Polymers*, chapter 7, pages 182–221. Cambridge University Press, Cambridge, 1st edition.

Djabourov, M., Nishinari, K., and Ross-Murphy, S. B. (2013c). Techniques for the characterization of physical gels. In *Physical Gels from Biological and Synthetic Polymers*, chapter 2, pages 18–63. Cambridge University Press, Cambridge, 1st edition.

Draget, K. I. and Nordgård, C. T. (2015). RiXOVA A new approach to cancer treatment targeting the extracellular matrix.

Draget, K. I., Skjåk Bræk, G., and Smidsrød, O. (1994). Alginic acid gels: the effect of alginate chemical composition and molecular weight. *Carbohydrate Polymers*, 25(1):31–38.

Draget, K. I. and Taylor, C. (2011). Chemical, physical and biological properties of alginates and their biomedical implications. *Food Hydrocolloids*, 25(2):251–256.

Duraiyan, J., Govindarajan, R., Kaliyappan, K., and Palanisamy, M. (2012). Applications of immunohistochemistry. *Journal of Pharmacy and Bioallied Sciences*, 4(6):307–9.

Edward, J. (1955). *Chem. Ind. London, 1102*.

Feitelson, M. A., Arzumanyan, A., Kulathinal, R. J., Blain, S. W., Holcombe, R. F., Mahajna, J., Marino, M., Martinez-Chantar, M. L., Nawroth, R., Sanchez-Garcia, I., Sharma, D., Saxena, N. K., Singh, N., Vlachostergios, P. J., Guo, S., Honoki, K., Fujii, H., Georgakilas, A. G., Amedeo, A., Niccolai, E., Amin, A., Ashraf, S. S., Boosani, C. S., Guha, G., Ciriolo, M. R., Aquilano, K., Chen, S., Mohammed, S. I., Azmi, A. S., Bhakta, D., Halicka, D., and Nowsheen, S. (2015). Sustained proliferation in cancer: mechanism and novel therapeutic targets. *Semin Cancer Biol*, 35:25–54.

Fingleton, B. and Lynch, C. (2010). Cancer in Context: Importance of the Tumor Microenvironment. In Zent, R. and Pozzi, A., editors, *Cell-Extracellular Matrix Interactions in Cancer*, chapter 3, pages 43–63. Springer.

Forgacs, G., Newman, S. A., Hinner, B., Maier, C. W., and Sackmann, E. (2003). Assembly of Collagen Matrices as a Phase Transition Revealed by Structural and Rheologic Studies. *Biophysical Journal*, 84(2):1272–1280.

Frantz, C., Stewart, K. M., and Weaver, V. M. (2010). The extracellular matrix at a glance. *Journal of Cell Science*, 123(24):4195–4200.

Fujita, H., Ohuchida, K., Mizumoto, K., Nakata, K., Yu, J., Kayashima, T., Cui, L., Manabe, T., Ohtsuka, T., and Tanaka, M. (2010). α-Smooth muscle actin expressing stroma promotes an aggressive tumor biology in pancreatic ductal adenocarcinoma. *Pancreas*, 39(8):1254–1262.

Gasperini, L., Mano, J. F., and Reis, R. L. (2014). Natural polymers for the microencapsulation of cells. *Journal of The Royal Society Interface*, 11(100):20140817–20140817.

Goodwin, J. and Hughes, R. (2008). Introduction. In *Rheology for Chemists: An Introduction*, chapter 1, pages 2–13. The Royal Society of Chemistry, Cambridge.

Gopinathan, A., Morton, J. P., Jodrell, D. I., and Sansom, O. J. (2015). GEMMs as preclinical models for testing pancreatic cancer therapies. *Disease Models & Mechanisms*, 8:1185–1200.

Grant, G. T., Morris, E. R., Rees, D. A., Smith, P. J., and Thom, D. (1973). Biological interactions between polysaccharides and divalent cations: The egg-box model. *FEBS Letters*, 32(1):195 – 198.

Grasdalen, H. (1983). High-field, 1H-n.m.r. spectroscopy of alginate: sequential structure and linkage conformations. *Carbohydrate Research*, 118:255–260.

Han, Z. and Lu, Z.-R. (2017). Targeting fibronectin for cancer imaging and therapy. *J. Mater. Chem. B*, 5(4):639–654.

Haug, A. (1964). *Composition and properties of alginate*. Doctoral thesis, NTH.

Haug, A., Larsen, B., and Smidsrød, O. (1974). Uronic acid sequence in alginate from different sources. *Carbohydrate Research*, 32(2):217–225.

Haug, A., Myklestad, S., Larsen, B., and Smidsrød, O. (1967). Correlation between Chemical Structure and Physical Properties of Alginates. *Acta Chemica Scandinavica*, 21:768–778.

Herman, I. M. (1993). Actin isoforms. *Current Opinion in Cell Biology*, 5(1):48–55.

Hessmann, E., Patzak, M. S., Klein, L., Chen, N., Kari, V., Ramu, I., Bapiro, T. E., Frese, K. K., Gopinathan, A., Richards, F. M., Jodrell, D. I., Verbeke, C., Li, X., Heuchel, R., Löhr, J. M., Johnsen, S. A., Gress, T. M., Ellenrieder, V., and Neesse, A. (2017). Fibroblast drug scavenging increases intratumoural gemcitabine accumulation in murine pancreas cancer. *Gut*, 1:1–11.

Hezel, A. F., Kimmelman, A. C., Stanger, B. Z., Bardeesy, N., and Depinho, R. A. (2006). Genetics and biology of pancreatic ductal adenocarcinoma. *Genes & Development*, 20:1218–1249.

Hinz, B., Phan, S. H., Thannickal, V. J., Galli, A., Bochaton-Piallat, M. L., and Gabbiani, G. (2007). The Myofibroblast: One function, Multiple origins. *American Journal of Pathology*, 170(6):1807–1816.

Isola, J. and Tuominen, V. J. (2010). ImmunoRatio, accessed 3 March 2017. `http://153.1.200.58:8080/immunoratio/?locale=en`.

Kalluri, R. (2003). Basement membranes: Structure, assembly and role in tumour angiogenesis. *Nature Reviews Cancer*, 3(6):422–433.

Kalluri, R. and Cosgroves, D. (2000). Assembly of type IV collagen. *Journal of Biological Chemistry*, 275(17):12719–12724.

Kavanagh, G. M. and Ross-Murphy, S. B. (1998). Rheological characterisation of polymer gels. *Progress in Polymer Science*, 23:533–562.

Kezwon, A. and Wojciechowski, K. (2014). Effect of temperature on surface tension and surface dilational rheology of type I collagen. *Colloids and Surfaces A: Physicochemical and Engineering Aspects*, 460:168–175.

Landini, G. (2015). Colour Deconvolution, accessed 5 March 2017. `http://www.mecourse.com/landinig/software/cdeconv/cdeconv.html`.

Lee, H. W., Park, Y. M., Lee, S. J., Cho, H. J., Kim, D. H., Lee, J. I., Kang, M. S., Seol, H. J., Shim, Y. M., Nam, D. H., Kim, H. H., and Joo, K. M. (2013). Alpha-smooth muscle actin (ACTA2) is required for metastatic potential of human lung adenocarcinoma. *Clinical Cancer Research*, 19(21):5879–5889.

Lee, K. Y. and Mooney, D. J. (2012). Alginate : properties and biomedical applications. *Progress in Polymer Science*, 37(1):106–126.

Lipman, N. S., Jackson, L. R., Weis-Garcia, F., and Trudel, L. J. (2005). Monoclonal versus polyclonal antibodies: distinguishing characteristics, applications, and information resources. *ILAR journal / National Research Council, Institute of Laboratory Animal Resources*, 46(3):258–68.

Lodish, H., Berk, A., Zipursky, S. L., Matsudaira, P., Baltimore, D., and Darnell, J. (2000). Collagen: The Fibrous Proteins of the Matrix. In *Molecular Cell Biology*, chapter 22. W. H. Freeman, New York, 4 edition.

Lu, P., Weaver, V. M., and Werb, Z. (2012). The extracellular matrix: a dynamic niche in cancer progression. *The Journal of cell biology*, 196:395–406.

MacKintosh, F. C., Käs, J., and Janmey, P. A. (1995). Elasticity of Semiflexible Biololymer Networks. *Physical Review Letters*, 75(24):4425–4429.

Mahadevan, D. and Von Hoff, D. D. (2007). Tumor-stroma interactions in pancreatic ductal adenocarcinoma. *Molecular Cancer Therapeutics*, 6(4):1186–1197.

Mardle, S. (2007). The selection of reporter labels. In Renshaw, S., editor, *Immunohistochemistry*, chapter 3, pages 33–44. Scion Publishing Limited, Cambridge, 1st edition.

Mezger, T. R. (2014). *Applied Rheology*. Anton Paar, Graz, 1st edition.

Miner, J. H. (2010). The Extracellular Matrix: An Overview. In Zent, R. and Pozzi, A., editors, *Cell-Extracellular Matrix Interactions in Cancer*, chapter 1, pages 1–18. Springer, London, 1st edition.

Muiznieks, L. D. and Keeley, F. W. (2013). Molecular assembly and mechanical properties of the extracellular matrix: A fibrous protein perspective. *Biochimica et Biophysica Acta*, 1832:866–875.

Nagase, H. and Woessner, F. J. (1999). Matrix Metalloproteinases. *The Journal of biological chemistry*, 274(31):21491–21494.

Nelson, D. and Cox, M. (2013). The Three-Dimensional Structure of Proteins. In *Lehninger Principles of BIochemistry*, chapter 4, pages 115–157. W. H. Freeman and Company, sixth edition.

Onley, C. (2007). Antibodies for immunohistochemistry. In Renshaw, S., editor, *Immunohistochemistry*, chapter 2, pages 1–31. Scion Publishing Limited, Cambridge, 1st edition.

Owen, J., Punt, J., Stranford, S. A., and Jones, P. (2013). Cancer and the Immune System. In *Kuby Immunology*, chapter 19, pages 627–651. W.H. Freeman and Company, New York, 7th edition.

Pankov, R. and Yamada, K. M. (2002). Fibronectin at a glance. *Journal of Cell Science*, 115(20):3861–3863.

Pawar, S. N. and Edgar, K. J. (2012). Alginate derivatization: A review of chemistry, properties and applications. *Biomaterials*, 33(11):3279–3305.

Picout, D. R. and Ross-Murphy, S. B. (2003). Rheology of biopolymer solutions and gels. *The Scientific World Journal*, 3:105–21.

Plodinec, M., Loparic, M., and Aebi, U. (2010). Atomic Force Microscopy for Biological Imaging and Mechanical Testing across Length Scales. *Cold Spring Harbor Protocols*, 2010(10).

Pontiggia, O., Sampayo, R., Raffo, D., Motter, A., Xu, R., Bissell, M. J., De Kier Joffé, E. B., and Simian, M. (2012). The tumor microenvironment modulates tamoxifen resistance in breast

cancer: A role for soluble stromal factors and fibronectin through $\beta 1$ integrin. *Breast Cancer Research and Treatment*, 133(2):459–471.

Raisio. Benecol, accessed 20 September 2017. `http://www.benecol.com/`.

Ramos-Vara, J. A. and Miller, M. A. (2014). When Tissue Antigens and Antibodies Get Along: Revisiting the Technical Aspects of Immunohistochemistry-The Red, Brown, and Blue Technique. *Veterinary Pathology*, 51(1):42–87.

R&D Systems (2014). IHC/ICC Protocol Guide. `http://www.sciencegateway.org/protocols/pdf/ihc_icc_protocol_guide.pdf`.

Reiner, M. (1964). The Deborah Number. *Physics Today*, 17(1):62.

Renshaw, S. (2007). Immunohistochemical staining techniques. In Renshaw, S., editor, *Immunohistochemistry*, chapter 4, pages 45–96. Scion Publishing Limited, Cambridge, 1st edition.

ResearchGate (2015). Does anyone have a protocol for quantifying IHC images in ImageJ?, accessed 5 March 2017. `https://www.researchgate.net/post/Does_anyone_have_a_protocol_for_quantifying_IHC_images_in_ImageJ`.

Ross-Murphy, S. B. (1984). Rheological methods. In Chan, W, S, H., editor, *Biophysical Methods in Food Research*, chapter 4, pages 138–200. Blackwell Scientific Publications.

Ross-Murphy, S. B. (1991). Incipient behaviour of gelatin gels. *Rheologica Acta*, 30(5):401–411.

Ross-Murphy, S. B. (1992). Structure and rheology of gelatin gels: recent progress. *Polymer*, 33(12):2622–2627.

Ross-Murphy, S. B. (1995). Structure–property relationships in food biopolymer gels and solutions. *Journal of Rheology*, 39:1451–1463.

Saper, C. B. (2009). A Guide to the Perplexed on the Specificity of Antibodies. *Journal of Histochemistry & Cytochemistry*, 57(1):1–5.

Scherer, G. W. (1989). Mechanics of syneresis I. Theory. *Journal of Non-Crystalline Solids*, 108(1):18–27.

Schindelin, J., Arganda-Carreras, I., Frise, E., Kaynig, V., Longair, M., Pietzsch, T., Preibisch, S., Rueden, C., Saalfeld, S., Schmid, B., Tinevez, J.-Y., White, D. J., Hartenstein, V., Eliceiri, K., Tomancak, P., and Cardona, A. (2012). Fiji: an open-source platform for biological-image analysis. *Nature Methods*, 9(7):676–682.

Scholzen, T. and Gerdes, J. (2000). The Ki-67 protein: From the known and the unknown. *Journal of Cellular Physiology*, 182(3):311–322.

Skalli, O., Ropraz, P., Trzeciak, A., Benzonana, G., Gillessen, D., and Gabbiani, G. (1986). A monoclonal antibody against alpha-smooth muscle actin: a new probe for smooth muscle differentiation. *The Journal of Cell Biology*, 103:2787–2796.

Sklarew, R. J., Bodmer, S. C., and Pertschuk, L. P. (1990). Quantitative imaging of immunocytochemical (pap) estrogen receptor staining patterns in breast cancer sections. *Cytometry*, 11(3):359–378.

Smidsrød, O. and Moe, S. M. (2008). *Biopolymer Chemistry*. Tapir academic press, Trondheim, 1st edition.

Sodek, K. L., Brown, T. J., and Ringuette, M. J. (2008). Collagen I but not Matrigel matrices provide an MMP-dependent barrier to ovarian cancer cell penetration. *BMC Cancer*, 8(1).

Stading, M. and Hermansson, A. M. (1990). Viscoelastic behaviour of β-lactoglobulin gel structures. *Topics in Catalysis*, 4(2):121–135.

Stark, A. and Eibl, G. (2015). Pancreatic Ductal Adenocarcinoma. *Pancreapedia*.

Takahashi, S., Leiss, M., Moser, M., Ohashi, T., Kitao, T., Heckmann, D., Pfeifer, A., Kessler, H., Takagi, J., Erickson, H. P., and Fässler, R. (2007). The RGD motif in fibronectin is essential for development but dispensable for fibril assembly. *Journal of Cell Biology*, 178(1):167–178.

Taylor, C. R., Shi, S.-R., Barr, N. J., and Wu, N. (2006). Techniques of Immunohistochemistry: Principles, Pitfalls and Standardization. In Dabbs, D., editor, *Diagnostic Immunohistochemistry*, chapter 1, pages 1–42. Elsevier, Pittsburg, 2nd edition.

te Nijenhuis, K. (2007). On the nature of crosslinks in thermoreversible gels. *Polymer Bulletin*, 58:27–42.

Timell, T. E. (1964). The Acid Hydrolysis of Glycosides. *Canadian Journal of Chemistry*, 42:1456–1472.

Tønnesen, H. H. and Karlsen, J. (2002). Alginate in Drug Delivery Systems. *Drug Development and Industrial Pharmacy*, 28(6):621–630.

True, L. D. (2008). Quality control in molecular immunohistochemistry. *Histochemistry and Cell Biology*, 130(3):473–480.

Tuominen, V. J., Ruotoistenmäki, S., Viitanen, A., Jumppanen, M., and Isola, J. (2010). ImmunoRatio: a publicly available web application for quantitative image analysis of estrogen receptor (ER), progesterone receptor (PR), and Ki-67. *Breast Cancer Research*, 12(4):1–12.

Visse, R. and Nagase, H. (2003). Matrix metalloproteinases and tissue inhibitors of metalloproteinases: Structure, function, and biochemistry. *Circulation Research*, 92(8):827–839.

Wang, J. P. and Hielscher, A. (2017). Fibronectin: How its aberrant expression in tumors may improve therapeutic targeting. *Journal of Cancer*, 8(4):674–682.

Weitz, D., Wyss, H., and Larsen, R. (2007). Oscillatory rheology: Measuring the viscoelastic behaviour of soft materials. *G.I.T Laboratory Journal*, 11(3-4):68–70.

Winslow, T. (2009). Pancreas anatomy, accessed 13 November 2017. `https://www.ncbi.nlm.nih.gov/pubmedhealth/PMHT0015631/`.

Wøien, S. M. H. (2015). *The Effect of G-block on the Extracellular Matrix Barrier to Molecular Diffusion*. Master thesis, Norwegian University of Science and Technology.

Wolfgang, C., Herman, J., Laheru, D., Klein, A., Erdek, M. A., Fishman, E. K., and Hruban, R. H. (2013). Recent Progress in Pancreatic Cancer. *CA Cancer J Clin.*, 63(5):318–348.

Wu, C.-C., Ding, S.-J., Wang, Y.-H., Tang, M.-J., and Chang, H.-C. (2005). Mechanical properties of collagen gels derived from rats of different ages. *Journal of Biomaterials Science, Polymer Edition*, 16(10):1261–1275.

Yamashita, M., Ogawa, T., Zhang, X., Hanamura, N., Kashikura, Y., Takamura, M., Yoneda, M., and Shiraishi, T. (2012). Role of stromal myofibroblasts in invasive breast cancer: Stromal expression of alpha-smooth muscle actin correlates with worse clinical outcome. *Breast Cancer*, 19(2):170–176.

Yan, C. and Pochan, D. J. (2010). Rheological properties of peptide-based hydrogels for biomedical and other applications. *Chemical Society Reviews*, 39(9):3528–3540.

Yang, Y. L., Leone, L. M., and Kaufman, L. J. (2009). Elastic moduli of collagen gels can be predicted from two-dimensional confocal microscopy. *Biophysical Journal*, 97(7):2051–2060.

Yuan, S.-m. (2015). α-Smooth Muscle Actin and ACTA2 Gene Expressions in Vasculopathies. *Brazilian Journal of Cardiovascular Surgery*, 30(6):644–649.

Zhong, Q. and Daubert, C. R. (2013). Food Rheology. In Kutz, M., editor, *Handbook of Farm, Dairy and Food Machinery Engineering*, chapter 15, pages 403–426. Elsevier Inc., 2nd edition.

Zuidema, J. M., Rivet, C. J., Gilbert, R. J., and Morrison, F. A. (2014). A protocol for rheological characterization of hydrogels for tissue engineering strategies. *Journal of Biomedical Materials Research Part B: Applied Biomaterials*, 102(5):1063–1073.

Appendix A

ImmunoRatio

The data presented here is the data used to make the graphs in the immunohistochemistry part of the result section. It is also the data used for the t-tests and ANOVA tests. After the staining procedure each slide was photographed at six different areas. There were taken three pictures in each lobe at a 20x magnification, a total of six images per slide. The requirements each image had to meet are listed in in part ??. The web appliation utilized can be accessed from: *http://153.1.200.58:8080/immunoratio/?locale=en* and the basic mode was used. The raw data from the webpage ImmunoRatio as well as the calculated variance and standard deviation (SD) of the sample group are displayed withing this appendix. The variance and SD are based on the sample group within the population (n-1) as not all of the tumor sections were included in the analysis.

Table A.1: The DAB$^+$/nuclear straining results obtained from the ImmunoRatio website for each of the three antibodies (collagen IV, fibronectin and α-SMA), the mean value of areas in each tumor and the standard deviation (St. Dev) for each tumor.

Collagen								
Tumor	**Area 1**	**Area 2**	**Area 3**	**Area 4**	**Area 5**	**Area 6**	**Mean**	**St. Dev**
433	57.40	75.90	68.30	85.50	87.20	74.70	74.83	11.09
436	53.00	48.60	70.80	83.80	62.60	65.10	63.98	12.65
438	54.50	84.30	82.10	42.50	12.50	33.60	51.58	28.08
523	58.20	65.90	75.20	55.60	65.80	61.00	63.62	6.99
524	90.80	88.80	86.90	84.50	93.70	90.20	89.15	3.20
527	78.20	70.60	82.70	86.70	69.10	84.00	78.55	7.29
528	58.10	64.60	63.10	70.10	72.30	77.50	67.62	7.01
Fibronectin								
Tumor	**Area 1**	**Area 2**	**Area 3**	**Area 4**	**Area 5**	**Area 6**	**Mean**	**St. Dev**
432	54.90	49.90	41.3	55.20	53.50	38.50	48.90	7.30
433	49.80	49.10	43.8	54.10	38.50	45.10	46.70	5.40
435	49.00	52.10	40.40	44.30	34.60	35.70	42.70	7.10
436	56.90	48.10	49.80	44.00	42.30	51.50	48.80	5.30
438	41.90	50.10	35.90	30.10	49.50	30.70	39.70	8.90
523	38.50	55.00	43.80	56.70	30.50	43.70	44.70	9.90
524	45.50	51.30	59.00	46.30	59.80	37.60	49.90	8.60
525	22.60	51.60	52.10	24.00	32.90	34.60	36.30	12.90
527	42.20	36.60	45.20	51.20	34.60	36.80	41.10	6.30
530	32.10	28.70	38.50	32.90	26.70	43.70	33.80	6.30
SMA								
Tumor	**Area 1**	**Area 2**	**Area 3**	**Area 4**	**Area 5**	**Area 6**	**Mean**	**St. Dev**
432	46.20	45.40	46.40	48.40	46.00	60.90	48.90	6.00
433	54.70	52.30	54.60	51.90	51.50	50.70	52.60	1.70
434	43.30	40.80	54.70	48.50	51.40	57.70	49.40	6.50
436	60.00	61.10	51.10	54.40	55.30	51.80	55.60	4.10
439	58.50	64.60	53.40	54.40	53.00	47.00	55.20	5.90
523	37.10	43.00	26.70	45.30	45.80	35.10	38.80	7.40
524	30.10	43.60	30.70	37.00	38.40	33.60	35.60	5.10
525	47.60	41.40	20.90	44.20	28.10	27.60	35.00	10.80
527	44.20	32.60	37.90	55.70	35.70	57.40	43.90	10.50
529	35.10	43.30	42.60	48.60	44.80	43.30	43.00	4.40

Appendix B

Protocols for immunohistochemistry

B.1 Immunostaining protocol

1. Deparafination and rehydration

Heating cabinet	30 min at 60 C
Neo-Clear	2 x 10 min
Absolute alcohol	2 x rinse
96%, 80%, 70%	Rinse
Destilled water	Rinse
3% H_2O_2	10 min
Destilled water	1-2 min

2. Heat induced epitope retrieval

Sections are placed in a plastic container with antigen retrieval buffer (10 mM Citratebuffer pH 6 or 10 mM Trisbuffer pH 9) and this is placed in a microwave at either 90 W (small container) or 160 W (large container) for 15 minutes. Let the sections cool down to room temperature in the container on bench.

3. Immunostraining

Rinsing buffer	5 min
Primary antibody [a]	1 h room temperature or over night at 4 degrees
Rinsing buffer	3 x 5 min
Dako EnVision secondary antibody	30 min
Rinsing buffer	2 x 5 min
DAB$^+$	1-5 min (evaluate under microscope)
Destilled water	5 min

[a] Primary antibody diluted with antibody dilution

4. Counterstaining and mounting

Hematoxylin	8-10 sec
Lukewarm water	2-3 min
Mount with Glycergel	

B.2 Rinsing buffer and antibody diluent

Rinsing buffer − stock diluent

9,70 g THAM, Sigma
66,12 g THAM HCl, Sigma
87,68 g NaCl
1000 ml destilled water

Adjust pH to 7,4. This is a 10x stock diluent. To make the rinsing buffer- take 1:10 of stock dilution and destilled water. Add 500 μl of TWEEN 20% VWR Chemicals.

Antibody diluent

0,5 g bovine serum albumine, Sigma

50 ml 50 mM TBS stock pH 7,4

25 μl Tween 20, VWR Chemicals

B.3 Example of a full experimental set-up

An example of a full experimental set-up using the optimized paramteters for fibronectin is shown in Table B.1).

Table B.1: Example of an experimental set up using fibronectin optimized parameter as an example. The example shows the antibody dilution used, the amount of time incubated with primary antibody and the amount of time the DAB+ was left on each slide. The secondary antibody was incubated for 30 minutes for all of the slides.

#	Name	Treatment	Antibody dilution	Incubation	DAB+ (sec)
1	432 A	Saline, 4 doses, control	1:50	1 h RT	55 ± 5
2	433 A	Saline, 4 doses, control	1:50	1 h RT	55 ± 5
3	434 A	0.5 mg/kg, 4 doses	1:50	1 h RT	55 ± 5
4	435 A	0.5 mg/kg, 4 doses	1:50	1 h RT	55 ± 5
5	436 A	25 mg/kg, 4 doses	1:50	1 h RT	55 ± 5
6	437 A	25 mg/kg, 4 doses	1:50	1 h RT	55 ± 5
7	438 A	560 mg/kg, 4 doses	1:50	1 h RT	55 ± 5
8	439 A	560 mg/kg, 4 doses	1:50	1 h RT	55 ± 5
9	523	Saline, 10 doses, control	1:50	1 h RT	55 ± 5
10	524	Saline, 10 doses, control	1:50	1 h RT	55 ± 5
11	525	0.5 mg/kg, 10 doses	1:50	1 h RT	55 ± 5
12	526	0.5 mg/kg, 10 doses	1:50	1 h RT	55 ± 5
13	527	25 mg/kg, 10 doses	1:50	1 h RT	55 ± 5
14	528	25 mg/kg, 10 doses	1:50	1 h RT	55 ± 5
15	529	560 mg/kg, 10 doses	1:50	1 h RT	55 ± 5
16	530	561 mg/kg, 10 doses	1:50	1 h RT	55 ± 5
17	Mouse kidney	N/A (positive control)	1:50	1 h RT	55 ± 5
18	IgG control	N/A	1:50	1 h RT	55 ± 5
19	Negative control	N/A	AB diluent only	1 h RT	55 ± 5

B.4 Optimization process for antibodies

B.4.1 Collagen IV

Table B.2: Optimization process of anti-Collagen IV. Positive control for anti-Collagen IV was human colon.

Part 1	**Dilution**	**pH**	**DAB+ (sec)**	**Incubation**
	1:50	6	120	O.N
	1:100	6	60	O.N
	1:50	9	30	O.N
	1:100	9	30	O.N
	Negative control	9	30	O.N
Part 2	**Dilution**	**pH**	**DAB+ (sec)**	**Incubation**
	1:200	9	115	O.N
	1:400	9	264	O.N
	1:800	9	301	O.N
	Negative control	9	120	O.N
Part 3	**Dilution**	**pH**	**DAB+ (sec)**	**Incubation**
	1:75	9	115	O.N
	1:150	9	264	O.N
	1:800	9	301	O.N
	Negative control	9	120	O.N
Part 4	**Dilution**	**pH**	**DAB+ (sec)**	**Incubation**
	1:150	9	95	O.N
	1:150	9	100	O.N
	1:150 (positive control)	9	100	O.N
	Negative control	9	270	O.N
	Negative control	9	280	O.N

B.4.2 Fibronectin

Table B.3: Optimization process of anti-Fibronectin. Positive control for anti-Fibronectin was in part 2 human kidney with tumor and in part 3 and part 4 the positive control was mouse kidney.

Part 1	**Dilution**	**pH**	**DAB+ (sec)**	**Incubation**
	1:100	6	251	1h RT
	1:100	9	65	1h RT
	Negative control	6	300	1h RT
	Negative control	9	300	1h RT
Part 2	**Dilution**	**pH**	**DAB+ (sec)**	**Incubation**
	1:100	9	30	O.N
	1:200	9	35	O.N
	1:300	9	50	O.N
	1:400	9	55	O.N
	1:300 (positive control)	9	70	O.N
	Negative control	9	120	O.N
Part 3	**Dilution**	**pH**	**DAB+ (sec)**	**Incubation**
	1:50	9	50	O.N
	1:50 (positive control)	9	255	O.N
	Negative control	9	120	O.N
Part 4	**Dilution**	**pH**	**DAB+ (sec)**	**Incubation**
	1:50	9	70	1h RT
	1:50 (positive control)	9	250	1h RT
	1:50 (positive control)	9	500	1h RT
	Negative control	9	250	1h RT

B.4.3 α-SMA

Table B.4: Optimization process of anti-α-SMA. For part 1,2 and 3 an antibody from DAKO for α-SMA was tested and in part 4 an antibody from Abcam was tested. Positive control for anti-α-SMA was in part 2 human colon, in part 3 it was human mammillary glands and in part 4 mouse duodenum was used. In part 5 the positive control for 1:200 was human mammillary glands and for the 1:1600 dilution mouse duodenum was used. In part 6 the positive control was mouse duodenum.

Part 1	**Dilution**	**pH**	**DAB+ (sec)**	**Incubation**
	1:400 (DAKO)	6	60	1h RT
	1:400 (DAKO)	9	55	1h RT
	Negative control	6	120	1h RT
	Negative control	9	120	1h RT
Part 2	**Dilution**	**pH**	**DAB+ (sec)**	**Incubation**
	1:100 (DAKO)	6	25	1h RT
	1:200 (DAKO)	6	30	1h RT
	1:300 (DAKO)	6	60	1h RT
	1:400 (DAKO)	6	85	1h RT
	1:400 (positive control) (DAKO)	6	90	1h RT
	Negative control	6	120	1h RT
Part 3	**Dilution**	**pH**	**DAB+ (sec)**	**Incubation**
	1:50 (DAKO)	6	50	O.N
	1:50 (positive control) (DAKO)	6	255	O.N
	Negative control	6	120	O.N
Part 4	**Dilution**	**pH**	**DAB+ (sec)**	**Incubation**
	1:50 (Abcam)	6	60	1h RT
	1:50 (Abcam)	6	55	1h RT
	1:50 (positive control) (Abcam)	6	120	1h RT
	Negative control	6	150	1h RT
Part 5	**Dilution**	**pH**	**DAB+ (sec)**	**Incubation**
	1:75 (Abcam)	6	40	O.N
	1:100 (Abcam)	6	40	O.N
	1:200 (Abcam)	6	50	O.N
	1:200 (positive control) (Abcam)	6	240	O.N
	1:1600 (positive control) (Abcam)	6	300	O.N
Part 6	**Dilution**	**pH**	**DAB+ (sec)**	**Incubation**
	1:75 (Abcam)	6	90	1h RT
	1:100 (Abcam)	6	135	1h RT
	1:200 (Abcam)	6	210	1h RT
	1:100 (positive control) (Abcam)	6	170	1h RT
	1:75 (DAKO)	6	45	1h RT
	Negative control	9	240	1h RT

B.5 Datasheet- Collagen IV

The datasheet for the antibody for collagen IV is enclosed here as it appears that it is no longer available online up on searching for it.

Anti-Collagen IV

Polyclonal Antibody
Cat. # AB8201
Lot # 2621744
pack size: 100 µg
FOR RESEARCH USE ONLY
NOT FOR USE IN HUMANS
Store at 2-8 °C

Certificate of Analysis
page 1 of 2

Applications	Species Cross-Reactivity	Antibody Isotype	Epitope/ Region	Host Species	Molecular Weight	Accession #
IH(P)	H, M, R	IgG	N/A	Rb	164 kDa	P02463

Background

Collagen is a long, fibrous structural protein whose function is quite different from the globular proteins such as enzymes. Tough bundles of collagen called collagen fibers are a major component of the extracellular matrix that supports most tissues and gives cells structure from the outside, but collagen is also found inside certain cells. Collagen has great tensile strength, and the main component of fascia, cartilage, ligaments, tendons, bone, and teeth. It strengthens blood vessels and plays a role in tissue development. There are 28 types of collagen described in literature.

Collagen Type IV forms the structural integrity of the basement membrane and is present in the placenta and eye lens. It also serves as part of the filtration system in capillaries and the glomeruli of nephron in the kidney. Collagen IV may inhibit endothelial cell proliferation and angiogenesis via mechanisms involving cell surface proteoglycans and the alpha and beta integrins of endothelial cells.

Presentation

Purified rabbit polyclonal IgG in buffer containing 0.02 M Sodium Phosphate, pH 7.6, 0.25M NaCl containing 0.1% Sodium Azide.

Concentration

1 mg/mL

Specificity

Recognizes native collagen Type IV

Species Cross-reactivity

Tested to react in human, mouse and rat samples.

Immunogen

Collagen IV native protein purified from murine sarcoma basement membrane.

Molecular Weight

164 kDa

Method of Purification

Protein G Purified

Storage and Handling

Stable for 1 year at 2-8°C from date of shipment.

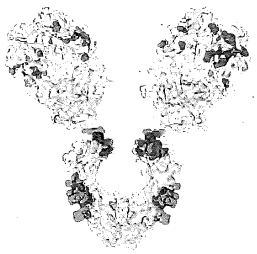

Quality Control Testing

Routinely evaluated by immunohistochemistry on human intestinal tissue.

Immunohistochemistry Analysis:

A 1:50-1:500 dilution of this lot detected strong membrane staining of basement membrane in the lamina propria of formalin-fixed, paraffin-embedded human intestinal tissue.

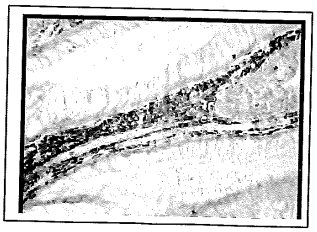

Immunohistochemistry Analysis:
Staining on formalin-fixed, paraffin-embedded human intestinal tissue. Tissue pretreated with citrate buffer, pH 6.0 using high heat epitope retrieval techniques. Antibody diluted to 1:100 and detected using Millipore's IHC Select HRP-DAB detection kit protocol (Cat .No. DAB050). Immunoreactivity is seen as strong membrane staining of basement membrane in the lamina propria.

APPLICATION LEGEND: **WB** Western Blotting **IP** Immunoprecipitation **IC** Immunocytochemistry **IF** Immunofluorescence **IH(P)** Immunohistochemistry (Paraffin)
SPECIES LEGEND: **H** Human **M** Mouse **R** Rat **Rb** Rabbit **WR** Most Common Vertebrates

upstate | CHEMICON | Linco
THE EXPERTISE OF UPSTATE®, CHEMICON® AND LINCO® IS NOW A PART OF MILLIPORE

Please visit www.millipore.com for additional product information, test data and references.
Submit your published journal article, and earn credit toward future Millipore purchases. Visit www.millipore.com/publication_rewards to learn more!

Rev.B/2014-09-18/AB8201CA/RB

Appendix C

Rheology

C.1 Example of raw data

The raw data presented here is an example of some of the raw data obtained from the rheometer and its computer program ”rSpace for Kinexus”. After obtaining the raw data it was exported to Excel. The data displayed here is intended to serve as an example of rheological data used in this thesis. The data stems from a sample of collagen dissolved in 2 ml acetic acid before being mixed with 555 μl DPBS and 47 μl 7.5% sodium bicarbonate. The sample was made and tested on the 21st of July.

Table C.1: Example of relevant rawdata from the Rheometer for a collagen sample run on the 21st of July. The data displayed is from a temperature ramp 4-37°C with constant strain and frequency (0.1% and 1 Hz).

Time (s)	Temperature (C)	Frequency (Hz)	Complex shear strain (%)	G' (Pa)	G" (Pa)	Phase angle (δ)	Torque (N m)
30	4,32	1	0.0989905	0.103	0.2772	69.61	4.91E-09
60	4.62	1	0.100084	0.134	0.2531	62.09	4.80E-09
90	5	1	0.0998367	0.1411	0.2525	60.81	4.84E-09
120	5.46	1	0.100147	0.1554	0.2454	57.66	4.87E-09
150	5.95	1	0.100973	0.1408	0.2354	59.12	4.64E-09
180	6.47	1	0.100281	0.1357	0.2237	58.76	4.40E-09
210	6.99	1	0.100855	0.1449	0.2318	57.98	4.62E-09
240	7.52	1	0.100818	0.1494	0.2377	57.86	4.74E-09
270	8.05	1	0.1013	0.1375	0.233	59.46	4.59E-09
300	8.57	1	0.102322	0.1589	0.2116	53.1	4.54E-09
330	9.1	1	0.0999464	0.1443	0.2246	57.28	4.47E-09
360	9.62	1	0.10026	0.1421	0.2227	57.46	4.44E-09
390	10.14	1	0.0998685	0.1489	0.2309	57.18	4.60E-09
420	10.66	1	0.100539	0.1611	0.2218	54.02	4.62E-09
450	11.17	1	0.100228	0.1667	0.2328	54.38	4.81E-09
480	11.68	1	0.0998538	0.1698	0.2155	51.76	4.59E-09
510	12.19	1	0.100332	0.1857	0.2255	50.53	4.91E-09
540	12.7	1	0.101077	0.199	0.2218	48.11	5.05E-09
570	13.21	1	0.0995449	0.2151	0.2309	47.02	5.26E-09
600	13.72	1	0.0994731	0.2462	0.2342	43.57	5.66E-09
630	14.23	1	0.099348	0.2853	0.273	43.74	6.57E-09
660	14.73	1	0.09926	0.3491	0.2907	39.79	7.56E-09
690	15.24	1	0.0991979	0.4712	0.3312	35.1	9.57E-09
720	15.75	1	0.098968	0.6443	0.3966	31.62	1.26E-08
750	16.25	1	0.0989919	0.9281	0.492	27.93	1.74E-08
780	16.76	1	0.0982321	1.379	0.6307	24.57	2.50E-08
810	17.27	1	0.098404	2.098	0.8389	21.8	3.73E-08
840	17.78	1	0.0989782	3.228	1.099	18.81	5.66E-08
870	18.28	1	0.0987016	5.008	1.442	16.06	8.62E-08
900	18.77	1	0.0959471	7.399	1.912	14.49	1.23E-07
930	19.26	1	0.0981678	10.77	2.449	12.82	1.82E-07
960	19.75	1	0.0964177	15.53	3.084	11.23	2.56E-07
990	20.24	1	0.0978939	21	3.744	10.11	3.50E-07
1.02E+03	20.75	1	0.098406	27.69	4.639	9.51	4.63E-07
1.05E+03	21.27	1	0.104067	35.08	5.344	8.66	6.19E-07
1.08E+03	21.78	1	0.101461	43.55	6.399	8.36	7.48E-07
1.11E+03	22.28	1	0.100114	50.85	7.159	8.01	8.61E-07
1.14E+03	22.79	1	0.0993703	58.08	7.819	7.67	9.76E-07
1.17E+03	23.3	1	0.0990224	64.78	8.235	7.24	0.000001083
1.20E+03	23.8	1	0.0969616	70.65	8.925	7.2	0.000001157
1.23E+03	24.31	1	0.0986259	76.11	9.387	7.03	0.000001267
1.26E+03	24.81	1	0.101304	80.39	7.708	5.48	0.000001371
1.29E+03	25.31	1	0.101587	85.9	10.24	6.8	0.000001472
1.32E+03	25.82	1	0.10774	89.81	10.18	6.46	0.000001632
1.35E+03	26.32	1	0.0998767	93	10.24	6.28	0.000001566
1.38E+03	26.83	1	0.101526	96.79	10.62	6.26	0.000001656
1.41E+03	27.34	1	0.104039	100.4	8.987	5.11	0.000001758
1.44E+03	27.84	1	0.096946	105.5	11.49	6.21	0.000001724
1.47E+03	28.34	1	0.0973624	109.2	11.85	6.19	0.000001792
1.50E+03	28.84	1	0.111238	112.8	11.97	6.06	0.000002114
1.53E+03	29.34	1	0.103813	116.1	11.93	5.87	0.00000203
1.56E+03	29.84	1	0.0995244	119.9	11.84	5.64	0.000002009
1.59E+03	30.34	1	0.101564	124.9	12.37	5.66	0.000002136
1.62E+03	30.84	1	0.0996266	128.8	12.43	5.52	0.000002159
1.65E+03	31.35	1	0.101649	132.7	12.55	5.4	0.00000227
1.68E+03	31.85	1	0.100581	136.2	13.24	5.55	0.000002306
1.71E+03	32.35	1	0.100783	140.5	13.91	5.65	0.000002384
1.74E+03	32.85	1	0.0995703	145.7	12.92	5.07	0.00000244
1.77E+03	33.35	1	0.101347	150	13.91	5.3	0.000002558
1.80E+03	33.85	1	0.105084	153.7	14.56	5.41	0.000002719
1.83E+03	34.36	1	0.0974855	156.8	12.57	4.58	0.00000257
1.86E+03	34.86	1	0.0978397	162.2	14.11	4.97	0.00000267
1.89E+03	35.36	1	0.0997899	170.7	15.31	5.12	0.000002866
1.92E+03	35.86	1	0.10073	175.5	14.6	4.76	0.000002972
1.95E+03	36.36	1	0.100402	181	15.31	4.83	0.000003057
1.98E+03	36.86	1	0.0997749	187.6	16.08	4.9	0.000003147

C.2 Programmed sequences on rheometer

C.2.1 Collagen sequence

	Temperature ramp (1°C/min)	Temperature hold (5h)	Frequency sweep	Strain sweep
Temperature (°C)	4 - 37	37	37	37
Frequency (Hz)	1	1	0.01 - 10	1
Strain (%)	0.1	0.1	0.1	0.01 - 100

C.2.2 Gelatin sequence

	Temperature ramp (1°C/min)	Temperature hold (1h)	Temperature ramp (1°C/min)
Temperature (°C)	60 - 20	20	20 - 60
Frequency (Hz)	1	1	1
Strain (%)	0.1	0.1	0.1

C.2.3 ConCordix sequence

	Temperature ramp (2°C/min)	Temperature hold (15 min)	Temperature ramp (2°C/min)
Temperature (°C)	60 - 20	20	20 - 60
Frequency (Hz)	1	1	1
Strain (%)	0.1	0.1	0.1

C.2.4 Collagen sequence- additional temp hold

	Temperature ramp (1°C/min)	Temp. hold (5 h)	Frequency sweep	Strain sweep	Temp. hold (1 h)
Temperature (°C)	4 - 37	37	37	37	37
Frequency (Hz)	1	1	0.01 - 10	1	1
Strain (%)	0.1	0.1	0.1	0.01 - 100	0.1

C.3 Datasheet- Rat tail collagen

For life science research only.
Not for use in diagnostic procedures.

Roche

Collagen (rat)

From rat tail tendon
Lyophilizate, cell culture grade

Cat. No. 11 179 179 001

3 vials of 10 mg

Version 16
Content version: November 2013

Store at +2 to +8°C

Product overview

Formulation
Lyophilized, cell culture grade, free of microorganisms as tested using an established microbiological enumeration test.

Preparation
Collagen is purified from rat tail tendon by a modification of the method of Bornstein (1, 2). Collagen from rat tail consists mainly of type I collagen.

Reconstitution
It is recommended to dissolve the lyophilizate in sterile 0.2% acetic acid (v/v). For best results, dissolve the cell culture grade lyophilizate in sterile 0.2 % acetic acid (v/v). In sterile 0.2 % acetic acid (v/v), this product can be used in cell culture without further filtration.

For the preparation of collagen gels, the content of the bottle should be dissolved in 3.3 ml sterile 0.2% acetic acid (v/v) each. This results in a final concentration of 3 mg/ml.

For coating culture dishes the final concentration should be 1 – 2 mg/ml.

For dissolving: do not stir, just pour the acetic acid onto the lyophilizate and let it stand for several hours until it has dissolved. For fully dissolve the product an incubation for up to a maximum of 24 h at +15 to +25°C may be required.

Biological activity
The collagen is tested for the promotion of adherence of human umbilical vein endothelial cells (HUV-EC).

Working concentration
The recommended concentration for the coating of cell culture vessels is 5 $\mu g/cm^2$.

For the production of collagen gels a final concentration of 2 – 3 mg/ml is used.

Species specificity
Collagen (rat tail) is active on most vertebrate cells.

Application
- Collagen (rat tail) is used as a substrate for the culture of cells.
- Collagen (rat tail) can either be used for the
  - coating of surfaces (culture vessels, slides, cover slips, etc.) or
  - for the preparation of collagen gels.

Storage/ stability
Stable at +2 to +8°C until the expiration date printed on the label.

The reconstituted solution in sterile acetic acid is also stable at+2 to +8°C.

Procedures and required material

Coating cell culture dishes with collagen

Overview
Rat tail collagen is useful for cultivating cells which need a substrate to grow and to proliferate. Collagen as a substrate is used in the form of either a thin film of dried collagen or a hydrated collagen gel (3–12). A thin film of dried collagen is prepared by spreading the collagen solution onto the surface of a dish and air dried.

Additional reagents required
- sterile 0.2% acetic acid (v/v)
- medium or buffer for washing purposes

Procedure
Coating of cell culture dishes with collagen (= collagen film). Please refer to the following table.

Step	Action
1	Dissolve each vial of the lyophilized Collagen with 5 ml sterile 0.2% acetic acid (v/v) to give a final concentration of 2 mg/ml.
2	Pipette 2.5 µl of this solution (2 mg/ml) per 1 cm^2 surface area to be coated (5 $\mu g/cm^2$). This can be increased or decreased to fit the application.
3	Carefully spread the collagen solution with a sterile rubber policeman on the bottom of the culture dish.
4	Air dry for about 60 min at +15 to +25°C in the laminar flow hood.
5	It is possible, but not essential, to wash the coated surface with medium or buffer.
6	The dishes can be used immediately or stored under sterile conditions.

Preparation of collagen gels

Overview
Collagen gels can be prepared by a number of different procedures.

One method consists of exposing ammonia vapor to the collagen solution (see method 1).

Another method consists of adjusting the pH and ionic strength of the collagen solution (see method 2).

For the three dimensional culture of various cell types, the rat tail collagen gel has proved to be an easy and useful system. For the two systems working instructions are given below. Work should be done under a laminar flow hood.

Handling instructions
- To allow for the formation of a homogenous gel and to avoid clump formation do not or only very carefully move culture vessels during gel formation.
- After attachment of the cells, the gel can be detached from the dish with a sterile pipette tip and allowed to float in the medium.

Additional material required
- 0.2% acetic acid (v/v), pH 3.0 or 1 mM hydrochloric acid, pH 3.0
- phenolred (optional)
- 25% ammonia solution (v/v)
- cell culture medium
- 35-mm petri dish
- 60–mm petri dish

Method 1

Please refer to the following table.

Step	Action
1	Dissolve each vial of the lyophilized Collagen in 3.3 ml sterile 0.2% acetic acid (v/v), pH 3.0 or 1 mM hydrochloric acid, pH 3.0. This gives a final concentration of 3 mg/ml. If 2 µl/ml phenolred is added, the change of the pH is easier to control.
2	Let it stand overnight for swelling up.
3	Pipette 100 µl of this collagen solution per 1 cm^2 surface area to be covered into the culture vessel. This gives an approximately 1 mm thick collagen gel layer.
4	The collagen solution is then exposed to ammonia vapors at +15 to +25°C or +37°C.
5	An example for preparing a collagen gel in a 35-mm dish: • Pipette 100 µl 25% ammonia solution (v/v) into a 60-mm petri dish. • A 35-mm dish containing 1ml collagen solution is placed in the 60-mm dish which is then closed. If phenolred is present in the collagen solution, the change of the pH can be easily observed (color change to neutral). • If there is no pH indicator in the collagen solution the 35-mm dish should be removed after max. 2 min. If the gel layer is thicker the gel needs longer to solidify.
6	After about 2 min the gel should be solidified. Equilibrate the gel with an appropriate amount of medium for 30 min. This is necessary to remove excess ammonia which is toxic to the cells. A longer period for equilibration is needed for a thicker collagen layer.
7	Aspirate the medium.
8	Then the cell can be seeded onto the gel.

Additional reagents required

- sterile 0.2% acetic acid (v/v), pH 3.0 or 1 mM hydrochloric acid, pH 3.0.
- sterile 10 × (5 ×) concentrated medium, with sodium bicarbonate, pH 7.4,

  Check the instructions provided by the supplier of the 10 × (5×) concentrated medium regarding the appropriate amount of sodium bicarbonate for the specific medium used.
- sterile (10 ×) 0.2 M Hepes, pH 7.3 [dilute 1 M Hepes tissue culture tested, 1 : 5 with sterile double dist. water]

Method 2

Please refer to the following table.

Step	Action
1	Dissolve each vial of the lyophilized Collagen in 3.3 ml sterile 0.2% acetic acid (v/v), pH 3.0 or 1 mM hydrochloric acid, pH 3.0. This gives a final concentration of 3 mg/ml.
2	Mix the following solutions at +2 to +8°C, avoid the formation of air bubbles: • 1 (or 2) parts of sterile 10 × (5 ×) concentrated medium, with sodium bicarbonate, pH 7.4, • 1 part of sterile (10 ×) 0.2 M Hepes, pH 7.3 [dilute 1 M Hepes tissue culture tested, 1 : 5 with sterile double dist. water], • 8 (or 7) parts of the sterile collagen solution. The mixture remains liquid at +2 to +8°C.
3	Pipette 100 µl of this neutralized collagen solution per 1 cm^2 surface area to be covered into the culture vessel. This gives an approximately 1 mm thick collagen gel layer.
4	Incubate for approx. 2–3 h at +15 to +25°C or at 37°C in a humidified atmosphere to allow gel formation. The culture dishes can be stored at +2 to +8°C under sterile conditions.
5	Before inoculating the cell suspension it is recommended to cover the gel with medium for about 15 min for equilibration.
6	The cells are plated as usual. To allow the formation of a homogeneous gel and to avoid clump formation do not or very carefully move culture vessels during gel formation.

Subculture of cells

To subculture the cells, the collagen gel can be digested with collagenase (*e.g.*, collagenase A*, 0.1% in HBSS for approximately 10 to 20 min or until the gel is digested at +37°C).

The cells can be recovered and washed by centrifugation.

Cells must be washed, to be completely free of collagenase if they are to be cultured on collagen again. If the cells are in clumps, single-cell suspensions can be prepared by further digestion with trypsin/EDTA* or dispase*.

Embedding cells in collagen gels

For embedding cells in collagen gel, suspend the cells in medium at 100× their final desired concentration and mix 1 part of the cell suspension with 100 parts of neutralized collagen solution at +2 to +8°C.
Pipette an appropriate volume into the culture vessel and incubate at +15 to +25°C or +37°C.
Add medium to the cells immediately after the gel has solidified.

The ratio of cell suspension to collagen solution can be varied but this will result in a variation of the gel consistency.

Changes to Previous Version

- Clarification of step in Method 2 using 10 × (5 ×) concentrated medium.
- Editorial changes.
- Licence disclaimer added

References

1 Bornstein, M. B. (1958), *Lab. Invest.* **7**, 134–137.
2 Michalopoulos, G. & Pitot, H. C. (1975), *Exp. Cell Res.* **94**, 70–78.
3 Iversen, P. L. et al. (1981) *In Vitro* **17**, 540–552.
4 Yang, J. et al. (1979) *Proc. Natl. Acad. Sci. USA* **76**, 3401–3405.
5 Yang, N. S. et al. (1981) *Cancer Res.* **41**, 4093–4100.
6 Yang, J. et al. (1980) *Proc. Natl. Acad. Sci. USA* **77**, 2088–2092.
7 Sinha, D. K. & Pazik, J. E. (1986) *In Vitro* **22**, 519–524.
8 Montesano, R. & Orci, L. (1988) *Proc. Natl. Acad. Sci. USA* **85**, 4894–4897.
9 Methods Enzymol. (1982) 82, Part A: Extracellular Matrix, Section I. Collagen, 3–555.
10 Kleinmann, H. K. et al. (1981) *J. Cell Biol.* **88**, 473–485.
11 Yang, J. & Nandi, S. (1983) *Int. Rev. Cytol.* **81**, 249–286.
12 Kleinmann, H. K. et al. (1987) *Anal. Biochem.* **166**, 1–13.

*available from Roche Applied Science

Contact and Support

To ask questions, solve problems, suggest enhancements and report new applications, please visit our **Online Technical Support Site**.

To call, write, fax, or email us, visit the Roche Applied Science homepage, **www.roche-applied-science.com**, and select your home country. Country-specific contact information will be displayed.

Roche Diagnostics GmbH
Sandhofer Strasse 116
68305 Mannheim
Germany

C.4 Datasheet- Gelatin

GELITA
Improving Quality of Life™

CERTIFICATE OF ANALYSIS

Order no.: 166868
Batch No.: 631150 Production Date: 01.09.2011 Expiry time: 5 years

GELITA® Bovine Gelatine
150 Bloom, Ph.Eur.
Pharmaceutical Grade

Customer: Ayanda AS Tromsoe, Norway

Parameter	Test Method	Specification	Test Result	
Jelly strength	Ph. Eur./GME (6,67%)	140 - 160	156	g Bloom
Viscosity	GME (6,67%, 60° C)	3,3 - 4,0	3,5	mPa.s
Loss on drying	Ph. Eur./GME (16 h, 105 °C)	9,0 - 15,0	11,1	%
pH	6,67 %, 60 °C	5,0 - 5,9	5,6	
Conductivity	Ph. Eur. (1%, 30°C)	<= 1000	90	µS/cm
Peroxides	Ph. Eur./GME	<= 10	corresponding	mg/kg
Chromium*	ICP-OES	<= 10,0	corresponding	mg/kg
Iron*	ICP-OES	<= 30,0	corresponding	mg/kg
Zinc*	ICP-OES	<= 30,0	corresponding	mg/kg
Sulphur dioxide*	Ph. Eur./GME	<= 10	corresponding	mg/kg
Total Aerob.Microb.Count	Ph. Eur./USP	< 1000	corresponding	cfu/ g
Total Yeast/Mould Count	Ph. Eur./USP	< 100	corresponding	cfu/ g
Escherichia coli	Ph. Eur./USP	0	negative	/ g
Salmonella	Ph. Eur./USP	0	negative	/ 10 g

* The parameter is monitored according to an internal quality programme

This certificate was made electronically and therefore it is valid without a signature
signed: Dr. Andreas Probst on 07.09.2011

Product release
Quality assurance: Dr. Andreas Probst 07.09.2011
Material management: Gunter Grab 07.09.2011

STDANA-5-26.07.2010/AWKNR2-2010062400/HOFMANN/166868/07.09.2011 12:54:07
GELITA AG - Uferstraße 7 - D-69412 Eberbach

Page 1 of 1

C.5 Frequency sweep data

Table C.2: The recorded G' value at 1 Hz and at 10 Hz as well as the increase in G' between 1 Hz and 10 Hz during the frequency sweep. The strain and temperature were kept constant (0.1% and 37°C). It took the program 4 minutes to go from 1 Hz to 10 Hz.

Name	G' (Pa) at 1 Hz	G' (Pa) at 10 Hz	Increase (%)
B1	2158	2291	5.8
B2	931.1	976.9	4.6
B3	1723	1803	4.4
C1*	927	1055	12.1
C2	3378	3526	4.2
C3	1499	1566	4.3
C4	-	-	
D1*	1804	1911	5.6
D2	2522	2605	3.2
D3	3629	3670	1.1
D4	2818	3002	6.1
E1*	4836	5038	4.0
E2	1315	1399	6.0
E3	2090	2201	5.0
E4	637.1	689.1	7.5

Table C.3: Changes in G' modulus value from the end of the temperature hold, through the frequency sweep and strain sweep as well as the overall percentage increase in G' modulus through the entire period and also for a 4 minute interval. The 4 minute interval corresponds to the time it took for the instrument to go from 1-10 Hz in the frequency sweep.

Name	G' (Pa) temp. hold	G' (Pa) in freq. sweep	G' (Pa) in strain sweep	Increase (%) overall	Increase (%) 4 min
B1	2069	2158	2210	6.4	0.9
B2	908.2	931.1	950.7	4.4	0.6
B3	1700	1720	1740	2.3	0.3
C1*	987.9	927	734.2	- 34.5	-3.7
C2	3131	3378	3512	10.8	1.9
C3	1410	1499	1500	6.0	0.9
C4	-	-	-	-	-
D1*	1666	1804	1423	- 17.1	-1.9
D2	2482	2522	2559	1.6	0.4
D3	3328	3629	3602	7.6	1.1
D4	2645	2818	2876	8.0	1.2
E1*	4751	4836	2249	- 111.2	-7.5
E2	1235	1315	1360	9.2	1.4
E3	2070	2090	2124	2.4	0.4
E4	620	637.1	671.6	7.6	1.1

C.6 Gelling kinetics

Table C.4: Overview of the various concentrations of dissolved G-block in 1:10 DPBS stock added in the making of collagen gel. The values for $G'_{20\%}$ and $T_{20\%}$ are calculated from G'_{max}. Due to numerous K019 error codes for parallel C4 at the 2.50 mg/ml G-block concentration this parallel is excluded from data analysis.

Treatment	Parallel name	G'_{min}	G'_{max}	$G'_{20\%}$	$T_{20\%}$ (°C)
No G-block	A1	4.54	112.80	22.56	20.00
No G-block	A2	0.26	61.46	12.29	21.00
No G-block	A3	0.10	187.60	37.52	21.50
5.00 mg/ml G-block	B1	1.73	138.20	27.64	25.00
5.00 mg/ml G-block	B2	0.31	164.80	32.96	25.50
5.00 mg/ml G-block	B3	0.75	193.3	38.66	25.80
2.50 mg/ml G-block	C1	0.52	37.36	7.47	25.00
2.50 mg/ml G-block	C2	3.06	54.31	10.86	27.00
2.50 mg/ml G-block	C3	1.02	69.42	13.88	26.00
2.50 mg/ml G-block	C4	-	-	-	-
1.25 mg/ml G-block	D1	1.50	14.99	2.99	18.00
1.25 mg/ml G-block	D2	0.08	27.43	5.49	28.50
1.25 mg/ml G-block	D3	0.18	70.23	14.05	27.00
1.25 mg/ml G-block	D4	2.19	67.62	13.52	26.50
0.62 mg/ml G-block	E1	0.37	46.04	9.21	24.00
0.62 mg/ml G-block	E2	0.78	81.08	16.22	26.00
0.62 mg/ml G-block	E3	0.24	72.41	14.48	27.00
0.62 mg/ml G-block	E4	1.10	40.21	8.04	27.00

Appendix D

Examples of R-scrips

D.1 Immunohistochemistry

```
#for fib 43x
PercentGr1.1 <- Percent1[1:12]
PercentGr1.2 <- Percent1[13:30]
#t-test, 2-halet 0.05 p
t.test(PercentGr1.1, PercentGr1.2, conf.level = 0.95)
#for fib 52x
PercentGr2.1 <- Percent2[1:12]
PercentGr2.2 <- Percent2[13:30]
#t-test
t.test(PercentGr2.1, PercentGr2.2, conf.level = 0.95)
#plot
boxplot(Percent1~Treatment1, data=tempfibIHC,
ylab="% DAB+/Nuclear staining",
names=c("432", "433", "435", "436", "438"))
boxplot(Percent2~Treatment2, data=tempfibIHC,
ylab="% DAB+/Nuclear staining",
names=c("523", "524", "525", "527", "530"))
#ANOVA Fibronectin 43x og 52x
```

```
testGr1 = aov(Percent1~Treatment1, data = tempfibIHC)
summary(testGr1)
TukeyHSD(testGr1, conf.level = 0.95)

testGr2 = aov(Percent2~Treatment2, data = tempfibIHC)
summary(testGr2)
TukeyHSD(testGr2, conf.level = 0.95)
```

D.2 Rheology

```
GrA <- T_20StoreMod[1:3]
GrB <- T_20StoreMod[4:6]
GrC <- T_20StoreMod[7:9]
GrD <- T_20StoreMod[10:13]
GrDadjust <- T_20StoreMod[11:13]
GrE <- T_20StoreMod[14:17]
Control <- T_20StoreMod[1:3]
Treated <- T_20StoreMod[4:17]
#t-test, 2-halet 0.05 p
t.test(Control, Treated, conf.level = 0.95)
t.test(GrA, GrB, conf.level = 0.95)
t.test(GrA, GrC, conf.level = 0.95)
t.test(GrA, GrD, conf.level = 0.95)
t.test(GrA, GrDadjust, conf.level = 0.95)
t.test(GrA, GrE, conf.level = 0.95)
#ANOVA and Tukey
Temp = aov(T_20StoreMod~Treatment, data = X20PercentofTmax)
summary(Temp)
TukeyHSD(Temp, conf.level = 0.95)
```